Co-funded by the European Union's Horizon 2020 research and innovation programme under Grant Agreement no. 691797

STORE&GO

Innovative large-scale energy storage technologies and Power-to-Gas concepts after optimisation

D6.4

Report on the model of the power system with PtG

Due Date	31 October 2018 (M32)
Deliverable Number	D6.4
WP Number	WP6
Responsible	E. Bompard
Author	E. Bompard,S. Bensaid, G. Chicco, A. Mazza
Reviewer	F. Maréchal, EPFL, H. Blanco (RUG)
Status	Started / Draft / Consolidated / Review / Approved / **Submitted** / Accepted by the EC / Rework

Dissemination level

✘	**PU**	Public
	PP	Restricted to other programme participants (including the Commission Services)
	RE	Restricted to a group specified by the consortium (including the Commission Services)
	CO	Confidential, only for members of the consortium (including the Commission Services)

Table of Contents

Acronyms

AC	Alternate current
CCGT	Combined Cycle Gas Turbine
DA	Day-Ahead
DCOPF	DC Optimal Power Flow
DG	Distributed Generation
DUOPF	DC Unit de-commitment Optimal Power Flow
GDP	Gross Domestic Product
HV	High Voltage
ID	Intra-Day
LSE	Load Serving Entities
mpc	Matpower Case-file
MV	Medium Voltage
OC	Overcurrent
OCGT	Open Cycle Gas Turbine
OV	Overvoltage
PEM	Proton Exchange Membrane
PtG	Power-to-Gas
pu	per unit
PV	Photovoltaic
RES	Renewable Energy Sources
RPF	Reverse Power Flow
ROR	Run-On-River plant (hydro power plant)
SA	Simulated Annealing
SNG	Synthetic Natural Gas
TYNDP	Ten Year Network Development Plan

Executive Summary

The project STORE&GO aims to investigate all the aspects regarding the integration of large-scale Power-to-Gas (PtG) at European level, by exploiting it as means for long term storage. One of the aspects that should be properly addressed is the beneficial impact that the integration of PtG plants may have on the electricity system. During the project, the framework of analysis regarding the electricity system integrating PtG plants has been introduced in Deliverable 6.1 “Report on opportunities and options for PtG in power systems” [1], where the authors presented a holistic view aiming to compare the features of PtG plants and electricity systems, giving the basis for the successive analysis. The studies regarding the electricity network have to address two basic questions: i) how much is the impact on the operation of the system of integrating PtG and ii) how PtG can impact on the electricity grid development. For properly addressing the two questions, two Deliverables have been scheduled: the current Deliverable 6.4 “Report on the model of the power system with PtG” and the Deliverable 6.6 “Report on the impacts of the PtG on selected scenarios”, due in M42. The current Deliverable D6.4 aims to i) introduce the models for investigating the integration of PtG in electricity system (i.e., model of the plant, transmission system model, distribution networks model), ii) provide some initial hints regarding the positive impact of PtG on the transmission system with the current and future level of Renewable Energy Sources (RES) penetration, and iii) analyse the impact on the operation of the distribution system in some meaningful case studies. The study regarding the impact on the grid development will be addressed in D6.6: due to this, the complete study regarding the point ii) on future scenarios will be faced in D6.6 as well, because it is strictly connected on the future development of the electricity infrastructure on which the PtG can have an impact.

As mentioned above, one of the goals of this Deliverable is the introduction of the models which will be used during the next investigations. This Deliverable presents a model of a PtG plant, which takes into account the entire chain of the plant, by eventually introducing the electrical “PtG node”, which is able to emulate the limits in accepting electricity due to the different elements composing the plant. The model developed is a first order model, and it is based on a real response of an alkaline electrolyser operating in one of the project demo sites (i.e., Falkenhagen, Germany). The model considers the presence of an H_2 buffer, and can be scaled up according to the nominal power chosen.

The Deliverable presents different network models aiming to properly represent both the transmission and distribution grids. In particular, the study regarding the transmission network is organized by considering three network samples. The first network is the European configuration of the CIGRE’ HV Transmission System [2]. The network presents all the typical characteristics of the European network, and was used as simple case for testing the calculation code. In this simple example, the results in presence of strong wind show that the installation of PtG will help to reduce the unbalancing that has to be faced by the slack bus of the network.

The second transmission network considered is the simplified version of the European 400kV system [3], covering most of continental Europe (17 countries). It is composed of 1254 nodes and more than 1900 branches. The model presents the geographical location of the nodes, allowing the overlapping of the physical layer (i.e., the network itself) with the resources layer (i.e., the potential of renewable energy sources). The loads have been updated thanks to the data available on the ENTSOE website [4]. The simulations show that with the load and generation condition referred to the year 2017, the presence of 7.2 GW of PtG reduces considerably both the peak (~45%) and the duration (>95%) of the unbalance due to the difference between the expected RES production and their actual value. The study has been carried out by using a model solving an Optimal Power Flow (OPF) based on the values of the hourly load based on ENTSOE data and the expected value, based on available and accessible free databases. The variation with respect to the expected value of RES has been

emulated by means of synthetic profiles obtained by adapting for the specific case procedure existing in literature and based on real data.

The third transmission network considered is a simplified EU network, composed of 256 nodes: it represents the results obtained by clustering the EU transmission network (composed of more than 6000 nodes), and uses standard values for the HV lines. Also this case has been run by using the script composed of two OPFs, and also in this case the results are good: on the basis of load and generation of 2017, the use of 10 GW of PtG allowed to reduce considerably the unbalance caused by the difference between expected and actual RES production, both in terms of time duration (~90%) and power peak (~50%).

Some hints regarding the future scenarios [5] for the network #T3 have also been provided: in particular, the same siting and sizing of the case 2017 led to have lower performances both in terms of duration and peak reduction, by suggesting the necessity of further studies for choosing the most appropriate installation sites, as well as the plant sizes (that will be presented in D6.6).

The study on the distribution system presents two networks, representing a rural area [6] and a semi-urban area [7]. The first one is considered as a good representative example for the distribution grid in the south of Italy: this choice has been done because one of the demo site (Troia, Italy) is installed in an area whose network can be represented by this kind of sample. For the same reason, by considering the location of the second demo site (Solothurn, Switzerland) a semi-urban network has been chosen to be meaningful for the case under study because composed of a downtown and some peripheral areas supplied by a single network.

The cases studied on the distribution networks allow to shown the impact that PtG can have in case:

1. reverse power flow, with all the network constraints respected
2. increase of the hosting capacity of the distribution network, by increasing the penetration of installed RES [8] (that means, the constraints are no longer respected in the base cases)

The results show that the placement of some PtG plants (whose size and number differ for the two case studies) is beneficial for the network, and it is able to alleviate or even eliminate the issues affecting the network. In particular the reverse power flow, thanks to the installation of PtG, is reduced at least 67% (in the rural network with 80% of PV penetration, case $2 \leq L \leq 3$) up to even 100% (with consequent elimination of the reverse power flow in the semi-urban network with 30% of PV penetration, method 2b). The penetration of RES has been calculated based on the irradiance value of July. An optimization algorithm has been run, for properly choosing size and installation sites of the PtG plants. A check regarding the absence of problems caused by the PtG plants has been also done for other months, for which the production of PV is lower than in July.

1 Introduction

The impact of Power-to-Gas (PtG) technology on electricity system is fundamental for investigating the potential of this technology for allowing the larger and larger penetration of Renewable Energy Sources (RES) in the European electricity systems.

The study of the implementation of PtG and its effect on the electricity system is analysed by the following different stages, reported in two different Deliverables:

- Deliverable 6.4:" Report on the model of the power system with PtG"
- Deliverable 6.6: "Report on the impacts of the PtG on selected scenarios"

The first Deliverable is the current one and aims to describe all the models involved in the study (such as the types of network implemented, information regarding the load and generation profiles, the model used for representing the PtG node in the network and so on), to show some hints regarding the operation of the transmission system with PtG by considering both current and future scenarios, and the results referring to the distribution system operation.

The second Deliverable (issued at M42), will contain the detailed simulation regarding the role of PtG in the electricity system reinforcement, as well as the complete studies regarding the operation of the transmission system according to the long term scenarios developed in Task 6.2.

For the studies carried out in Task 6.3, five different networks have been used, i.e., three transmission networks (the former as proof of concept for testing the model, and the latter two representing the European transmission system) and two distribution networks (with different characteristics, aiming to represent the networks existing in the demo sites).

The content of this Deliverable is organised as follows: Section 2 presents the electrical PtG node, Section 3 presents the models developed for studying the use of PtG plants connected to the transmission system, whereas Section 4 presents the first results obtained using the models above cited. Section 5 focuses on the description of the distribution system models used, whereas Section 6 presents the results obtained by running the models. The conclusions are reported in Section 7, whereas five appendixes present details regarding the calculation of PV power starting from the value of irradiance, some notes regarding day-ahead and intraday market, an introduction to the optimal power flow problem, a description of the scripts used for the transmission system case studies and a brief presentation of the Simulated Annealing (an optimization method used for the distribution system studies).

2 The “electrical” PtG node: plant model assumptions

As mentioned later in Section 3.8.1, the electricity system is composed of different types of nodes, and the goal of this Section is to present the assumptions made for building what can be called PtG node. The PtG node is a schematic representation of the entire PtG chain (electrolyser + buffer + methanation) that interacts with the electricity network at which it is connected. So, a feedback comes from the downstream part of the plant (i.e., the chemical process and the installed buffer), by limiting the possibility of the plant of absorbing electricity from the network, and thus having an effect on the possibility for the PtG plant to participate in the network stabilisation. Moreover, the PtG node has all the ingredients for scaling up the plants or even change the type of electrolyser.

This work aims to analyse the behaviour of electricity grids, in which AEC-based PtG systems are considered and the electric input profile is linked to intermittent renewable energy sources. The choice of the type of electrolyser is due to the presence of real measurement data provided by the demo site of Falkenhagen (Germany), which allows to have a real-world based model, based on the facility belonging to a partner of the project.

It is worth to note that the other types of electrolyser can be chosen for updating the model according to the latest technology (for example the Proton Exchange Membrane (PEM) electrolysers).

The PtG plant consists of an AEC-based electrolyser, which converts water into hydrogen through electrolysis. Then, the hydrogen could be stored into a tank or mixed with carbon dioxide in order to produce methane in a methanation unit. A simplified scheme of the PtG process can be seen in Figure 2-1.

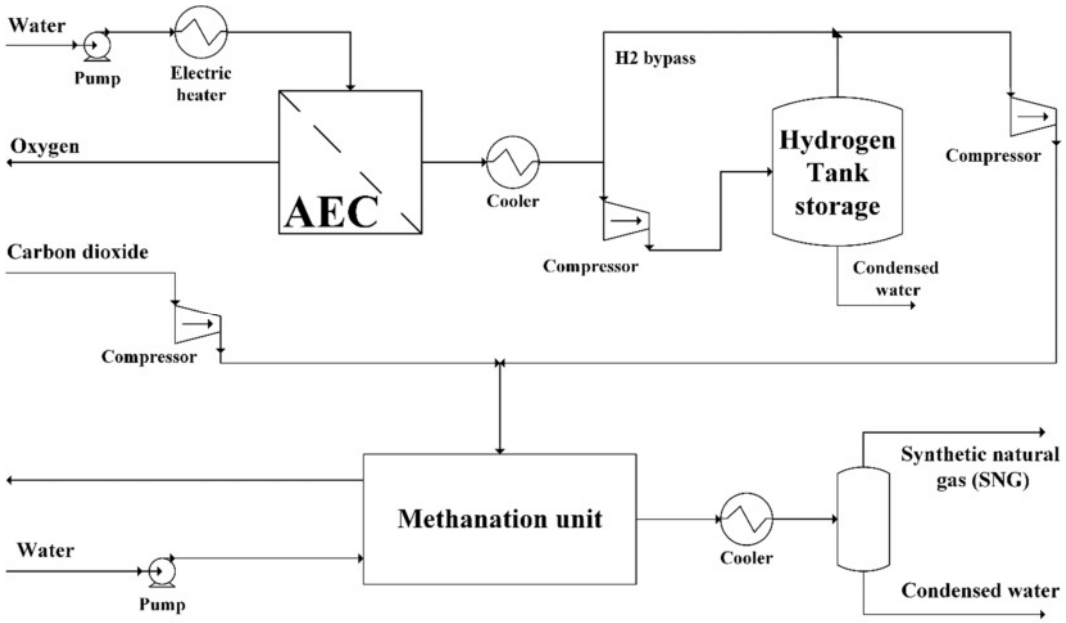

Figure 2-1: Simplified AEC-based Power-to-Gas process scheme considering an H_2 storage.

The low temperature-based electrolyser is characterised through to a power-to-hydrogen efficiency (e.g. about 55 %), whereas the methanation unit is characterized by a certain value of the CO_2 conversion (i.e., about 99 %). In order to perform a better assessment of the system, a PtG plant model was developed in a MATLAB environment. This PtG model was built taking into account the dynamics (start-ups, shutdowns and partial loads) of a real AEC-based electrolyser. In addition, the electrical input to the PtG plant is comparable with the load of the electrolyser, thus all the auxiliary consumptions were considered.

2.1 AEC electrolyser model

The dynamic AEC-electrolyser response was obtained from the data of a test carried out at the project demo site in Falkenhagen on a 2 MW AEC-electrolyser, which was constituted of 6 AEC modules (330 kW each one). The test had a duration of about 11.5 h, and the set point of the electrolyser was periodically changed with steps of different amplitude to explore a large number of operating conditions, as shown in Figure 2-2. These tests (undertaken by Uniper, one of the partners of the project) highlighted that the AEC-based electrolyser had a fast response when the setpoint changed; therefore, its response could be modelled for the purpose of forecasting the behaviour of the AEC-based electrolyser when it is coupled with an intermittent RES-based electric profile.

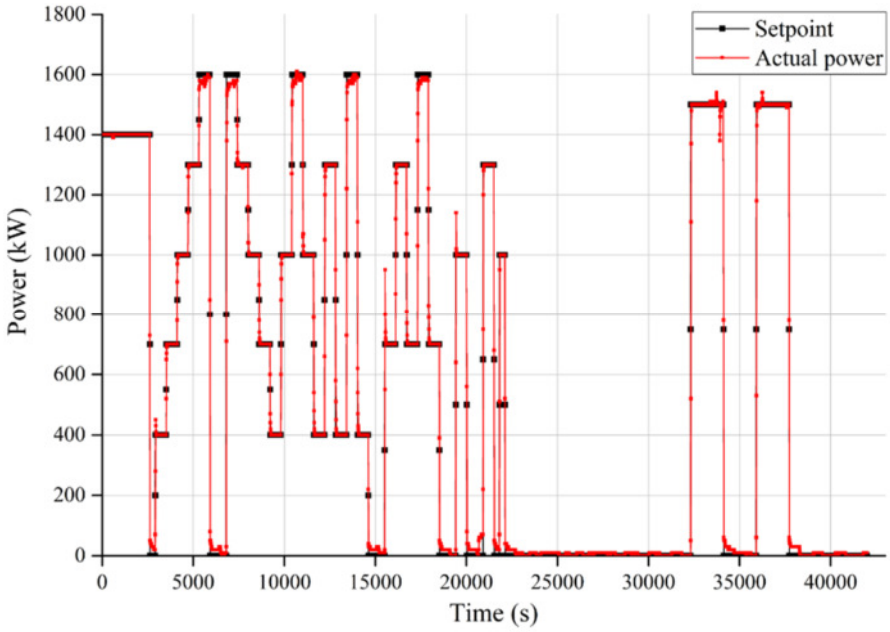

Figure 2-2: Falkenhagen test on an AEC-based electrolyser

The easiest model to describe the AEC-based electrolyser behaviour is a first order system with delay, which is characterized by 3 parameters; the mathematical model of its response to a step is described by means of equation (1) [9][10].

$$\begin{cases} y(t) = 0 & \text{If } t < \alpha \\ y(t) = A \cdot K \cdot \left[1 - \exp\left(-\dfrac{t-\alpha}{\tau}\right)\right] & \text{If } t \geq \alpha \end{cases} \quad (1)$$

In this equation, y is the actual power of the AEC-based electrolyser (MW), A is the step amplitude of the set point (MW), K is the gain of the system, α is the time delay of the response (s), τ is the time constant of the system (s) and t represents the time (s). The gain could be evaluated by means of equation (2), where $y(\infty)$ is the actual power of the electrolyser after a large period of time (stationary condition).

$$K = \frac{y(\infty)}{A} \quad (2)$$

Whereas, the two time parameters (α and τ) were estimated by means of the Sundaresan and Krishnaswamy's method [11], according to equations (3) and (4), respectively. The two parameters were calculated using two characteristic points of the response curve: t_1 represents the time in which the response reaches the 35.3% of the stationary value $y(\infty)$; while, t_2 is estimated as the time in which the response reaches the 85.3% of the final value $y(\infty)$.

$$\alpha = 1.3 \cdot t_1 - 0.29 \cdot t_2 \quad (3)$$

$$\tau = 0.67 \cdot (t_2 - t_1) \quad (4)$$

For the purpose of evaluating the three parameters (K, τ and α), four steps with the same amplitude were considered. More in detail, the four steps were obtained between 3450 s and 5400 s (see Figure 2-2), where the step amplitude (A, MW) was 0.3 MW. Therefore, the first order system with delay model interpolates carefully the actual power data, as illustrated in Figure 2-3. The estimated parameters (K = 1; τ = 11.73 s; α = 14.62 s) allow the actual power of the AEC-based electrolyser to be calculated by means of the model of its dynamic response. The response is exponential, thus, the stationary condition could be reached after about 60 s (the difference between the set point and the actual power is lower than 2 %).

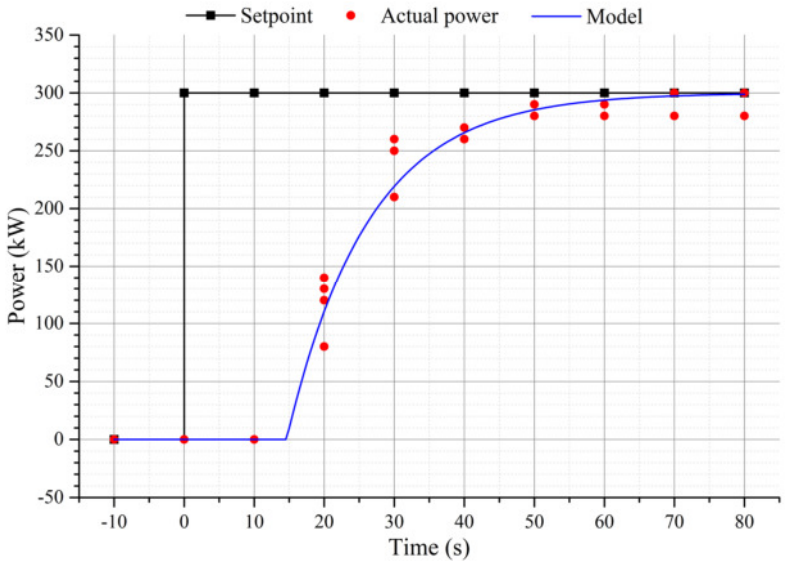

Figure 2-3: AEC-based electrolyser response model estimated using Falkenhagen test data (first order system with delay: K = 1; τ = 11.73 s; α = 14.62 s).

It is worth to note that, in general, these parameters depend on the characteristics of the single electrolyser, but they do not depend on the step amplitude, which is applied to that electrolyser. They could change, if the stack size varies; but in our case, 330 kW AEC stacks are considered. Thus, this size could be considered as an average size between 300 kW and 2-3 MW electrolysers due to the modularity of the technology.

2.1.1 AEC electrolyser efficiency

Another relevant feature of the electrolyser is its efficiency, which relates the absorbed electric power with the hydrogen chemical power. The power-to-H_2 efficiency (η_{el_H2}, LHV based) is a free parameter of the model. In our case study, the average value of the efficiency of the electrolyser is 57.6% and it has been provided by the project partner Uniper, managing the demo site of Falkenhagen. This value is in line of the reference efficiencies of low temperature-based electrolysers [12][13]. In addition, the hydrogen power was calculated using the volumetric hydrogen flow ($\dot{V}_{H2}$, m^3/h) measured during the test, according to equation (6). In this equation, p is the normal pressure (10^5 Pa), T the normal temperature (273.15 K), R is the ideal gas constant (8314 $J \cdot kmol^{-1} \cdot K^{-1}$), MW_{H2} represents the molar weight of the hydrogen (2.016 kg/kmol) and LHV_{H2} is the lower heating value of the hydrogen (120 MJ/kg).

$$P_{H2} = \eta_{el\_H2} \cdot P_{AEC} \quad (5)$$

$$P_{H2} = \frac{p \cdot \dot{V}_{H2}}{R \cdot T} \cdot \frac{MW_{H2} \cdot LHV_{H2}}{3600} \quad (6)$$

2.2 Methanation unit

The overall CO_2 conversion within the methanation unit was assumed at about 99 % [14] to ensure the synthetic natural gas (SNG) quality. Hence, the thermodynamic hydrogen-to-methane efficiency corresponds to 83 % on LHV basis (it is defined as the ratio between the chemical energy of the produced methane and the chemical energy of the hydrogen which is fed to the methanation unit). However, the methanation reaction is strongly exothermic, thus, 17 % of the hydrogen chemical energy (LHV basis) is released as heat of reaction (-164 kJ/mol) [13]. Moreover, all high-temperature items of equipment were thermally insulated to minimize heat losses and dissipations. Heat losses (Q, MW) were estimated according to equation (7), in which k represents the thermal conductivity ($W \cdot m^{-1} \cdot K^{-1}$) of a microporous insulation material [15], S is the surface heat exchange area (m^2), x is the insulation panel thickness (m), T_1 and T_2 are the temperatures (K) of the internal and external surface area, respectively.

$$Q = \frac{k \cdot 10^{-6}}{x} \cdot S \cdot (T_2 - T_1) \quad (7)$$

2.3 Compression and pumping power consumptions

The hydrogen produced within the AEC-based electrolyser could be compressed in a storage tank or it could be mixed with carbon dioxide in stoichiometric ratio equal to equation (4). In addition, the carbon dioxide may be compressed up to the methanation unit pressure. Finally, the water has to be pumped in the electrolyser. For all these processes electricity is needed, thus the power of the compressors ($P_{c,j}$, MW) and the power of the pump ($P_{p,H2O}$, MW) must be estimated according to equations (8) and (9), respectively. In these correlations, Z is the compressibility factor, R is the molar ideal gas constant, γ is the heat capacity ratio and η_c is the compression efficiency, which was set at 85% [16]. $T_{1,j}$ (K) and $p_{1,j}$ (bar) are the temperature and the pressure at the inlet of the j-th compressor; and lastly, $p_{2,j}$ (bar) is the pressure at the outlet of the equipment. Moreover, $\dot{n}_{in,j}$ is the molar flow (kmol/s) of the gas mixture at the inlet of the j-th compressor. In addition, p_M and p_{ATM} are the methanation unit pressure (MPa) and the atmospheric pressure (0.101325 MPa), respectively; MW_{H2O} is the water molar weight (18.016 kg/kmol), η_p is the efficiency of the pump which was assumed equal to 85 %, ρ_{H2O} i the water density (about 1000 kg/m^3), $\dot{n}_{H2}$ is the hydrogen molar flow (kmol/s) produced by the electrolyser and WC is the water conversion of the AEC-based electrolyser which was set equal to 75%.

$$P_{c,j} = Z_j \cdot \frac{R}{10^6} \cdot T_{1,j} \cdot \frac{\gamma_j \cdot \eta_{c,j}}{\gamma_j - 1} \cdot \left[\left(\frac{p_{2,j}}{p_{1,j}} \right)^{\frac{\gamma_j - 1}{\gamma_j \cdot \eta_{c,j}}} - 1 \right] \cdot \dot{n}_{in,j} \quad (8)$$

$$P_{p,H2O} = \frac{(p_M - p_{ATM}) \cdot MW_{H2O}}{\eta_p \cdot WC \cdot \rho_{H2O}} \cdot \dot{n}_{H2} \quad (9)$$

For instance, the specific energy consumption for CO_2 compression is 83.4 kJ/kg, while the specific energy consumption for H_2 compression is about 3300 kJ/kg, which correspond to 3.8 % of the produced SNG energy. In addition, the water flow has to be heated up to the electrolyser temperature, hence the molar enthalpy variation of the water flow is about 3770 kJ/kmol (1.9 % of the produced SNG energy).

2.4 Simulation algorithm of the AEC-based PtG plant model

The AEC-based PtG plant model, which was developed in this work, simulates the dynamic behaviour of a real AEC-based electrolyser coupled with a methanation unit. The simulation algorithm is illustrated in Figure 2-4 and has been developed in Matlab.

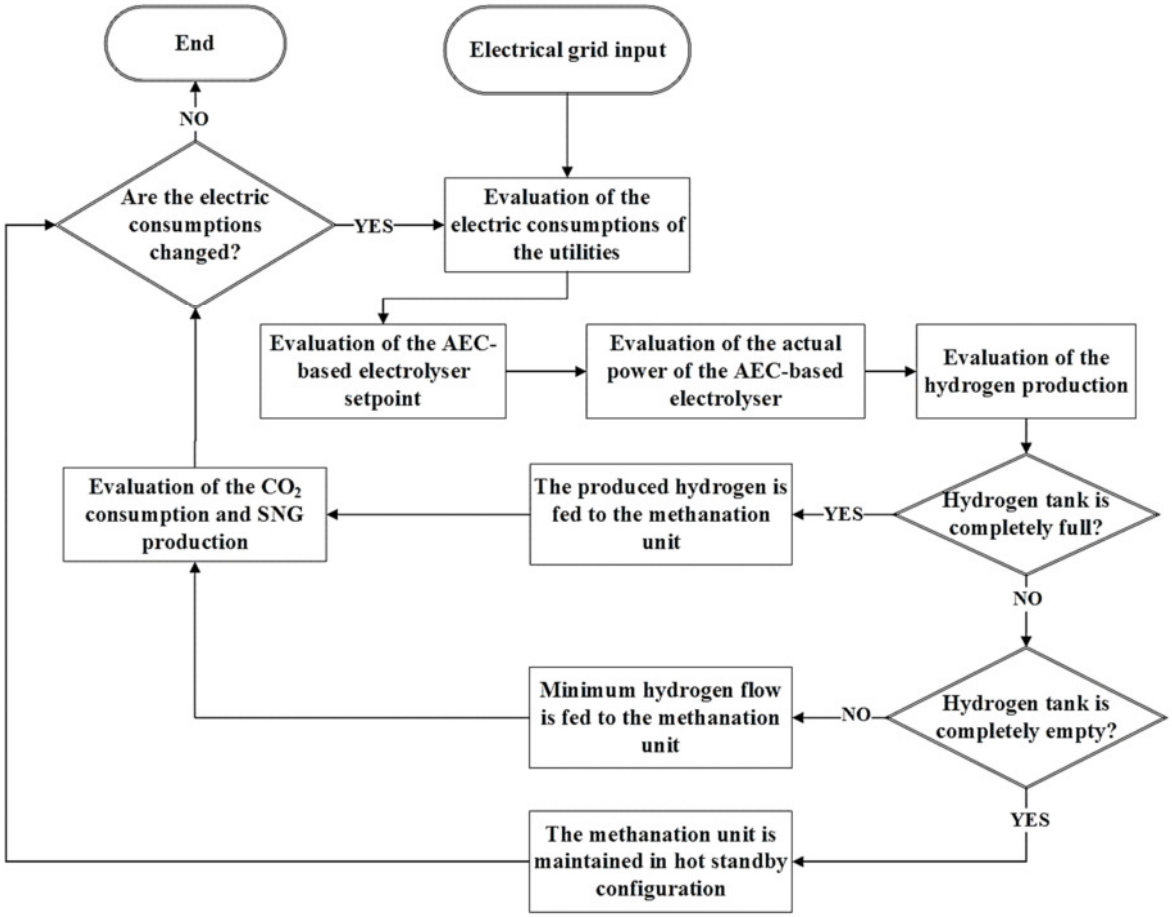

Figure 2-4: AEC-based P2G plant flowchart of the algorithm.

The simulation algorithm of Figure 2-4 consists of the following main instructions:

- **Setpoint** power of the AEC-based electrolyser: the setpoint is defined as the theoretical maximum operative power load at which the electrolyser may work. This maximum can correspond to either the power provided by the grid (when this power is lower than the nominal power of the electrolyser) or the nominal power of the electrolyser (in the case that the excess of power to be taken from the grid exceeds the nominal power of the electrolyser. Furthermore, also the consumption of the auxiliary services are taken into account. It is worth to note that the minimum power of the PtG plant is equal to 20% of the nominal power.

- **Actual power consumption of the AEC-based electrolyser**: the actual electric power consumption could be calculated using the dynamic model of the AEC-based electrolyser (first order system with delay, see equation (1)).

- **Hydrogen production**: the hydrogen flow could be evaluated taking into account the efficiency of the AEC-based electrolyser (see **Fehler! Verweisquelle konnte nicht gefunden werden.**).

- **Hydrogen tank**: the methanation unit is always fed with a minimum hydrogen flow (20% of the nominal power), if the electrolyser is operative. In addition, a certain amount of hydrogen could be sent to a hydrogen tank storage until the tank is completely full (the priority is filling the tank). This operation allows the methanation unit to be decoupled from the AEC-based electrolyser. The hydrogen produced by the AEC-based electrolyser is completely fed to the methanation unit, if the hydrogen tank is completely full. On the contrary, the stored hydrogen is fed to the methanation unit, if the electrolyser does not produce hydrogen, in order to produce continuously SNG. In this case, the methanation unit works at the minimum power load until the hydrogen tank is completely empty; then it could be turned off in standby conditions. A hot standby condition (it means that the equipment is maintained at the operative temperature conditions with auxiliary energy, in order to ensure a fast start up) was assumed for the main equipment (electrolyser and methanation unit).

- **Auxiliary consumptions**: all the consumptions of the auxiliary items of equipment are related to the amount of produced hydrogen. Firstly, the hydrogen could be compressed; secondly, the carbon dioxide has to be compressed; thirdly, the water has to be pumped and lastly it must be heated up to the AEC-based electrolyser.

- **Control of the setpoint**: the setpoint power of the electrolyser must be recalculated considering the new auxiliary consumptions, because the available electricity is comparable with the power absorbed by the electrolyser.

- **Methanation unit**: eventually, the amount of methane could be calculated using the CO_2 conversion, or alternatively, the hydrogen-to-SNG efficiency; thus, the SNG productivity could be estimated.

The summary of the assumption used for implementing the model is shown in Table 2-1.

Table 2-1: Parameters used for the PtG model

Parameter	Value
K	1
τ	11.73 [s]
α	14.62 [s]
$\eta_{power\text{-}to\text{-}H2}$	57.6 % (LHV basis)
$\eta_{power\text{-}to\text{-}SNG}$	83 % (LHV basis)
Conversion CO_2 in methanation unit	99 %
η_c	85 %
η_p	85 %
WC	75 %
P_{min}	$0.2P_n$
P_{max}	P_n

3 Description of the transmission networks and implementation for STORE&GO

The transmission system represents the backbone of the entire electricity system and traditionally has been the link between the generation units (usually located far from cities) and the load centres. For matter of clearness, the simplified schematic of the entire electricity system is shown in Figure 3-1 (the detailed description can be found in [17]).

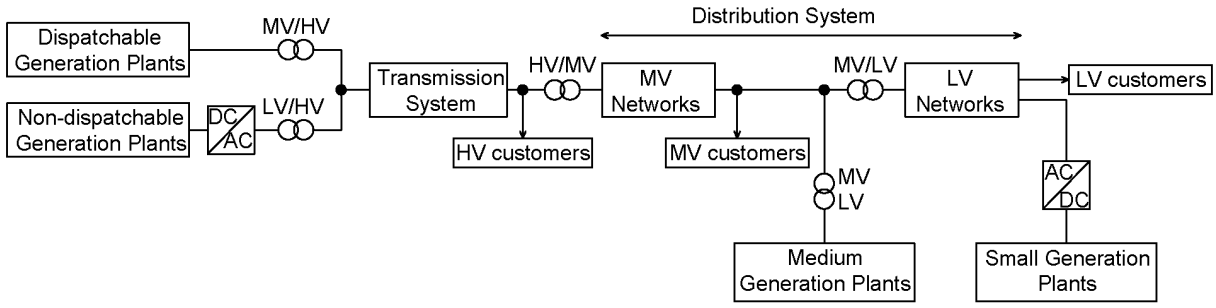

Figure 3-1: Representation of the electricity system

In Europe, the number of nodes is about 6000, and it is operated with different level of voltages, as reported in Table 3-1.

Table 3-1 Number of nodes composing the EU transmission system [18]

Voltage V_n [kV]	Number of Nodes
<220	327
220 ≤ V_n < 400	3683
400	2592
>400	19
Total number of nodes	6621

The detailed study of the integration of PtG into the transmission network needs the following features:

1. **Proper description of the transmission network**: this means the implementation of a realistic transmission system, in terms of physical parameters (e.g., resistance, reactance, length, line thermal limits and so on)
2. **Geographical coverage**: in the usual load flow analysis, the geographical coverage is not so much important. However, by handling with a new technology which aims to support the integration of RES in Europe, the geographical information is necessary
3. **Proper values of generation and loads**: the mix of generation and loads regarding the next decades (e.g., 2030 and 2040)
4. **Proof of concept**, for testing the algorithm

3.1 Existing models of the European transmission system

The most updated model of the European transmission system is the one related to the Ten Years Network Development Plan (TYNDP) 2016 [18], that is the so called “Stum Model”. Unfortunately, the model does not report any information regarding the geographical location of the different nodes, so cannot be used due to the lack of the point 2) of the above mentioned feature list.

A further source is [19], presented in the paper [20]: the model assumed a value of the transmission capacity linked to the voltage level of the line. However, the website does not report any information about the model itself.

Due to the aim of this Deliverable, the approach followed in the project STORE&GO was to merge different sources, for creating a simplified model of the European transmission system considering all the characteristics listed above. For this reason, three different databases were merged:

1) UCTE model of the European transmission network (internal source of POLITO), reporting the thermal limits of the lines (no information about neither the geographical coordination nor the types of generation)

2) Bialek model from PowerWorld® [21], reporting information about the types of generators installed (no information about neither the geographical coordination nor the thermal limits)

3) Geographical coordinates from the Bialek model stored in the repository [22] (no complete information about thermal limits)

The matching of the nodes among the three modesl was possible thanks to the partial information in all the models, for example the thermal limits of the transnational connection and the same node coding. This approach led to obtain the Network #T2, explained in Section 3.2.2.

Another source can be found in the Zenodo repository [23], and it was mentioned as source by [24]. This database has two drawbacks: it does not report the load for the nodes, and it has not any information about the transfer capacity. The first problem was solved in [24] by dividing the hourly load of all the EU countries based on the density of population at NUTS3 level. The same paper uses clustering technics for reducing the number of nodes by maintaining the main capacity corridor. However, the transmission limits (fully described in [18]) are not present in the repository [23], which thus cannot be used alone. Furthermore, the paper in any case is not considering the grid topology and the electrical distance among nodes, fundamental for properly studying the operation of the system.

On May 2018, a new and updated release of the model stored in the repository [23] was uploaded: this model can be found at the web-link [25] and in the repository [26]. The model has been validated in [27]: this model considers as thermal capacity the one obtained by considering, for every level of voltage, a defined type of conductor. The model allows as well to simplify the network, making an equivalent composed of 256 node.

Thanks to the presence of the code architecture, the input file has been also adapted for the network reported in [25], by creating the model #T3 reported in Section 3.2.3.

3.2 Description of the network models used

3.2.1 Description of the Network #T1

The first network used was the CIGRE European Configuration network [2]: the network is composed of 13 buses and all its elements are referred to the European network standards (e.g., voltage level types of lines and so on).

The representation of the network is shown in Figure 3-2-a. In the initial configuration, no RES power plants were installed. However, the taskforce has found as possible node for installation of a wind farm the bus 12, obtaining the configuration shown in Figure 3-2-b: as it is possible to see, an additional line has been added, as well as new reactors (for reactive power control).

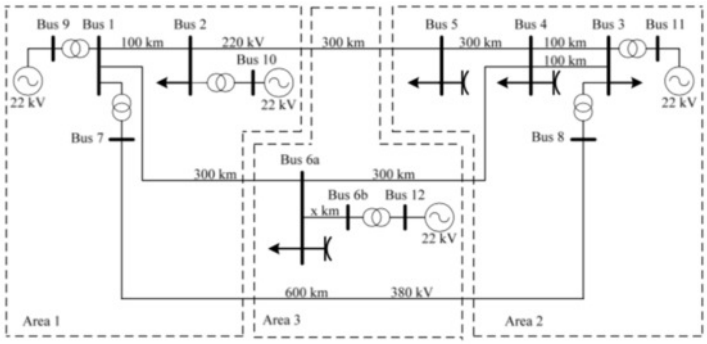

(a) Version without RES plants

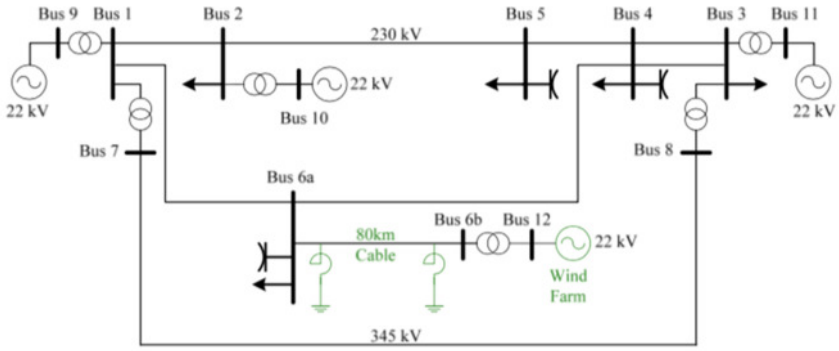

(b) Version with wind power plant

Figure 3-2: CIGRE HV Transmission Network: European configuration

The aim of this network was to clarify all the elements necessary for making possible a complete analysis of the transmission network by considering both RES and PtG. Furthermore, managing a smaller network helped to create a proper input file, which can be easily scaled up with larger network. An example of the calculation carried out by using this network is reported in Section 4.1. The analysis of the network has been made through the script detailed in Appendix D: Description of the script for the transmission network case studies.
After the initial calculations and tests, this network has not been longer used anymore, due to the lack of the geographical information about the nodes and the limited potential studies which were possible to do with it, by leaving the room to more meaningful networks, as the network #T2 and #T3 (presented in Section 3.2.2 and Section 3.2.3, respectively).

3.2.2 Description of the Network #T2

The Network #T2 aims to be representative of the entire European transmission system. The network is based on data provided Union for the Coordination of the Transmission of Electricity (UCTE) [3], which was the former name of the current European Network of Transmission System Operators for Electricity (ENTSO-E) [4]. This model is the simplified version of the European transmission network[1]. The information regarding the network are summarised in Table 3-2.

[1] The evolution of this model led to the Bialek model ([21]), whose current version does not provide any information regarding the thermal limits of the network.

Table 3-2 Information about the Network #T2

Buses	Branches	Generators	Load [GW]
1254	1944	378	~250

This model covers mostly of the continental Europe, and is representative of the following 17 European countries: Austria (AT), Belgium (BE), Croatia (HR), Czech Republic (CZ), Denmark (DK), France (FR), Germany (GE), Hungary (HU), Italy (IT), Luxemburg (LU), Netherlands (NL), Poland (PL), Portugal (PT), Slovakia (SK), Slovenia (SI), Spain (SP) and Switzerland (CH). The graphical representation of the geographical distribution of the model is depicted in Figure 3-3. The values of loads and their variation with the time have been updated on the basis of the data provided by [28], for the countries considered. The analysis of the network has been made through the script detailed in Appendix D: Description of the script for the transmission network case studies.

Figure 3-3: Representation of the model implemented [21]

3.2.3 Description of the Network #T3

The network #T3 is composed of 256 nodes [27]: it has been created by applying a *k-means* clustering technique at the European Network (over 6000 nodes) which was obtained by analysing the European Network Map [29]: this simplified network is fully composed of a 380kV equivalent network, connecting the different nodes, which fall in their own cluster. The capacity among the clusters depend on the connection existing among them: due to the fact that the model considers also lower voltage levels (220 kV and 300 kV), the equivalent capacities consider also those connections. Due to the absence of information regarding the real lines composing the original network, a simplification has been carried out, i.e., defined lines geometries have been considered, as shown in Table 3-3 [30].

Table 3-3: Properties transmission lines

Voltage [kV]	Current limit [A]	Power limit [MVA]
220	1290	492
300	1935	1005
380	2580	1698

The resulting network's summary is presented in Table 3-4, whereas the representation of the model georeferenced is shown in **Fehler! Verweisquelle konnte nicht gefunden werden.**.

Table 3-4: Network #T3 data summary

Buses	Branches	DC lines	Generators	Load [GW]
257	460	24	828	~360

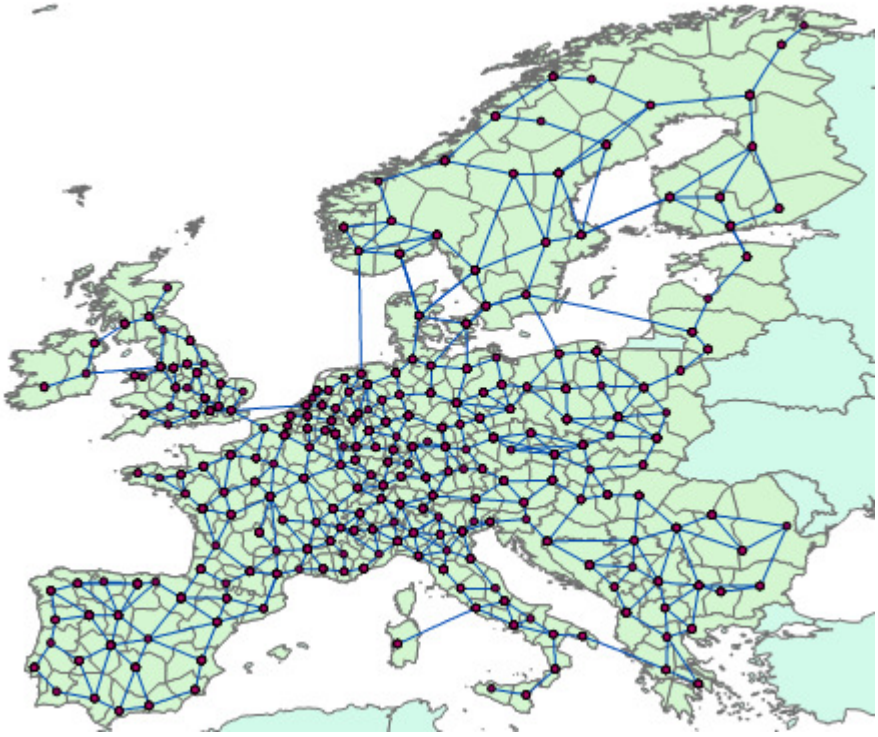

Figure 3-4: Representation of the network #T3

The network covers all the ENTSOE countries: Albania (AL), Austria (AT), Bosnia and Herzegovina (BA), Belgium (BE), Bulgaria (BG), Estonia (EE), Finland (FI), Croatia (HR), Czech Republic (CZ), Denmark (DK), France (FR), Germany (GE), Great Britain (GB), Greece (GR), Hungary (HU), Ireland (IE), Italy (IT), Latvia (LV), Lithuania (LT), Luxemburg (LU), Montenegro (ME), The former Yugoslav Republic of Macedonia (MK), Netherlands (NL), Norway (NO), Poland (PL), Portugal (PT), Romania (RO), Serbia (RS), Slovakia (SK), Slovenia (SI), Spain (SP), Sweden (SE) and Switzerland (CH)

The load profile in the original dataset referred to the year 2013: the share of load for every cluster has been obtained by considering a combination between the population and Gross Domestic Product (GDP) of each cluster.

The generation in the original dataset referred to the year 2013: at every node of the network more than one type of generator is connected. The types of generators considered in the model have been adapted ato the types of generators requested by the script created in the STORE&GO project explained in Appendix D: Description of the script for the transmission network case studies. The model considers also the presence of DC links existing in Europe, considered as part of the model.

Both generation and loads have been updated according to current and future scenarios, as shown in Sections 3.5, 3.6 and 3.7.

3.3 PV production for the European case

The variance of PV production within space and time brings the need to adequately represent PV production in our study case. This is the reason why a proper network model including georeferenced bus data was needed. This information allows to reach a good level of fidelity for both the installed capacity and the generation profile for each bus.

The installed PV capacity data has been gathered from the EMHIRES dataset [31], provided by the Strategic Energy Technologies Information System (SETIS). The EMHIRES dataset provide information about PV installed capacity at country level, by bidding zone, at NUTS 1 level and at NUTS 2 level. By assigning each bus to the corresponding NUTS 2 region it is possible to reach the highest level of spatial resolution available with this dataset.

The EMHIRES dataset also provides 30 years of hourly production levels, for each one of the previous spatial resolutions. However, this information is only enough for hourly analyses, so another source is needed in order to study the network at a higher temporal resolution. This has been achieved by using Bright's solar model [32]: this model, at given points coordinates, simulates a yearly irradiance profile with a temporal resolution of one minute that can be averaged according to the user's need.

PV profiles for each bus are then calculated from the irradiance profiles and the given installed PV capacity. Thanks to the formulation reported in Appendix A: Calculation of the AC power for PV fields, the power profiles are calculated [33].

3.4 Wind production for the European case

Wind generation has the property to be less distributed than PV generation. Since the EMHIRES dataset provides for the wind generation the same information as given for the PV generation, this source has also been used for characterising the wind in Europe.

As for the PV, another source is needed in order to reach a higher temporal resolution. Differently from the irradiance, wind speed cannot be assumed easily, since it highly depends from seasonality, turbine height and ground conformation. Moreover, each turbine model has its unique power characteristic. No reliable data with high spatial and temporal resolution have been found, so a different approach has been introduced.

Since capacities and hourly profiles were available from the EMHIRES dataset, the missing information was wind variability. By analysing a year worth of data from a real wind farm, a per unit profile has been extracted, with a temporal resolution of ten minutes. The wind variance has been characterized statistically through clusterization in order to elaborate a realistic synthetic wind profile. This way, the variability information from the real wind farm allowed to emulate the actual wind effect.

The clusterization method followed these steps:

- Description of the average wind production (taken from [31]) in discrete classes, indicating the production in pu with respect to the installed wind capacity.
- Calculation of the average hourly power production of the real wind farm, for all the months. This average production has been described in discrete classes (as made at the previous point for the data taken from [31]).
- Calculation of the difference between the actual values (measured every 10 minutes) of the real wind profiles and the average hourly value. By doing this, it is possible to obtain a

"variability profile" along all the year. This variability profile is labelled according to average hourly production classes. The result is a population of variability profiles corresponding to a defined hour and a defined month.

- A clustering of these populations of variance is applied (in our case ten clusters for each population), using a *k-mean* algorithm [34]. The result is for each population ten typical variance profiles, and their probabilities of occurrence.

- For each bus and for each hourly average value an extraction from the relative variability clusters is performed, for assigning a proper variability to the hourly production.

Validation for the method was needed, and it has been performed by analysing the autocorrelation of:

- the real data

- the real data averages added to the variance calculated via the described method

- the real data averages added to the variance values (not entire profiles) extracted randomly from the populations.

The autocorrelation results are presented in Figure 3-5, and show the effectiveness of the approach. The autocorrelation calculation shows clearly that the methodology introduced allows to obtain synthetic profiles closer to the real data than by simply using a random approach. This can be observed both at low lag values and at the value of the negative peak. Figure 3-6 shows an example of the profiles used in the autocorrelation test.

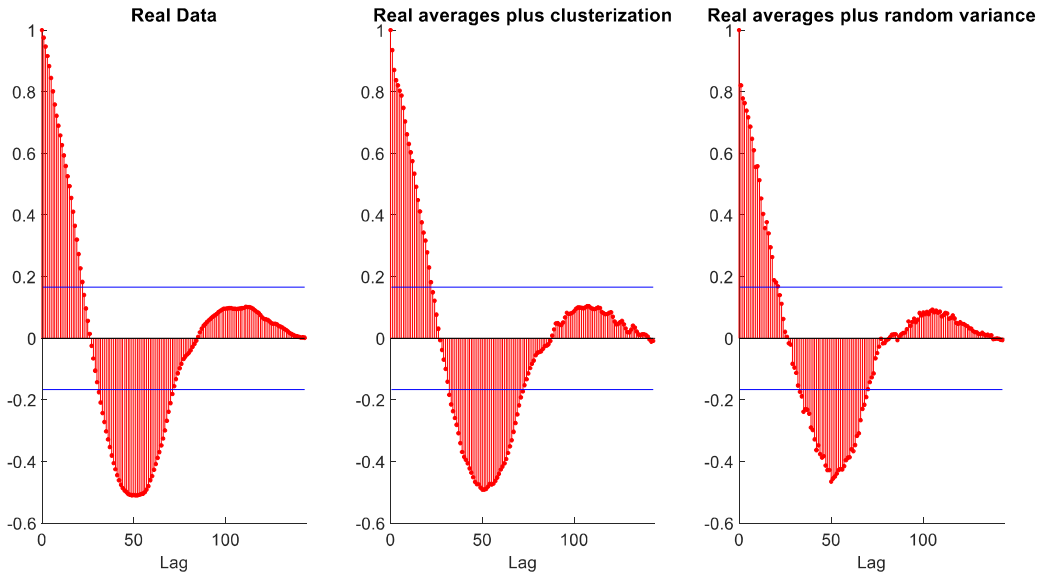

Figure 3-5: Wind profiles autocorrelation figures

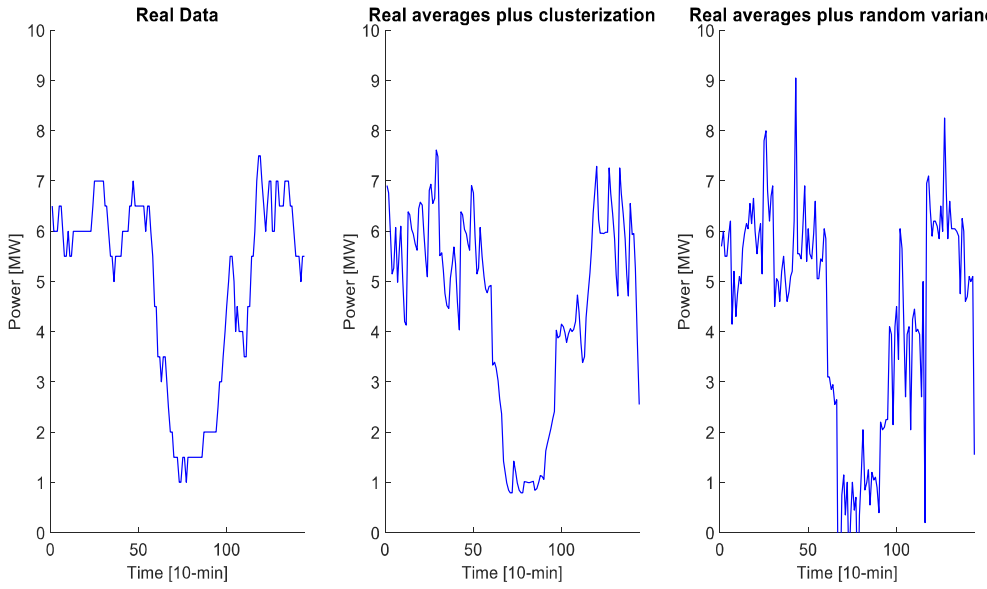

Figure 3-6: Wind profiles used in the autocorrelation test

3.5 Load profiles for the European case

The values of loads and their variation with time have been updated on the basis of the 2017 data provided by [28], for the countries considered. The power statistics offers yearly historical data for power consumption, provided with a temporal resolution of one hour, and country level as spatial resolution. The country-level load has been distributed within the buses of the same country by the nominal load of each bus, provided within the different network data.

3.6 Generation scenario for the European case

As for the load profiles, generation capacity of each network has been updated to match [35] 2017 data. The number of generators and their position has been kept the same as in network data, and then within each country, for each generator type, the capacity has been scaled up. Minimum stable power output, and ramp rate values have been considered for each type of generator. The data has been collected from [18]. Note that the ramp rate value for hydro generators is not the maximum technical possible, but a value for ordinary operation has been considered, since the model does not aim to recreate emergency situations.

3.7 Future scenarios for the European case

Beyond the most recent historical data, various scenarios can be used in the model. The selection of the scenario implies the choice of the desired load profile and scaled up baseline generation, based on the data obtained by [5]. The forecasts are part of the ENTSO-E TYNDP [18][36], which provides a detailed overview of possible European energy futures up to 2040.

In particular the scripts are able to handle the following baseline scenarios:

- **2025_BE Best Estimate**: it represents a medium-term scenario which is on track to meet the decarbonization targets set in place by EU for 2030. It is based on TSO perspective and on following all national and European current regulations.

- **2030_DG Distributed Generation**: it represents a prosumer-centric development, in which the end user technologies will be the focus. A high PV, batteries, and electric vehicles penetration is considered, and the use of smart home devices and dual fuel appliances, which can allow prosumers to switch energy following market conditions, is a reality.

- **2030_EUCO European Council**: using the EU reference Scenario 2016 as a base, it models the achievement of the 2030 climate and energy targets agreed by the European Council in 2014. Since its similarities, this scenario replaced the 2030_GCA within the TYNDP framework

- **2030_ST Sustainable Transition**: it summarizes a quick, yet sustainable, CO_2 reduction by replacing coal and lignite power plants with gas ones. Oil use in heavy transport is also displaced by gas. This particular focus causes a slower electrification of heat and transports, but allows to reach the EU goal of 80-95% CO_2 reduction in 2050.

- **2040_DG Distributed Generation**: see 2030_DG.

- **2040_GCA Global Climate Action**: opposed to ST scenarios, full speed decarbonization is the global objective, achieved by large-scale renewables and nuclear power plants deployment. Electrification of residential and commercial heat leads to an important decrease of gas demand in this sector, and electrification is applied also to transports. The research for better energy efficiency is applied to all the sectors, and PtG production reaches the biggest development in comparison to the other scenarios.

- **2040_ST Sustainable Transition**: see 2040_ST.

Every scenario offers the possibility to choose between three load time-series, built to represent three different climatic conditions, i.e.:

- 1982 for dry conditions

- 1984 for normal conditions

- 2007 for wet conditions

A summary of the scenarios is presented in Figure 3-7 [36]. For more information about these scenarios, please refer to [5].

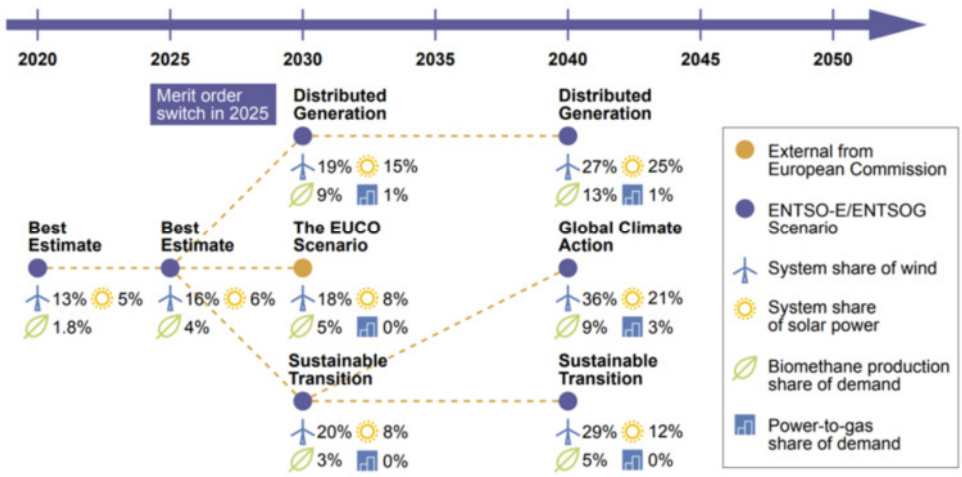

Figure 3-7: The scenario building framework for TYNDP 2018. RES share of demand for electricity and gas [36].

3.8 Power Flow and Optimal Power Flow

The resolution of problems involving the electricity network needs the calculation of the status of the network starting from an operational point. In particular, by starting from a condition characterized by a certain amount of load (composed by active and reactive power) and from the network parameters, it is possible to calculate the current flowing in the branches and the voltage at every node. All these aspects are complicated by the structure of the transmission network, which is meshed for allowing enough connection redundancy for guaranteeing the security of the system.

3.8.1 Nodes categorisation

In the network resolution, the nodes of the network can be divided in three categories:

- *PQ*: they traditionally represented the passive load of the network. The two letters “P” and “Q” indicate that the node is defined through an active power value (“P”) and reactive power value (“Q”). Today, this kind of representation is also used for generation nodes which are not acting voltage regulation (such as non-dispatchable generators producing only active power P, without any injection of reactive power Q)

- *PV*: these nodes are representative of the traditional generators. They are defined through a power injected P and the nodal voltage V. They are characterised by a “capability curve”, which delimitates the possible combined production of active and reactive power

- *Slack bus*: this is also called swing bus. It represents the reference node in the network calculation. Furthermore, it allows to cover all those quantities (such as the network losses) which are unknown at the beginning of the process, and are only known at the end of the iterative calculation

3.8.2 Power flow resolution methods: AC power flow vs DC power flow

The resolution of the network is based on the use of iterative methods, which can be solved by both active and reactive dispatching (i.e., AC-power flow methods) or only by active power dispatching (i.e., Decouple power, also called DC-power flow). The choice to use either the AC methods or the DC power flow depends on the type of network under analysis, the constraint in terms of time for making the calculation, and on the available information of network’s parameters.

The most used AC power flow methods are the so-called Newton-Raphson and Gauss-Siedel methods [37]. However, the solution of a large-scale network can be efficiently made by applying the decoupled power flow methods, which provide an approximate result of the load flow calculation. The principles which drive towards the use of this simplified method are the presence, in the transmission network, of two well defined “control channels”, which are the “active control channel” and the “reactive control channel”. The active control channel refers to the control of the “active power”, which in the transmission system is mainly based on the voltage angle values, whereas the reactive control channel refers to the reactive power control, mainly depending on the amplitude of the nodal voltages. These two channels are so “well defined” in the transmission network thanks to the low resistance value of the electrical conductor. This kind of considerations led to simplify the mathematical formulation of the Newton-Raphson methods, by making possible to have results good enough in less time [37]. In the case study considered in this report, the DC power flow has been used: the calculation software has been based on a Matlab® script, recalling the function developed by in the package Matpower [38].

3.8.3 Optimal power flow: description of the problem and resolution methods

A main role of PtG is to produce SNG by exploiting the excess of electricity produced by RES, and the installation of a number of PtG plants can help to stabilise the network. In this framework, the

PtG plants operate as *balancing elements*, by making possible the long term storage of the excess of electricity produced by RES.

In this Deliverable, the integration of PtG into the electricity system passes through an intraday Optimal Power Flow (OPF) based on the results of day-ahead OPF. The OPF consists of minimizing the total cost $f(\mathbf{x})$ of the electricity system through on an optimization problem.

The two above mentioned OPF aim to find the set of generators allowing the operation of the system at minimum generation cost. In particular, the first OPF dispatches the expected value of RES and the traditional generation through an economic merit order, whereas the second one aims to redispatch the traditional generators and the PtG for facing the unbalances caused by the variable nature of the RES. These two OPF aim to represent the day-ahead market and a (quasi) real-time market, on which PtG can operate for providing its services to the network. The script developed uses as coding environment Matlab®, and recall the function developing the OPF developed in Matpower [38].

A short overview of the concept of day-ahead market (DAM) and the real-time intra-day market (IDM) is presented in Appendix B: Day-ahead market and Intraday market, whereas few details regarding the OPF formulation can be found in Appendix C: OPF formulation.

4 Results for the cases #T1, #T2 and #T3

4.1 Network #T1

The network #T1 has been analysed by means of the script presented in Appendix D: Description of the script for the transmission network case studies, which is essentially based on a power flow algorithm. This implies that the largest generator is considered as the slack bus, and thus any excessive load variation (which cannot be faced properly by any of the generators connected to the network) can be solved by it.

The case studied considered a wind power plant connected to the node 12 and a PtG plant (in which only the dynamic characteristics of the electrolyser were considered) in node 6b, as suggested in [2]. Node 6b is in fact referred as a suitable location for studying the effect of the incorporation of large-scale renewable energy sources such as wind energy conversion systems in node 12.

The loads and the generators of the model are shown in Table 4-1 and Table 4-2, respectively[2]. By applying a combination of load profiles, the maximum peak power of the network was 8.65 pu.

Table 4-1: Load of the case study

Node	P [pu]	Q [pu]
2	2.85	2.00
3	3.25	2.44
4	3.26	2.44
5	1.03	0.62
6a	4.35	2.96
6b (PtG)	0.5	0

Table 4-2: Generators of the case study

Node	S_{rated} [pu]	P_{out} [pu]
1	7.00	5.00
2	5.00	2.00
3	5.00	3.00
12 (wind)	3.92	3.92
9 (slack)	-	-

The ramp rate chosen is equal to 0.1 pu/min, and the minimum power at which the plant can work is 20% of its nominal power.

A real wind farm per unit profile has been assigned to the wind generator, and it has been scaled up in order to match a certain percentage of the daily energy consumed by the loads. In our tests two percentages have been used, i.e., 10% and 20% of the total load energy.

The results of this simplified case study are reported in Figure 4-1 and Figure 4-2, which represent the imbalance of power that the slack cannot provide, at each minute: it is evident that the installation

[2] The values expressed in per unit (pu) are referred to S_b=100 MVA

of a relatively small PtG plant is able to help the stabilisation of the network, by reducing the variation of power that the slack has to face. Improvements can be seen as both reductions of the peaks of imbalance and removal of the minor fluctuations. Figure 4-3 shows the absorption profile of the PtG unit. Results are also reassumed in Table 4-3.

These results showed the goodness of the approach, which has been further developed for the networks #T2 and #T3.

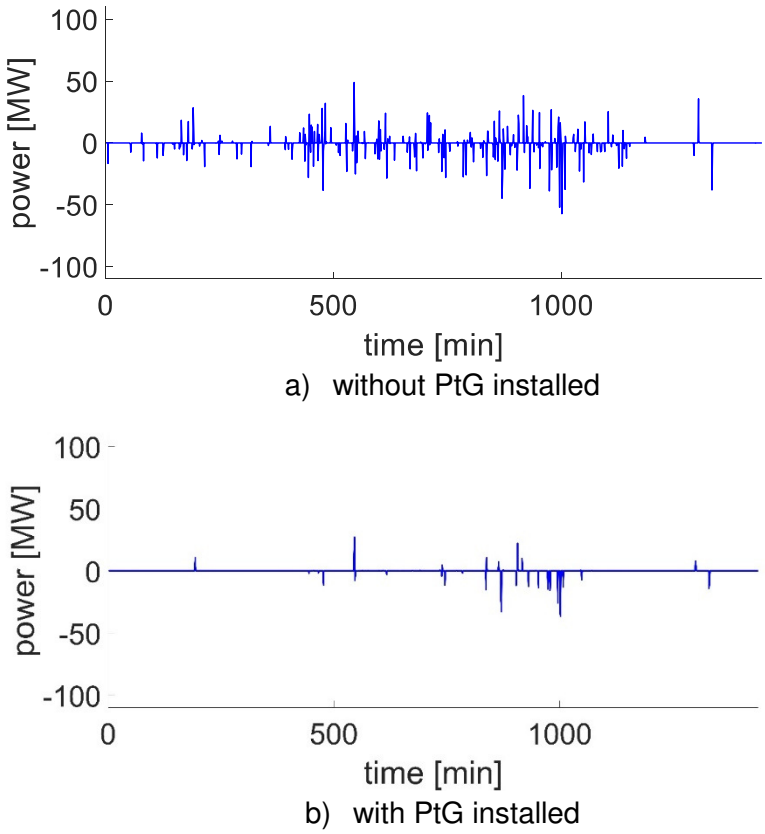

Figure 4-1: Power imbalance at slack bus, network #T1, 10% energy case

Table 4-3: Results for network #T1

Wind energy penetration	PtG status	Slack imbalance				
		Duration [min]	Difference [%]	Peak [MW]	Difference [%]	Average [MW]
10%	Off	246	-76.4%	57.1	-35.5%	11.1
	On	58		36.8		8.0
20%	Off	687	-37.8%	119.0	-8.8%	25.2
	On	427		108.5		22.1

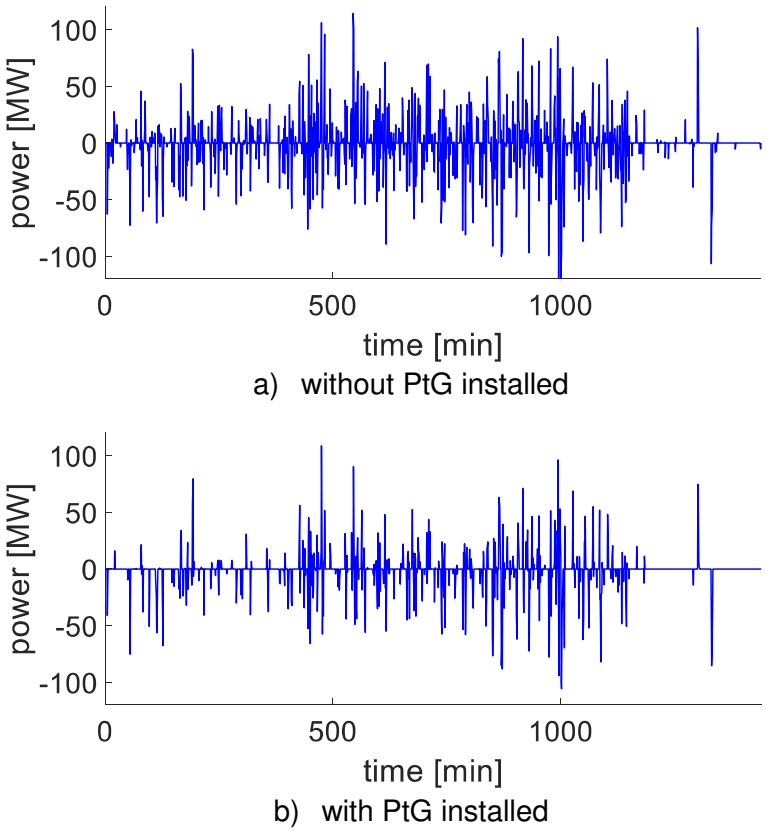

Figure 4-2: Power imbalance at slack bus, network #T1, 20% energy case

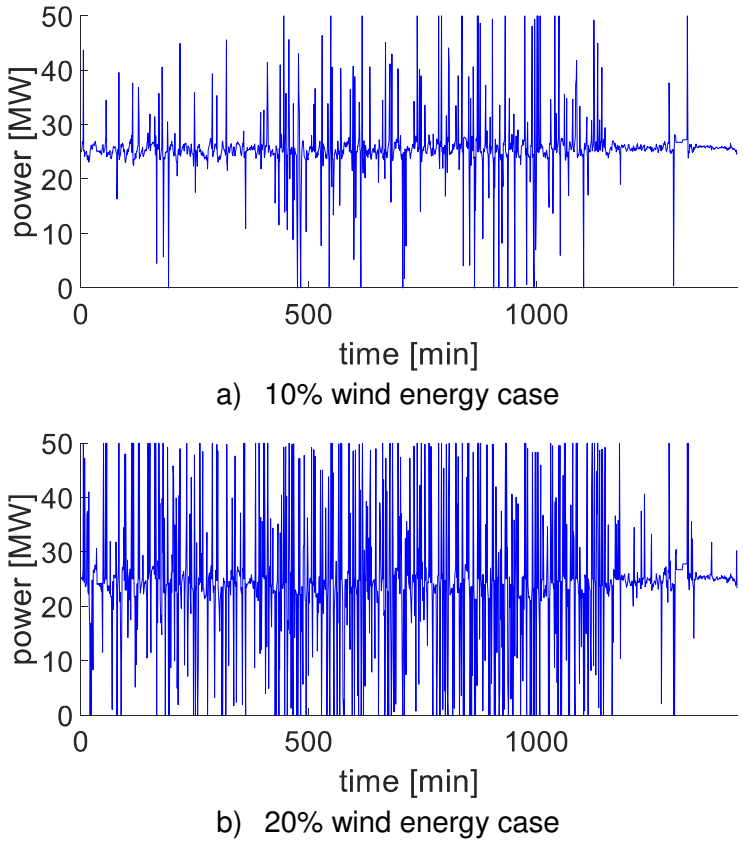

Figure 4-3: PtG power consumption in network #T1

4.2 Network #T2

The results shown for the network #T2 refer to two working days of the year, in January and July. The rationale behind this choice was to show two completely different types of seasonality, both for loads and RES production. In January the load reaches its peak of the year, while in July it is lower. RES production is different both for wind and PV, given the characteristics of winter and summer. The loads used are based on the European load values of 2017 and the capacity of the generators installed in the network has been updated to approximate the capacity of the same year. Table 4-4 shows RES capacity for the various countries.

Table 4-4: Generation capacity in Network #T2, 2017 scenario

Country	Conventional [MW]	Solar [MW]	Wind [MW]	RES penetration [%]
AT	22135	1031	2730	17.0
BE	15392	3380	2807	40.2
CH	21333	1664	75	8.2
CZ	18497	2040	308	12.7
DE	111449	42020	55072	87.1
DK	9671	907	5497	66.2
ES	75247	6970	23066	39.9
FR	109135	7646	13539	19.4
HR	4191	51	537	14.0
HU	8152	94	323	5.1
IT	103540	19662	9778	28.4
LU	1876	121	120	12.8
NL	21916	38	3641	16.8
PL	32395	186	5697	18.2
PT	14219	489	5090	39.2
SI	3534	270	3.3	7.7
SK	7301	530	3	7.3

Figure 4-4 shows with red line the RES power production imbalance between the forecasted value in day-ahead and the actual value that happens in intra-day, calculated as a sum for all RES plants of the network: this unbalance has to be solved by involving the traditional generators, that should adapt their production for maintaining the system in operation. The same figure shows in dashed blue the effect of 7.2 GW of PtG working in different network nodes[3]. The redistribution of the power among the different PtG plants has been based on size criterion: this means that, after the calculation of the unbalance of the network, the setpoints of every PtG plant have been fixed according to its size. In this particular example, the sizes of all the PtG plants have been fixed to 400 MW. The model of the PtG plant is the one shown in Section 2.

[3] It is worth to note that the siting and sizing of the PtG in the European transmission system, in these case studies, has not been optimized and it will be proper investigated in the deliverable D6.6 “Report on the impacts of the PtG on selected scenarios”. In this paper, PtG plants have been placed in correspondence with the biggest RES plants.

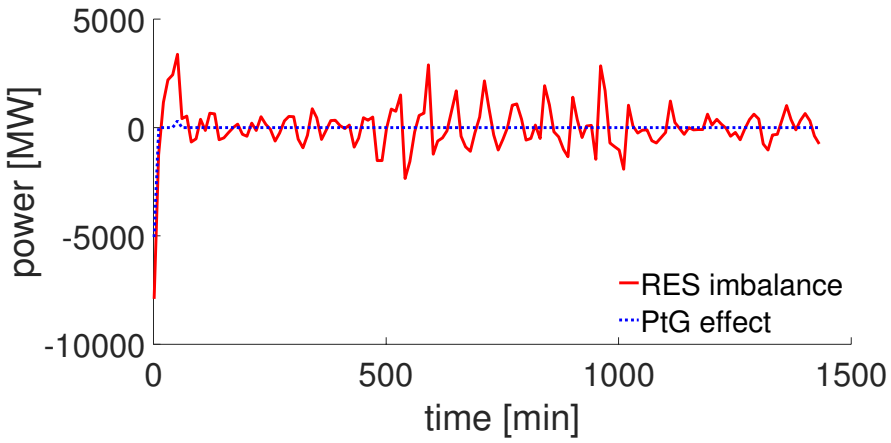

Figure 4-4: Total network RES imbalance before and after the PtG installation (10th January)

Since PtG plant setpoint is imposed by their size, and their size is the same, the responses of the PtG plants are also the same. An example of these responses is shown in Figure 4-5: the model follows in very good way the setpoint imposed. A detail of the response can be seen in Figure 4-6.

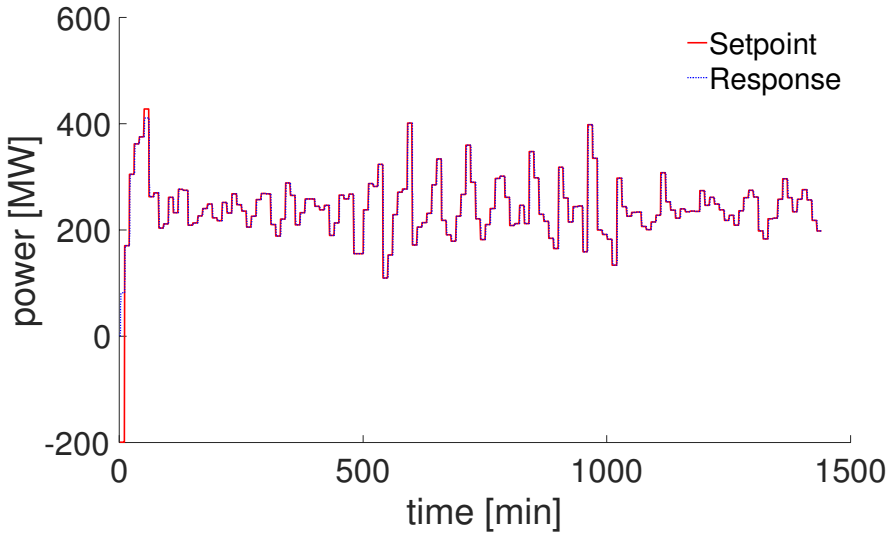

Figure 4-5: Setpoint and response of 400-MW PtG plant (10th January)

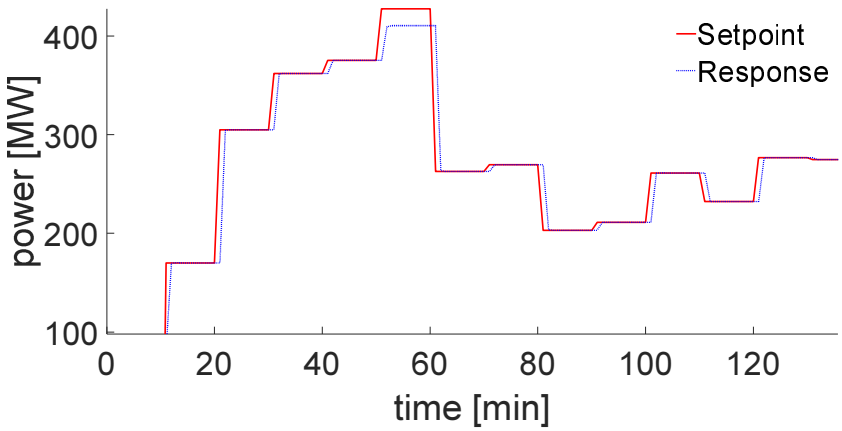

Figure 4-6: Detail of the setpoint and response of 400-MW PtG plant (10th January)

The same results related to July are shown in Figure 4-7 and Figure 4-8: it is evident that there is more variability to be faced in presence of the sunrise and sunset, where the power produced by the sun is increasing/decreasing in monotonic way.

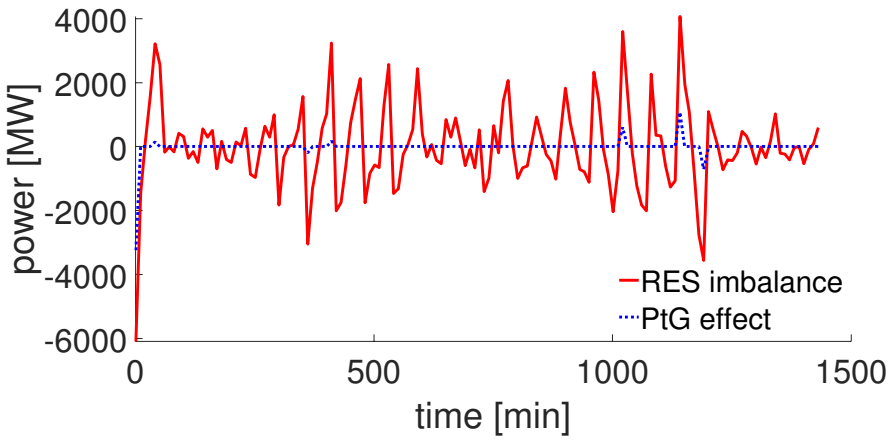

Figure 4-7: Total network RES imbalance before and after the PtG installation (3rd July)

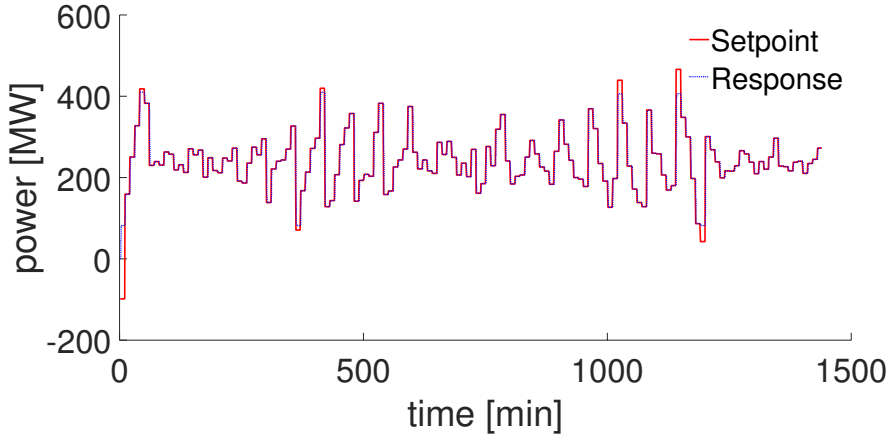

Figure 4-8: Setpoint and response of 400-MW PtG plant (3rd July)

For the two days considered, the beneficial effect of the installation of the PtG is shown in Table 4-5: the presence of PtG limits both the duration and the peak of the imbalance, helping the operation of the transmission network

Table 4-5: Performance of PtG in the network #T2

Scenario	PtG status	RES imbalance			
		Duration [min]	Difference [%]	Peak [MW]	Difference [%]
Network #T2 January	Off	1410	-98.6%	7910	-36%
	On	20		5060	
Network #T2 July	Off	1410	-95%	6094	-47%
	On	70		3244	

4.3 Network #T3

The results shown for the network #T3 also refer to two days of the year, in January and July, for the same rationale as explained in Section 4.2. The capacity of the generators installed is based on 2013 data (the original ones of the network, shown in Table 4-6) and then updated to 2017 through scenario selection. The loads values are based on 2017 data.

Table 4-6 Generation capacity in Network #T3, 2013 scenario

Country	Conventional [MW]	Solar [MW]	Wind [MW]	RES penetration [%]
AL	-	-	-	-
AT	19648	1981	404	12.1
BA	-	-	-	-
BE	12690	2172	3068	41.3
BG	5894	701	1041	29.6
CH	22141	60	756	3.7
CZ	7055	277	2067	33.2
DE	100594	43429	38411	81.4
DK	5635	5082	781	104.0
EE	2339	301	6	13.1
ES	58005	23003	6967	51.7
FI	12597	1082	11	8.7
FR	99117	10312	6192	16.7
GB	66505	13563	9000	33.9
GR	10936	1775	2444	38.6
HR	3002	384	44	14.3
HU	5269	328	29	6.8
IE	6132	2400	1	39.2
IT	74374	8750	19100	37.4
LT	1531	290	69	23.4
LU	1644	60	116	10.7
LV	2275	70	2	3.2
ME	-	-	-	-
MK	-	-	-	-
NL	21333	3641	1429	23.8
NO	30470	860	14	2.9
PL	33747	5186	87	15.6
PT	13117	4826	429	40.1
RO	12313	2923	1249	33.9
RS	-	-	-	-
SE	25074	3029	263	13.1
SI	2985	3	532	17.9
SK	6227	3	104	1.7

Figure 4-9 shows the total RES variability from the forecasts of the day-ahead OPF to the actual values in intra-day OPF: this unbalance is representative of the whole network, and has to be solved by involving the traditional generators that should adapt their production for maintaining the system

in operation. The same figure shows in dashed blue the effect of 10 GW of PtG, working in different network nodes[4], on the imbalance of power of the whole network. The redistribution of the power among the different PtG plants has been based on size criterion. In this particular example, the sizes of the PtG plants has been fixed 1 GW. The model of the PtG plant is the one shown in Section 2.

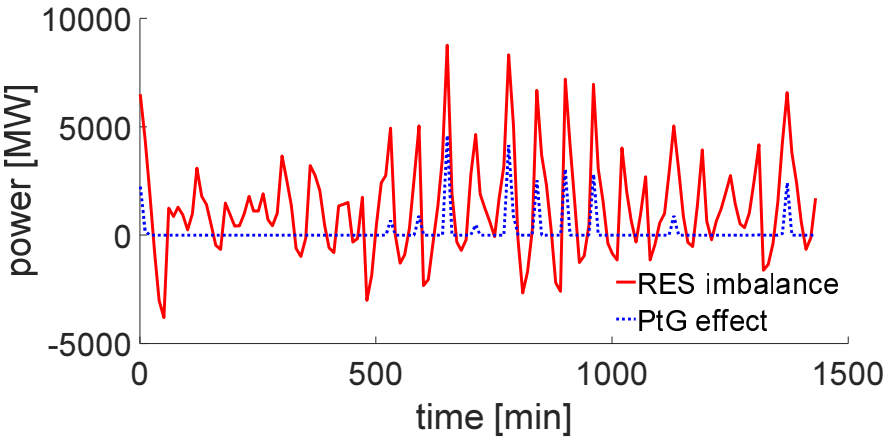

Figure 4-9: RES imbalance before and after the PtG installation (10th January, 2017 scenario), network #T3

Since PtG plants setpoint is imposed by their size, and their size is the same, the responses of the PtG plants are the same. An example of these responses is shown in Figure 4-10: the model follows in very good way the setpoint imposed. A detail of the response can be seen in Figure 4-11.

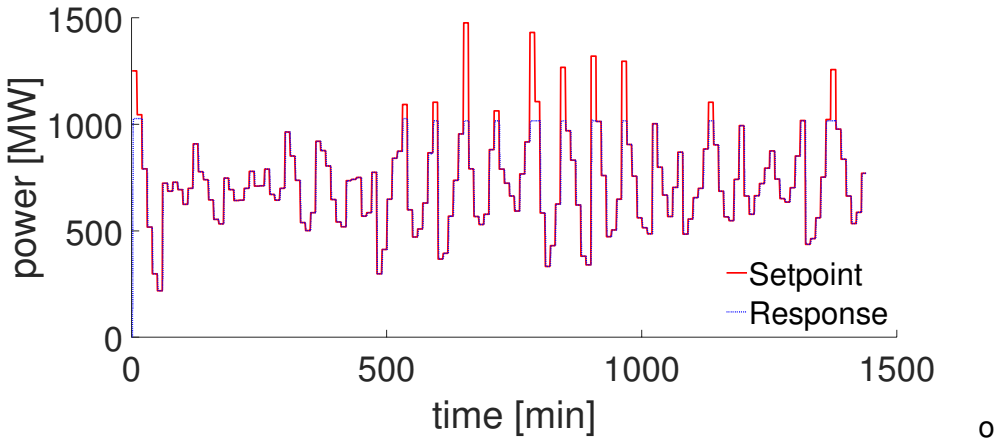

o

Figure 4-10: Setpoint and response of 1-GW PtG plant (10th January, 2017 scenario), network #T3

[4] It is worth to note that the siting and sizing of the PtG in the European transmission system, in these case studies, has not been optimized and it will be proper investigate in the deliverable D6.6 “Report on the impacts of the PtG on selected scenarios”. In this paper, PtG plants has been placed in correspondence of the biggest RES plants.

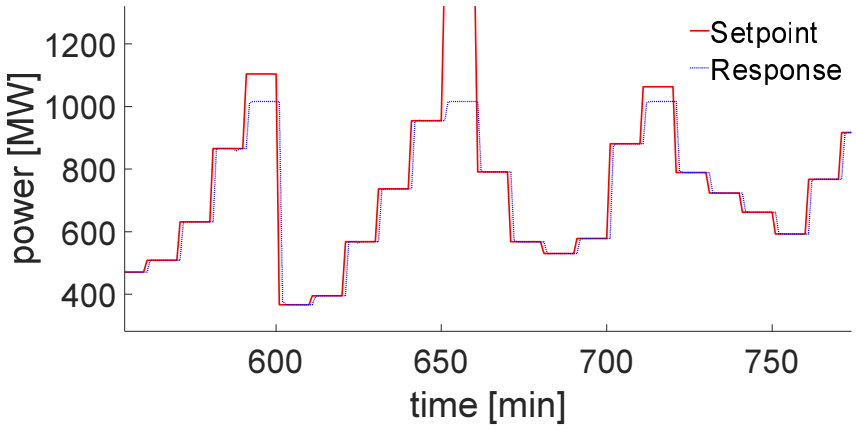

Figure 4-11: Detail of RES imbalance before and after PtG installation (10th January, 2017 scenario), network #T3

The same results related to July are shown in Figure 4-12, Figure 4-13, and Figure 4-8: it is evident that there is more variability to be faced in presence of the sunrise and sunset, where the power produced by the sun is increasing/decreasing in a monotonic way.

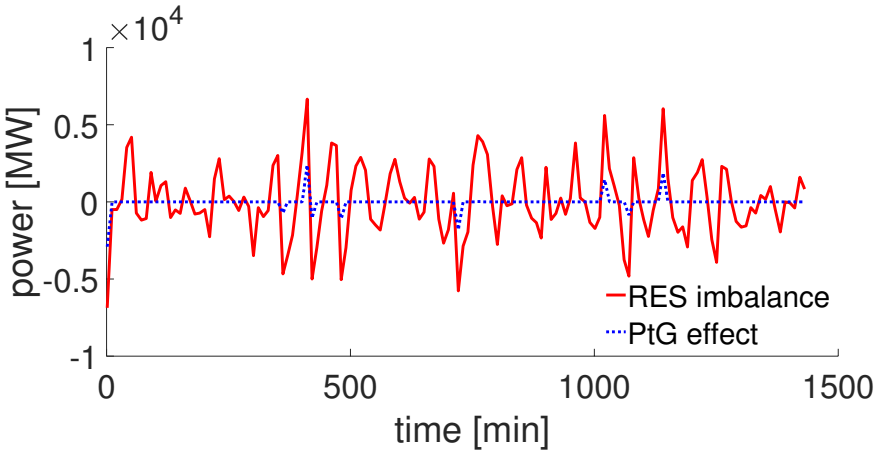

Figure 4-12: RES imbalance before and after the PtG installation (3rd July, 2017 scenario), network #T3

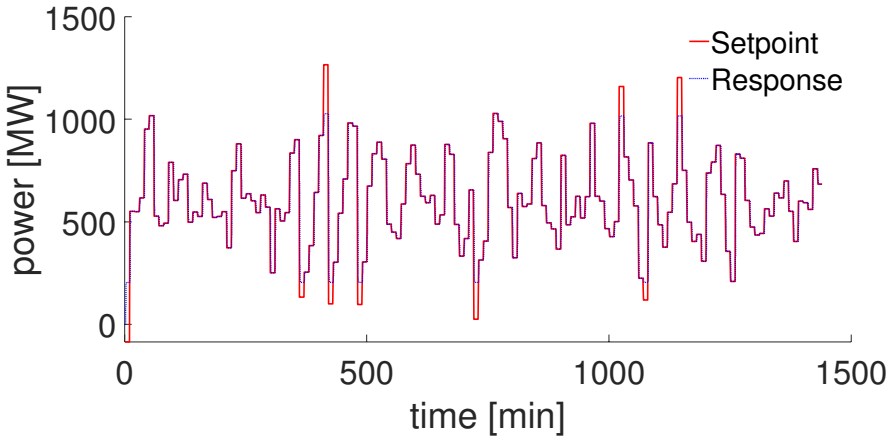

Figure 4-13: Setpoint and response of 1-GW PtG plant (3rd July, 2017 scenario), network #T3

The PtG effects for the two days of 2017 scenario are shown in Table 4-7: the presence of PtG, also in this case, limits both the duration and the peak of the imbalance, helping the operation of the transmission network.

Table 4-7: Performance of PtG in 2017 scenario, network #T3

Scenario		PtG status	RES imbalance			
			Duration [min]	Difference [%]	Peak [MW]	Difference [%]
Network January	#T3	Off	1440	-90%	8758	-47%
		On	150		4600	
Network July	#T3	Off	1440	-93%	8091	-53%
		On	100		3827	

Results for 2030 DG and 2040 GCA scenarios are also provided to show scenario selection functionality. PtG installed capacity and placement has not been altered from 2017 scenario results, in order to show how a solution that worked quite well in 2017 would perform if applied in future scenarios. Results are summarized in Table 4-8 for 2030 DG scenario and in Table 4-9 for 2040 GCA scenario, which shows how a growing RES capacity in the network reduces the effectiveness of the deployment of the same PtG plants set.

Table 4-8: Performance of PtG in 2030 DG scenario, network #T3

Scenario		PtG status	RES imbalance			
			Duration [min]	Difference [%]	Peak [MW]	Difference [%]
Network January	#T3	Off	1440	-64%	22186	-19%
		On	520		18029	
Network July	#T3	Off	1440	-60%	23895	-18%
		On	580		19639	

Table 4-9: Performance of PtG in 2040 GCA scenario, network #T3

Scenario		PtG status	RES imbalance			
			Duration [min]	Difference [%]	Peak [MW]	Difference [%]
Network January	#T3	Off	1440	-49%	32534	-13%
		On	730		28477	
Network July	#T3	Off	1440	-47%	33908	-12%
		On	770		29728	

As it can be seen in RES imbalance figures (Figure 4-14, Figure 4-16, Figure 4-18 and Figure 4-20), the effect of PtG units still exists, but it is less effective than the one within the 2017 scenario. Referring to the summary tables, the RES imbalance peak grows in future scenarios, given the RES installed capacity increases. Therefore, it is necessary to plan PtG sizing and siting in a proper way.

PtG unit responses, shown in Figure 4-15, Figure 4-17, Figure 4-19 and Figure 4-21, follow correctly their given setpoints. Compared to the 2017 scenario, the maximum setpoint required for each PtG unit doubles for the 2030 DG scenario (~1500MW to ~3000MW) and almost triples for the 2040 GCA

scenario (~1500MW to ~4000MW). This indicates that for properly facing the amount of RES installed, additional PtG capacity will be necessary.

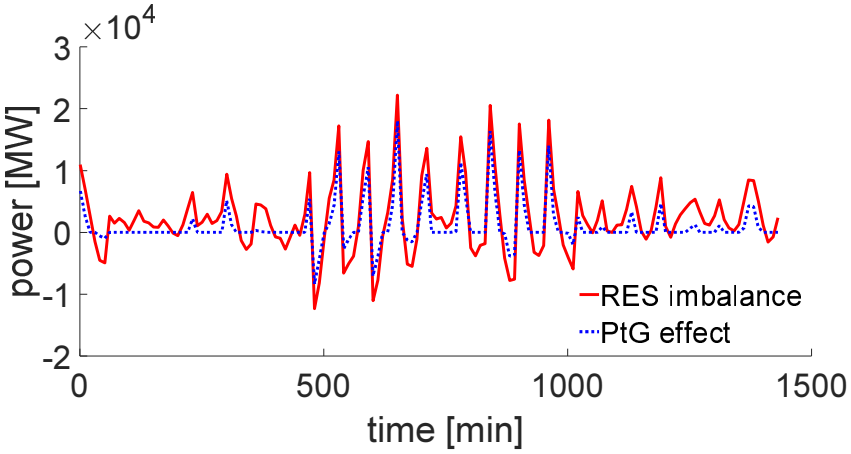

Figure 4-14: RES imbalance before and after the PtG installation (10th January, 2030 DG scenario), network #T3

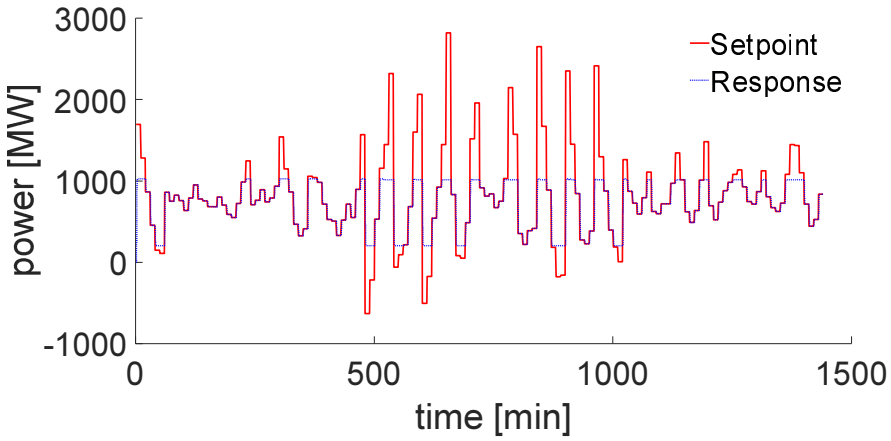

Figure 4-15: Setpoint and response of 1-GW PtG plant (10th January, 2030 DG scenario), network #T3

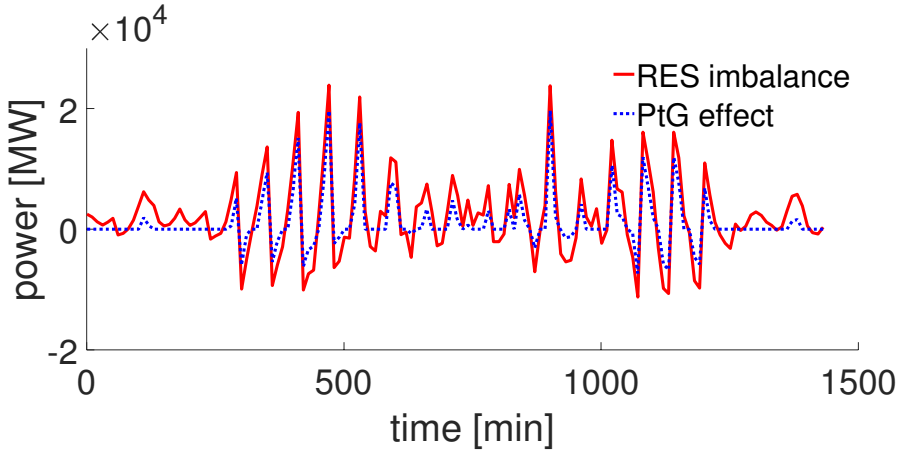

Figure 4-16: RES imbalance before and after the PtG installation (3rd July, 2030 DG scenario), network #T3

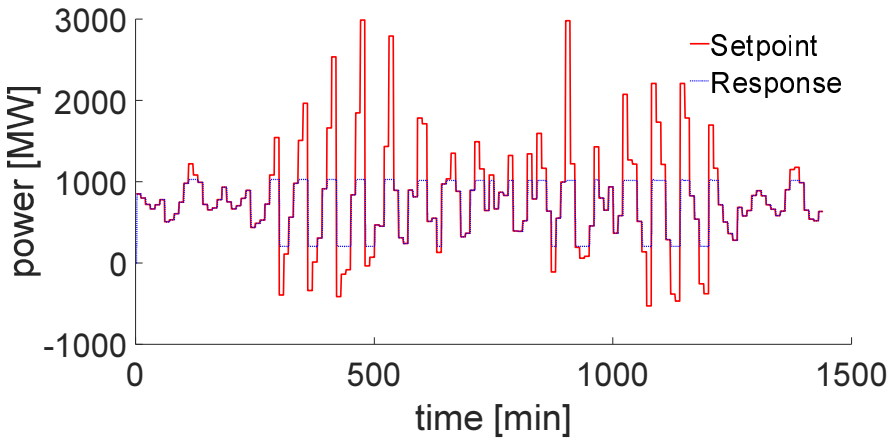

Figure 4-17: Setpoint and response of 1-GW PtG plant (3rd July, 2030 DG scenario), network #T3

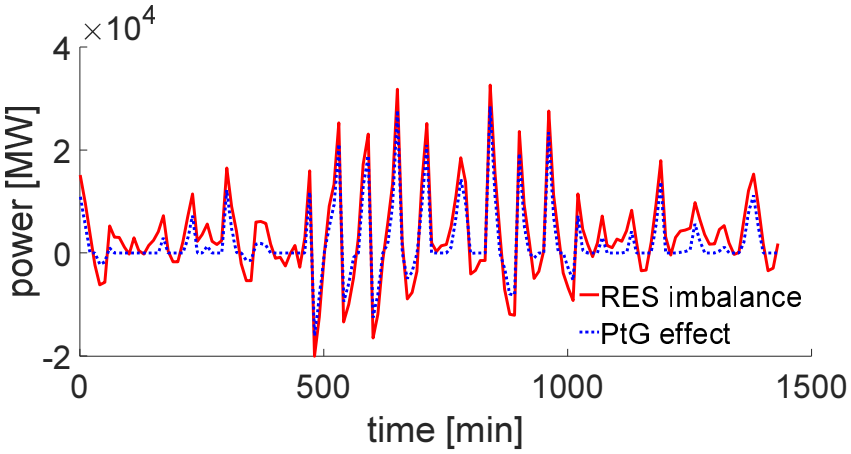

Figure 4-18: RES imbalance before and after the PtG installation (10th January, 2040 GCA scenario), network #T3

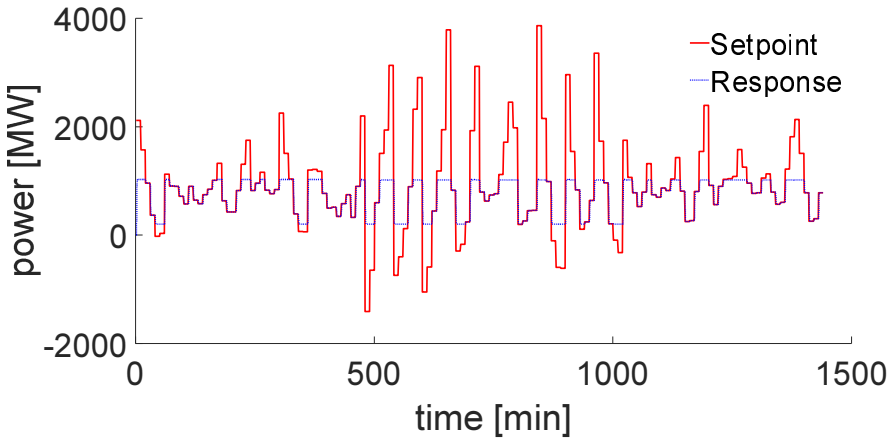

Figure 4-19: Setpoint and response of 1-GW PtG plant (10th January, 2040 GCA scenario), network #T3

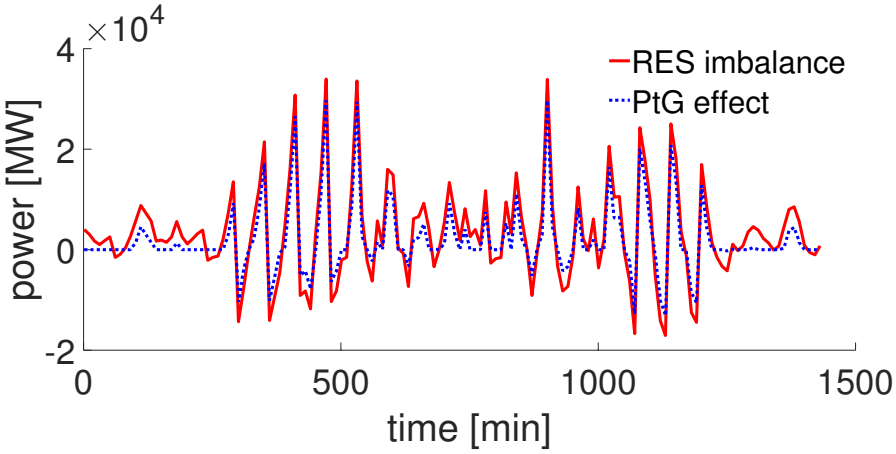

Figure 4-20: RES imbalance before and after the PtG installation (3rd July, 2040 GCA scenario), network #T3

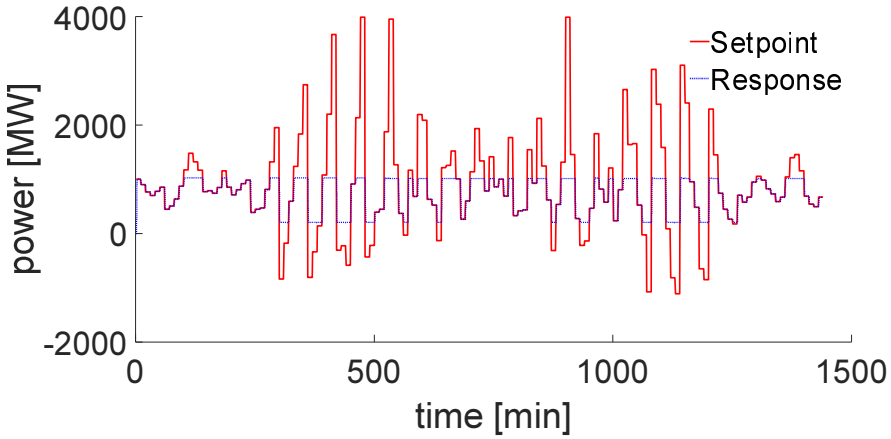

Figure 4-21: Setpoint and response of 1-GW PtG plant (3rd July, 2040 GCA scenario), network #T3

4.4 Transmission system result summary

The results obtained from the analysis of all the networks (network #T1, network #T2 and network #T3) presents a common result: *PtG helps the transmission networks by absorbing the RES variability*, which cannot be completely foreseen in advance. The magnitude of the RES impact will increase in the next years, as it can be seen comparing the 2017 scenario to the 2030 DG and 2040 GCA ones in network #T3, almost up to three times the 2017 level, and transmission networks needs to be ready for the future.

It is possible to understand how important it is to properly consider future scenarios, despite their uncertainty: a set of PtG plants that, installed in the conditions corresponding to the 2017 scenario, can reduce the duration of RES imbalance effects by ~92%, when applied in the 2030 DG and 2040 GCA scenarios, sees a reduced effect (from ~92% reduction of RES imbalance effects duration to ~62% and ~48%, respectively). The peak power reduction of the RES imbalance on the network follows a similar trend: being directly linked to the total capacity of PtG installed, the peak reduction decreases from ~50% for 2017 scenario down to ~18% and ~12% for the future scenarios.

These results make room for further investigations, which will be developed in the next Deliverable 6.6 “Report on the impacts of the PtG on selected scenarios”, due in M42 (August 2019).

5 Description of the distribution networks and implementation for STORE&GO

The distribution system is the portion of the system connecting the transmission system and the customers (Figure 3-1). The distribution system is composed of several networks, which can be either operated at Medium Voltage (MV) or Low Voltage (LV). Due to the nature of the investigation of the STORE&GO project (i.e., deployment of MW-scale PtG plant), this Deliverable considers only network samples operated at MV.

It is worth to note that the studies related to the distribution system are strictly depending on the network sample, nature of the load, weather conditions, and so on. Among all the network examples available in literature (see for example [39]), most of them are derived from North America standard networks and so not really fitting with the European reality. On the basis of these considerations, the idea was to choose network samples which could fit with the European reality, and possibly taking into consideration the geographical position of the demo sites. Based on the above premises, two networks samples were chosen, i.e.:

- Network #D1, representing a rural area
- Network #D2, representing a semi-urban area (small-medium town)

More details about the two samples are reported in Sections 5.1 and 5.2.

5.1 Description of the Network #D1

The Italian demo site is installed in a rural area. For this reason, a possible network that can be used is one of the networks developed in the project *ATLANTIDE* [6]. The project aimed to develop different network samples, representative for the Italian distribution system.

In particular, it is possible to use the country-side network (shown in Figure 5-1). This network is representative of a rural area, and it is supplied by a transmission system operated at 150 kV: this value is typical for the south of Italy, and hence this network has been considered meaningful for the demo site of Troia (Italy).

Figure 5-1: Schematic of the rural network from the project Atlantide [6]

The description of the network in terms of feeder, nodes and types of load is shown in Table 5-1. As shown, different types of load are considered, i.e., different load profiles, shown for completeness in Figure 5-2. The time step is 15 minutes, which represents the one among the typical time steps used for properly describing the behaviour of the electrical loads

Table 5-1: Main features of the case #D1

Feeder	Nodes	Residential	Industrial	Agricultural	PV
F1	3 – 27	7	2	16	1
F2	28 – 33	0	2	6	1
F3	34 – 55	13	3	9	3
F4	56	1	0	0	0
F5	57 – 69	5	3	12	0
F6	70 – 76	1	1	7	0
F7	79 – 103	13	3	17	0

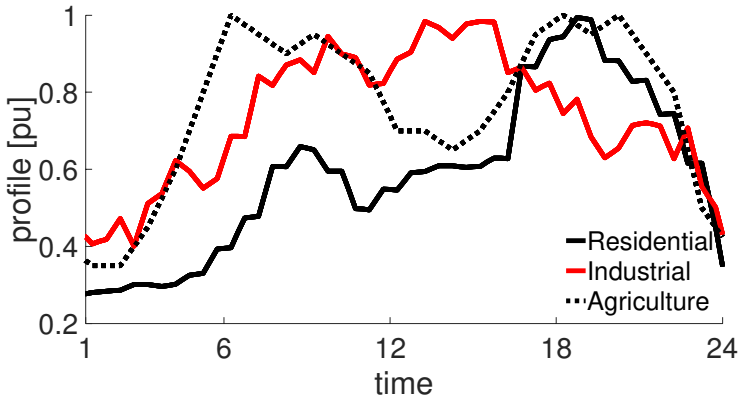

Figure 5-2: Load profiles used in the case study #D1

The network is composed of seven feeders, i.e., seven lines supplied by the HV/MV substation, 103 nodes and 102 closed branches, being the network radial.

The network contains three different types of load (i.e., residential, industrial, and agricultural), divided among the nodes as follows:

- 40 nodes with *residential loads*
- 14 nodes with *industrial loads*
- 67 nodes with *agricultural loads*
- 5 nodes with PV generation

5.2 Description of the Network #D2

The second network sample considered is the semi-urban network shown in [7]. The authors of the report collected data from 79 out of 190 European DSOs, which supply 70% of the total electricity served by all DSOs. This information was used for building 36 indicators and 10 of these indicators were considered the most representative for distribution networks. Based on them, the distribution network samples have been obtained using RNM (Reference Network Model). This is a useful software for large scale distribution planning developed by the Universidad Pontificia Comillas [40]. The description of the network is reported in Figure 5-3.

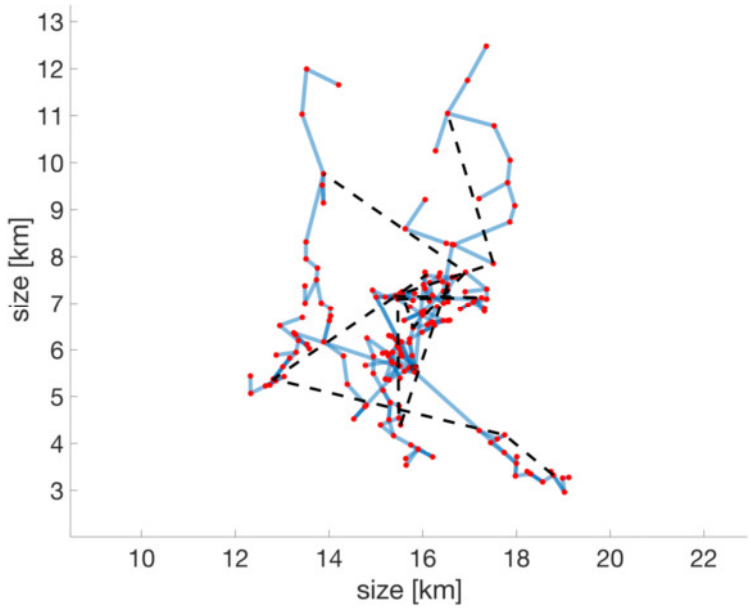

Figure 5-3: Semi-urban network. The dashed lines represent open branches, for guaranteeing the radiality of the network [7]

The original network consists of both MV and LV portions. The LV portions of the network are supplied by a MV node, through a transformer. Due to the goal of the study, the LV network portions have been distinguished on the basis of the MV node supplying them, and their loads summed up by forming the nodal load connected to the corresponding MV nodes.

The network is composed of ten feeders that means that the HV/MV transformer feeds ten different feeders.The technical specifications of the network are summarised in Table 5-2.

Table 5-2: Main features of the semi-urban network

LV consumers	MV consumer	Peak Power [MW]	HV/MV transformer [MVA]
~14,000	40	74.5	120

The original network reported only the nominal power of the connected load, without specifying neither the type, nor the load profiles. For making possible a complete analysis, the network has been modified, by labelling the loads according to types listed in Table 5-1, by adding two more types of loads representing the tertiary sector, i.e., commercial and offices (Figure 5-4).

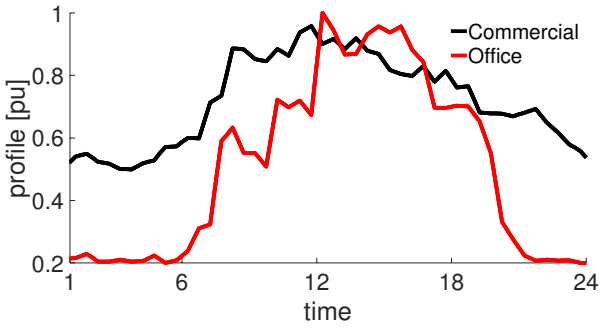

Figure 5-4: Adjunctive loads considered in the case #D2

The placement of the different types of loads was made by considering the length of the branches, to obtain a realistic load distribution (as shown in Table 5-3), based on the experience of the authors.

Table 5-3: Placement of the types of load according to the line length

Line length *L* [km]	% residential	% industrial	% commercial	% offices	% agriculture
$L \leq 0.15$	80	0	10	10	0
$0.15 < L \leq 0.3$	70	0	15	15	0
$0.3 < L \leq 0.5$	65	5	15	15	0
$0.5 < L \leq 0.8$	25	5	45	20	5
$0.8 < L \leq 1$	10	50	25	5	10
$1 < L \leq 3.5$	20	10	5	5	60

On the basis of Table 5-3, the final configuration is composed as follows:

- 201 nodes with *residential loads* and *tertiary loads* (commercial loads and office)
- 131 nodes with *industrial loads*
- 51 nodes with *agricultural loads*

The total load installed divided per types is shown in Table 5-4.

Table 5-4: Total amount of load (nominal power) per type [MW]

Residential	Industrial	Commercial	Offices	Agriculture
44	3.5	14	10.5	2.5

The nodes composing the feeders are shown in Table 5-5.

Table 5-5: Composition of the feeders for the case #D2

Feeder	Nodes	Total Length feeder [km]
F1	3, 11, 13, 25, 80, 85, 86, 105, 121, 122, 123, 125, 138	2.2
F2	16, 17, 37, 43 – 46, 48, 53, 56 – 58, 62, 70, 71, 74, 75, 81, 102	3.8
F3	21, 23, 29, 40 – 42, 47, 59, 60, 61, 66, 69, 91, 94, 96, 97, 100, 104, 114, 115	4.3
F4	18, 20, 33, 64, 65, 67, 68, 73, 77, 82, 83, 87, 88, 90, 95, 99, 101, 106, 107	5.9
F5	2, 22, 30, 49 – 52, 54, 55, 72, 76, 78, 79, 84, 89, 98, 103, 112, 117	4.2
F6	10, 27, 108 – 110, 113, 116, 118 – 120, 130 – 133, 135, 136, 143	4.5
F7	5, 8, 12, 26, 28, 35, 36, 39, 92, 93, 111, 124, 126, 127, 134, 139, 140, 142	3.0
F8	9, 15, 19, 137, 146 – 148, 150, 151, 153, 154, 158, 166, 167, 171	4.5
F9	1, 4, 6, 7, 34, 128, 129, 141, 144, 145, 149, 152, 160 – 163, 168, 170, 176, 177, 179 – 183, 185 – 187, 190, 194 – 196, 199, 201, 202	7.2
F10	14, 24, 31, 32, 38, 155 – 157, 159, 164, 165, 169, 172 – 175, 178, 184, 188, 189, 191 – 193, 197, 198, 200	6.0

5.3 PV profiles for distribution system case studies

According to the local nature of the distribution system and according to what was suggested in the Deliverable D5.2 “Interim report of benchmarks and analysis description and load profile definitions” [41], the information about the PV profiles have been based on [32], which refers to [42].

The model provides a synthetic irradiance profile expressed in [W/m^2], with sample 1-minute, which takes into account the geographical position of the installation site (i.e., latitude and longitude).

However, in order to obtain the power at AC side, the model reported in Appendix A: Calculation of the AC power for PV fields is used: this model requires as further input the temperature at the installation site, which has been obtained from the website PVGIS [43].

In total, four typical days have been considered, representing the different seasons (with different duration of the irradiance.

The four days for the two sites are reported in Figure 5-5 (for Solothurn) and in Figure 5-6 (for Troia). The two figures report the time and the value of normal production in four meaningful days of four months (i.e, January, April, July and October), as obtained by combining the 1-minute irradiance obtained by [32] and the temperature provided by [43], as explained in Appendix A: Calculation of the AC power for PV fields.

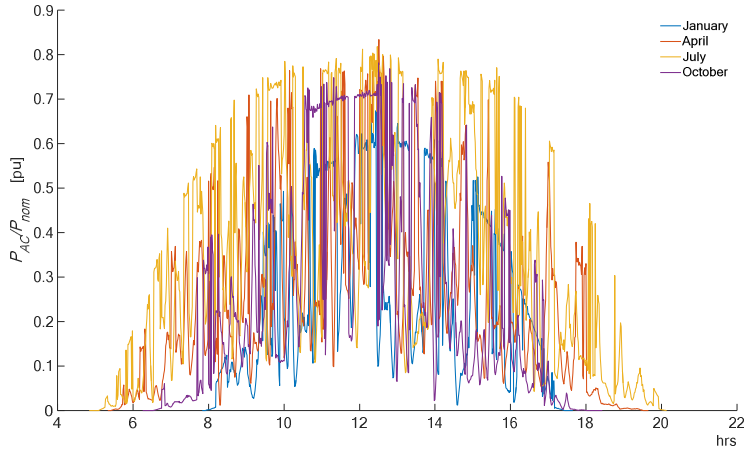

Figure 5-5: 1-minute PV daily production for Sothurn (in January, April, July and October)

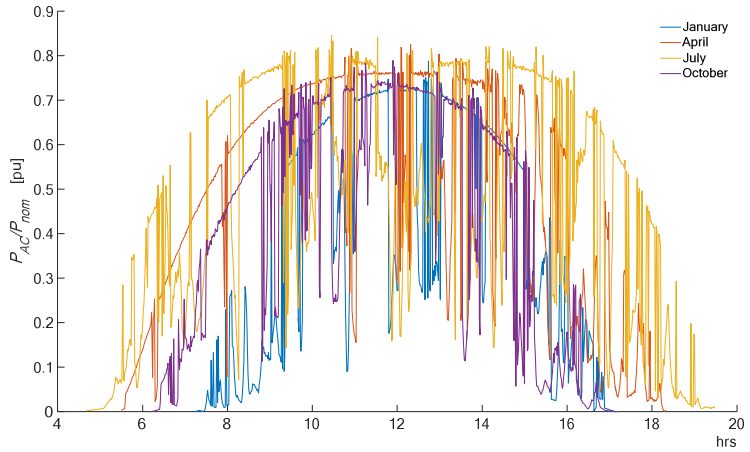

Figure 5-6: 1-minute PV daily production for Troia (in January, April, July and October)

For the demo site of Solothurn (Switzerland), the values of latitude and longitude are (47.209, 7.532). It has been also assumed an inclination of the PV panel of 35° and an orientation towards south. The height of the town is 432 m a.s.l.

For the demo site of Troia (Italy), the values of latitude and longitude are (41.360, 15.308). Also in this case, it has been assumed an inclination of the PV panel of 35° and an orientation towards south. The height of the city is 439 m a.s.l.

According to the Deliverable 6.1 “Report on opportunities and options for PtG in power systems” [1], one of the remarkable features is the maximum positive/negative change rate, shown in Table 5-6 for the two demo sites.

Table 5-6: Maximum positive/negative variation of PV production (in [%P_{nom}])

	Change rate	
	Solothurn	**Troia**
January	52%	+53%
	-47%	-57%
April	+60%	+63%
	-60%	-59%
July	+59%	+68%
	-61%	-63%
October	+61%	+55%
	-58%	-53%

The case studies have been created by imposing a penetration of renewables such that it creates some issues representative of the real world cases.

As pointed out in previous project Deliverables (the reader can refer to [1] and [41]) and as widely shown in literature (for example in [44]), the installation of large share of RES can create the following issues:

1. **Reverse power flow**: the reverse power flow is an issue both for the transmission system operator and the distribution system operator. In fact, the presence of an energy flowing from the distribution to the transmission network makes the interconnection between distribution system and transmission system equivalent to a non-controllable active node, which can create some difficulties in guaranteeing the correct operation of the electrical system. On the other hand, the presence of reverse power flow can create issues also at the distribution system, for example in terms of not proper protection schemes. The reverse power flow is calculated at the HV/MV connection point. Usually, this kind of problem is nowadays solved by cutting the excess of production or using some pilot battery-based storage [45].

2. **Overcurrent**: the large share of RES can create overcurrents along the feeders. These overcurrents can affect only a portion of the network (e.g., the last portion) or the entire network, depending on the level of load and distributed generation, together with the geographical position of the PV plants. It is worth to note that theoretically a condition with some branches affected by overcurrents could not be synonym of reverse power flow.

3. **Overvoltages**: this problem is characteristic especially of rural networks, composed of long feeders (also up to 10 km), and characterised by a high R/X ratio.

By starting from the base cases presented in Section 5.1 and 5.2, and by adding the generation profiles presented in Section 5.3, different case studies have been prepared, for properly testing the use of PtG in the distribution system context.

The PV plants have been installed in the network following two main drivers:

1) Installation based on the line length

2) Installation based on the loss allocation factors [46]:

    a. without any check regarding the network constraints

    b. by respecting the network constraints (i.e., voltage and current) [47]

The case 1) is used to create case studies characterized of PV plants installed in a well-defined portion of the network (for example at the end of long lines). This approach is a “topological approach”, and the problems created can be only reverse power flow, or reverse power flow together to another specific problem (for example only overvoltage and not overcurrent). This method has been applied on both case studies, i.e., network #D1 and network #D2.

Vice versa, the cases created following the approach 2.a) allows to analyse networks affecting by different problems at the same time (not only reverse power flow, but also both overvoltage and overcurrent conditions existing). However, this approach does not guarantee the presence of really dispersed generation throughout the entire network. For this reason, the method 2.b) has been also used: this methodology allows to isolate one problem (i.e., reverse power flow), by considering all the network constraints respected. Due to the different parameters of the two case studies, these two methodologies has been applied only at the network #D1 (no meaningful examples obtained by applying the methodology at network #D2).

Table 5-7 shows the cases studied for the distribution system #D1, whereas Table 5-8 reports the cases studied with the network #D2, both with the indications of the issues affecting the networks.

Table 5-7: Case studies for the network #D1

Method PV placement	Length [km]	PV penetration	Reverse PF	Overcurrent	Overvoltage
Method 1	$0<L\leq0.9$	50%	X	-	-
		60 %	X	-	-
		70 %	X	X	-
		80 %	X	X	-
	$2\leq L\leq 3$	50 %	X	-	-
		60 %	X	-	-
		70 %	X	-	X
		80 %	X	-	X
Method 2a	-	50 %	X	X	-
		60 %	X	X	-
		70 %	X	X	X
		80 %	X	X	X
Method 2b	-	50 %	X		
		60 %	X		
		70 %	X		
		80 %	X		

Table 5-8: Case studies for the network #D2

Network	Length [km]	PV penetration	Reverse PF	Overcurrent	Overvoltages
	$0<L\leq0.45$	50 %	X		
		60 %	X		
		70 %	X	X	
#D2		80 %	X	X	
	$0.5\leq L\leq 3$	30 %	X	X	
		40 %	X	X	X
		50 %	X	X	X
		60 %	X	X	X

The network issues are solved (or at least alleviated) by installing a number PtG plants in the network. The choice of the installation node and the size of the PtG plant is made through a probability-based heuristic optimization method called Simulated Annealing (SA), whose features are explained in Appendix E: Simulated Annealing.

It is worth to note the different nature of the issues existing in the network: on one hand, the reverse power flow represents an operational condition that, even not desirable, is not affecting the operational constraints of the network (i.e., thermal limits and voltages). On the other hand, the presence of overcurrent and overvoltages represent an abnormal condition, and the system operator has to prevent conditions like this one. So, *the case studies where overcurrents and overvoltages exist should be considered as extreme cases*: their aim is to demonstrate that PtG can effectively operate for allowing the allocation of large amounts of RES, by stabilising the network conditions.

5.4 Introduction of the PtG node into the calculation loop

In this network model the desired working point of the PtG unit is calculated at the current time step of the power flow, which is solved by means of the Backward Forward Sweep (BFS). As explained in Section 2, the response of the PtG unit is modelled as a first order system and only few electrolyser's working points are needed to generate the plant response. For this reason the variable N_{keep_step} is introduced. The numerical value of N_{keep_step} should be sufficient to rebuild the model response, by maintaining the model's accuracy with respect to the "correct response" (i.e., the ones based on the entire set of past working points)[5]. The flowcharts representing the main calculation loops are shown in Figure 5-7 and Figure 5-8.

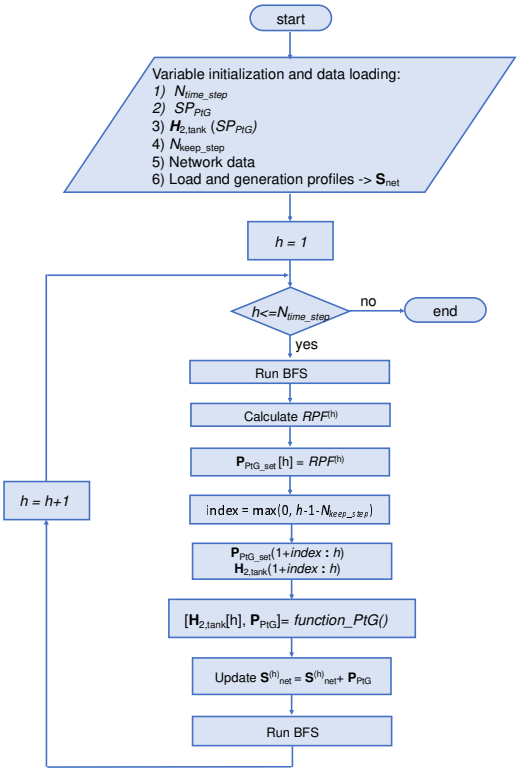

Figure 5-7: The main calculation loop of the distribution system, when only the setpoint needed for solving the reverse power flow is considered. The function called *function_PtG* represents the PtG node

[5] This method has been tested and the error is 10^{-18} with respect to the case in which all the working points are calculated.

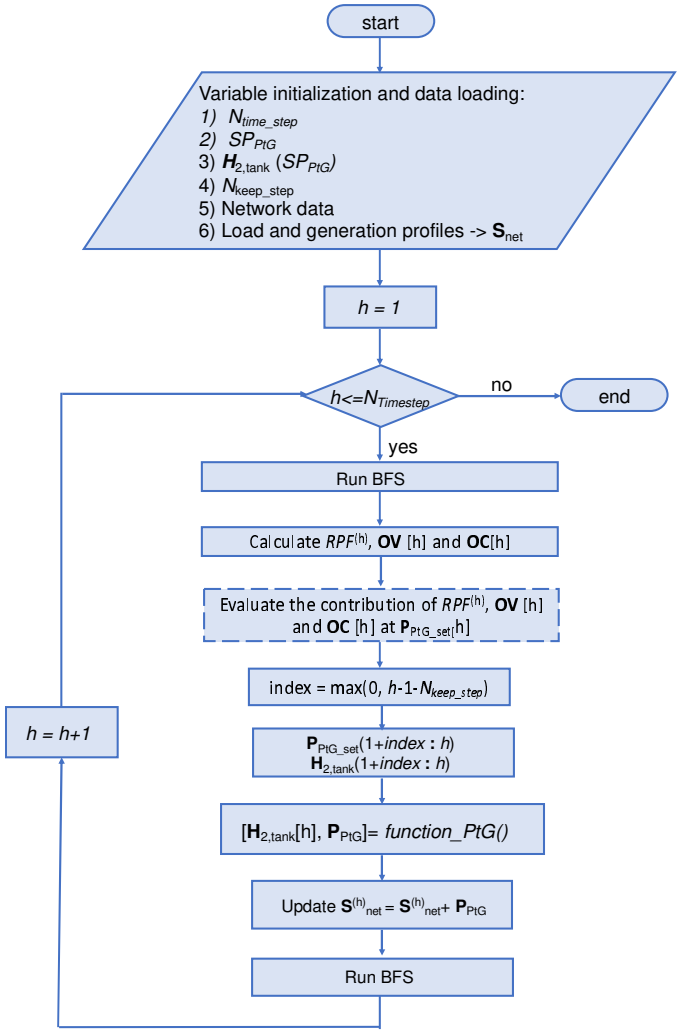

Figure 5-8: The main calculation loop of the distribution system, when the compound setpoint is considered. The function called *function_PtG* represents the PtG node

The difference between the two flowcharts lies in the way to calculate the power $\mathbf{P}_{PtG\_set}[h]$, representing the PtG setpoint at the time step *h*. In fact in the first case, the value of setpoint is evaluated only on the basis of the reverse power flow affecting the network, whereas in the latter case the set point is a compound value of different contributions, i.e., besides the reverse power flow contribution, also the overcurrent contribution and the overvoltage contribution. The set of the input data is reported in Table 5-9: among those parameters, only two are fixed for all the simulations, whereas all the others are case dependent, and so no default values are specified.

Table 5-9: Set of the input data of the main calculation cycle.

Initialized Variables	Description	Value
N_{time_step}	Number of BFS iterations (one of each minute of the day)	1440
N_{keep_step}	Number of points for run PtG model	10
SP_{PtG}	Size PtG plant	-
$\mathbf{H}_{2,tank}(SP_{PtG})$	Initial value of the volume of H2 in the tank	-
Network data	Lines parameter, incidence matrix, rate nodal power, lines thermal limits	-

Load and generation profiles	Load an generation profiles for evaluating $\mathbf{S}_{net}$	-
$\mathbf{S}_{net}$	Net nodal power	-

The explanation of the algorithm is based on the flowchart reported in Figure 5-8, which uses as PtG set point a compound signal taking into account reverse power flow (variable $RPF^{(h)}$), overvoltage (vector **OV**) and overcurrent (vector **OC**). After solving a BFS for iteration *h*, the variable $RPF^{(h)}$), **OC**[*h*] and overvoltage **OV**[*h*] are calculated: on the basis of the these three values, the compound PtG set point is created. The set points referring to them are calculated as follows:

- Component related to the reverse power flow: it is directly the value of reverse power flow
- Component related to the value of overcurrent **OC**[*h*]: it is the power needed to bring the overloaded branches to operate at 80% of their thermal limit (Figure 5-9)
- Component related to the value of overvoltage **OV**[*h*]: it is the power needed for bringing the nodes with overvoltage to operate at 1.05 pu[6] (Figure 5-10).

It is worth to note that the sum of these three contributions is one of the inputs of the node PtG function. If the number of time steps $h<N_{keep\_step}$, the entire past values of the variables $\mathbf{P}_{PtGset}$ and $\mathbf{H}_{2,tank}$ are passed as input. Otherwise, only the previous N_{keep_step} points of $\mathbf{P}_{PtGset}$ and $\mathbf{H}_{2,tank}$ are passed to PtG node function. In the loop, the values of $\mathbf{H}_{2,tank}$ and $\mathbf{P}_{PtG}$ are updated, being $\mathbf{P}_{PtG}$ the power absorbed by the PtG system: this value is fundamental for updating the value the $\mathbf{S}_{net}^{(h)}$ which is the vector containing all the power of the network, and then also the ones related to PtG plants. Finally, another BFS is calculated for the instant h, to update all the variables for taking into account the additional load composed of the PtG consumption.

This cycle is repeated for a number of iterations equal to the number of minutes of the day (or any other duration chosen by the user).

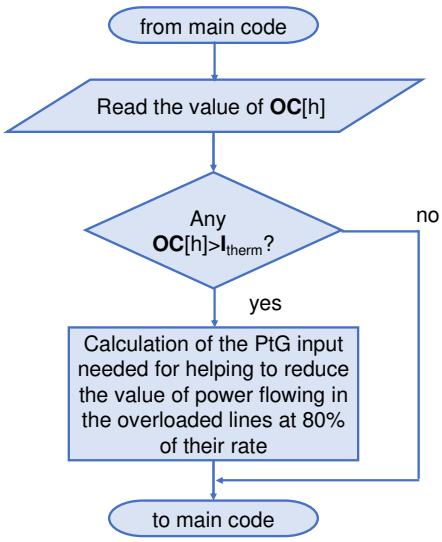

Figure 5-9: Loop of calculation of the setpoint value related to the overcurrent

[6] The resistance of the network is not negligible, so the impact of active power on voltage values is not negligible as well.

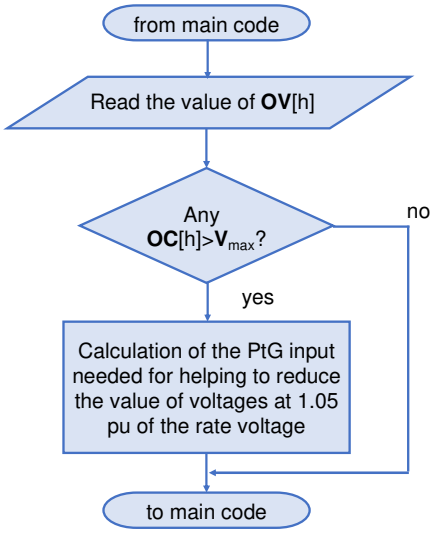

Figure 5-10: Loop of calculation of the setpoint value related to the overcurrent

6 Results for the cases #D1 and #D2

6.1 Conditions considered in the placement of PtG plants

The siting and sizing of PtG plants has been carried out, as specified in Section 5.4, by means of SA.

The values of the parameters used in the optimization method are reported in Table 6-1: the explanation of the symbols is reported for convenience in Appendix E: Simulated Annealing.

Table 6-1: Set of values used in the SA method

N_A	N_C	α	p_0	N_R	C_0	ρ_I	ρ_V
30-50	15-20	0.9	0.5	10-2015	16.8-600	5-100	3-6

The network condition considered that is the worst for the network that is in the month of July. In that condition the production of PV is really high and can cause severe issues to the network operation (see Sections 6.2.1, 6.3.1,6.4.1) The other three months (January, April and October), less critical, have been used to verify that the installed PtG plants do not create any additional network issues (see Sections 6.2.4, 6.3.3, 6.4.3)

6.2 Case #D1, Method 1

For the Case #D1, the sizes chosen for the PtG plant lie in the range 0.5 to 2 MW, and are connected to the MV network through a proper transformer. The range has been chosen for taking into account both the constraints due to the presence of the methanation process and the value of additional nodal loads that can be added at the MV rural network according to the rules usually employed by the DSOs. The model of PtG considered in the following simulation has been explained in Section 2.

6.2.1 Operation during July

As mentioned in Section 5.4, the placement of the PV plants through method 1 allows to create cases with plants connected to nodes belonging to either short or long lines. The distribution of the PV in the network is reported in Table 6-2: from the values shown, it is evident that some feeders can be characterised by high PV penetration in both cases (for example F7), whereas other (as F4 and F5) can remain even without any PV plants installed. In these two cases it is evident that the PV installations are very different feeder by feeder, so more concentration of PV installation exists in delimited zones of the networks.

Table 6-2: Distribution of the PV in the different feeders of network #D1, method 1

Length [km]	Feeder	PV Installed Power [MW]				
		40%	50%	60%	70%	80%
$0<L\leq0.9$	F1	3.42	3.61	5.218	5.963	6.708
	F2	1.06	1.85	1.618	1.850	2.081
	F3	0.65	0.80	1	1.146	1.290
	F4	0.66	0.80	1	1.149	1.293
	F5	1.79	2.18	2.730	3.126	3.510

	F6	0.54	0.66	0.835	0.9547	1.074
	F7	6.47	7.87	9.8459	11.252	12.659
$2 \leq L \leq 3$	F1	2.95	3.59	4.498	5.140	5.783
	F2	2.59	3.15	3.947	4.511	5.075
	F3	3.59	4.37	5.474	6.256	7.038
	F4	0	0	0	0	0
	F5	0	0	0	0	0
	F6	1.31	1.549	1.990	2.280	2.565
	F7	4.16	5.07	6.341	7.247	5.800

The results are summarised in Table 6-3: they show that the use of PtG is able to reduce the problems caused by the high penetration of RES in the distribution network under analysis. The size of the installed PtG plants (corresponding to the solutions reported in Table 6-3) are shown in Table 6-4.

An important aspect to consider is the exploitation of the installed plants: for this, it is necessary to consider the load factor of the plants, which will be evaluated in Section 6.2.3

For completeness, Table 6-5 shows the value of energy injected in the HV network after and before the installation of the PtG plants: the values highlight the good performance reaching by the network thanks to the installation of PtG plants.

Table 6-3: Comparison of the results before and after the installation of PtG, network #D1, method 1

Length [km]	PV penet	Rev. PF pre	Rev. PF post	Overcurr. pre	Overcurr. post	Overvolt. pre	Overvolt. post
$0<L \leq 0.9$	40 %	113	6	-	-	-	-
	50 %	211	4	-	-	-	-
	60 %	366	23	-	-	-	-
	70 %	454	152	360	0	-	-
	80 %	506	256	578	7	-	-
$2 \leq L \leq 3$	40 %	144	9	-	-	-	-
	50 %	232	8	-	-	-	-
	60 %	370	28	-	-	-	-
	70 %	429	182	-	-	463	0
	80 %	488	291	-	-	1297	9

Table 6-4: Size of the PtG plants (expressed in MW) and installation nodes, network #D1, method 1

Length [km]	PV penet	Size plant 1	Size plant 2	Size plant 3	Size plant 4	Installation nodes
$0< L \leq 0.9$	40 %	2.5	-	-	-	82
	50 %	2	2	0.5	2	85, 100, 27, 21
	60 %	2	2	2	1.5	85, 80, 93, 100
	70 %	2	2	2	2	85, 13, 80, 98

	80 %	2	2	2	2	83, 21, 84, 98
2 ≤ *L* ≤ 3	40 %	2	-	-	-	87
	50 %	2	1.5	2	2	85, 81, 93, 100
	60 %	2	2	2	1.5	85, 44, 93, 100
	70 %	2	1	2	2	82, 97, 21, 98
	80 %	2	1.5	2	2	82, 97, 48, 98

Table 6-5: Comparison of the results before and after the installation of PtG, network #D1, method 1 Energy of reverse power flow

Length [km]	PV penet	Rev. PF pre [MWh]	Rev. PF post [MWh]	Reduction [%]
0< *L* ≤0.9	40 %	1.02	0.051	-95.00
	50 %	5.78	0.086	-98.50
	60 %	20.38	0.39	-98.07
	70 %	36.25	3.06	-91.55
	80 %	50.96	10.39	-79.60
2 ≤ *L* ≤ 3	40 %	1.79	0.076	-95.74
	50 %	5.48	0.11	-97.94
	60 %	19.68	0.96	-95.14
	70 %	32.38	4.94	-84.76
	80 %	46.43	15.14	-67.40

The decrease of the objective function along the optimization process is shown in Figure 6-1. As a matter of example, the figure presents the results for the cases with 0< *L* ≤0.9 and penetrations of 50% and 80%: it is quite evident that the optimization allows to reach very good results, as well as that, with a proper control, the PtG is able to improve network conditions helping in distribution network stabilisation, definitely reducing the issues affecting the network.

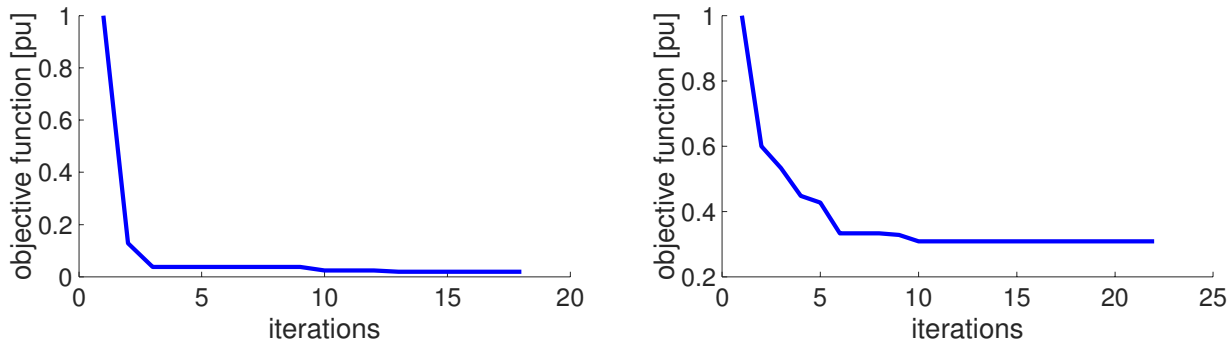

(a) 0< *L* ≤0.9 km, 50% PV penetration (b) 0< *L* ≤0.9 km, 80% PV penetration

Figure 6-1: Examples of objective function decrease along the iterations, network #D1, method 1

The improvement of the network condition can be seen also analysing the electrical features, such as voltage and currents. As shown in

Table 5-7, the cases 0< *L* ≤ 0.9 km with 70% and 80% of penetration of RES are affected by overcurrent as well: this condition is alleviated, or even solved as visualized in Figure 6-2. For example, Figure 6-2d refers to the case 0<*L* ≤0.9 km, 80% of PV penetration after the installation of PtG plants: even if still some overcurrents exist, they are very limited, as shown in Table 6-6, and do not affect the normal operation of the network.

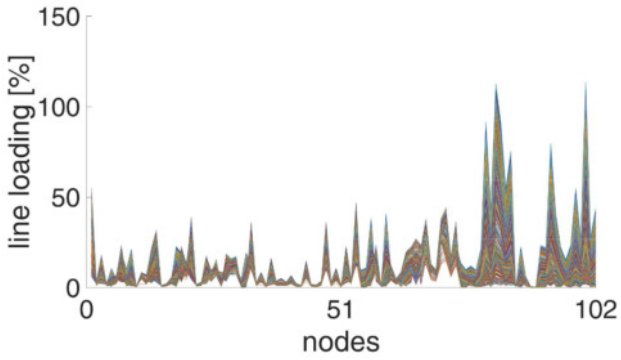

(a) 0< *L* ≤0.9 km, 70% PV penetration, before the installation

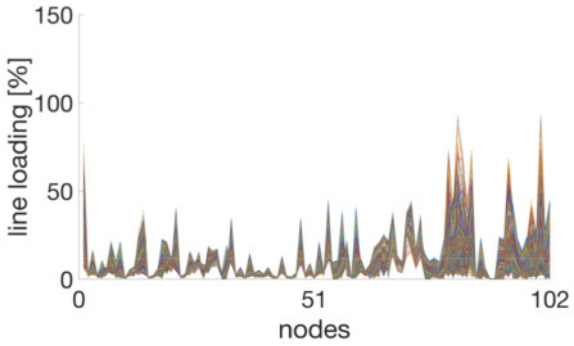

(b) 0< *L* ≤0.9 km, 70% PV penetration, after the installation

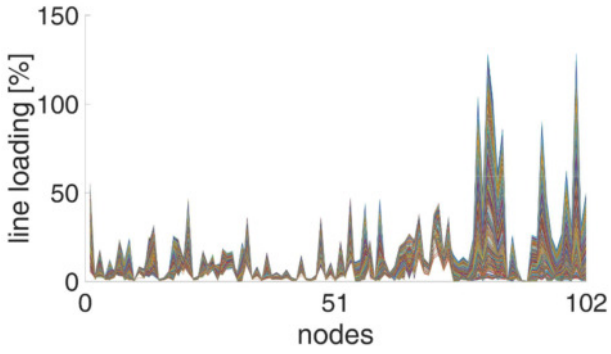

(c) 0< *L* ≤0.9 km, 80% PV penetration, before the installation

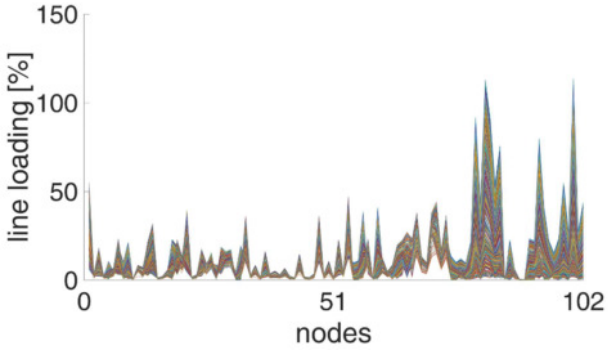

(d) 0< *L* ≤0.9 km, 80% PV penetration, after the installation

Figure 6-2: Overloading before and after the installation of PtG plants for the case #D1, subcase 0<*L* ≤0.9 km

Table 6-6: Magnitude of the overloading after the PtG installation, network #D1, 0<*L* ≤0.9 km, 80% penetration

Length [km]	PV penet	Overloaded branches	Magnitude	Persistence [min]
0< *L* ≤0.9	80 %	82	7.5%	2
		83	6.5%	3
		100	6.7%	2

For the cases 2< *L* ≤3 km, the network issues affecting the network are the reverse power flow and the overvoltages: as shown in Figure 6-3, the installation of PtG allows to improve the nodal voltage values. It is worth to note that for the case with 80% of PV penetration there are still remaining overvoltages, whose amplitudes in any case are very limited and persist for a short time, not affecting the proper network operation (Table 6-7).

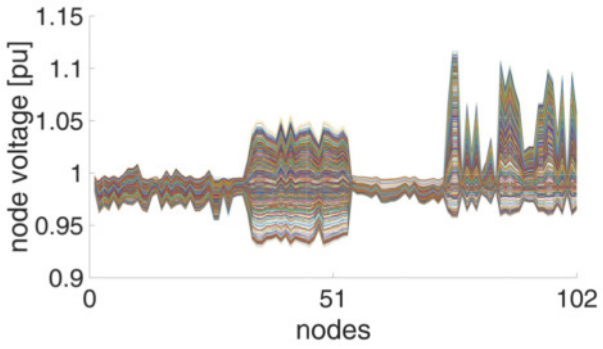

(a) 2≤*L* ≤3 km, 70% PV penetration, before the installation

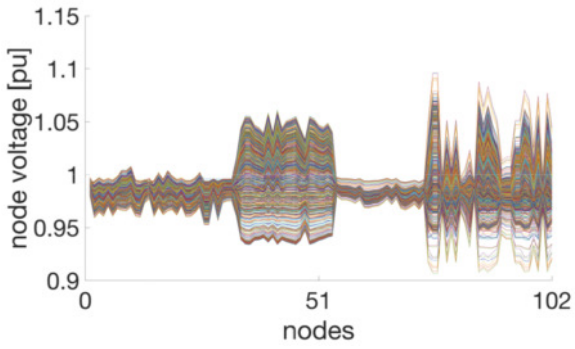

(b) 2≤*L* ≤3 km, 70% PV penetration, after the installation

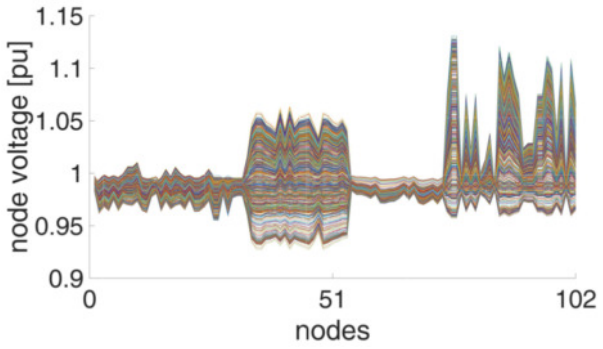

(c) 2≤*L* ≤3 km, 80% PV penetration, before the installation

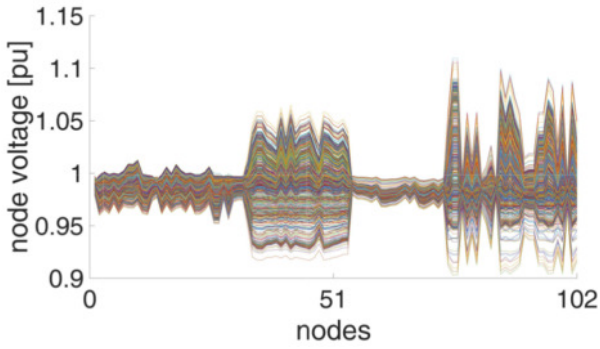

(d) 2≤*L* ≤3 km, 80% PV penetration, after the installation

Figure 6-3: Voltage values before and after the installation of PtG plants for the case #D1, subcase 2<*L* ≤3 km

Table 6-7: Magnitude of the overvoltage after the PtG installation, network #D1, 0<*L* ≤0.9 km, 80% penetration

Length [km]	PV penet.	Nodes	Magnitude	Persistence [min]
2≤ *L* ≤3	80 %	76	10.95%	4
		77	10.95%	4
		96	10.01%	1

An important key performance index is the value of power losses: Table 6-8 shows that the installation of PtG improves in percentual terms the network losses value. This improvement is due to the fact that the PtG plants are adjunctive loads, and they help to stabilise the network operation, by absorbing the excess of RES. It is worth to note that even if in some cases the increasing load slightly increases the losses in absolute terms, the percentage value of the losses are always improving.

Table 6-8: Value of power losses for the network #D1, method 1

Length [km]	PV penet.	Network losses [MWh]		Network losses [%]	
		pre-installation	post-installation	pre-installation	post - installation
0<*L* ≤0.9	40 %	3.08	3.02	2.17	1.85
	50 %	3.53	3.88	2.70	2.06
	60 %	4.23	3.55	4.08	1.90
	70 %	5.06	3.50	6.41	2.14
	80 %	5.88	3.84	9.88	2.63
2 ≤ *L* ≤ 3	40 %	3.06	2.75	2.23	1.74
	50 %	3.71	4.03	2.88	2.03
	60 %	4.88	4.69	4.78	2.69
	70 %	5.99	5.15	7.22	3.42
	80 %	7.31	5.59	11.51	4.27

6.2.2 Production of SNG

The production (in terms of energy) of SNG, with the different PV penetrations for the case 0< *L* ≤0.9 km, is shown in Figure 6-4: the production falls in the range 20 MWh – 80 MWh per day in July. The penetration of 60% is similar to the case with PV penetration of 70% SNG production, due to the relative localization of PV and PtG plants.

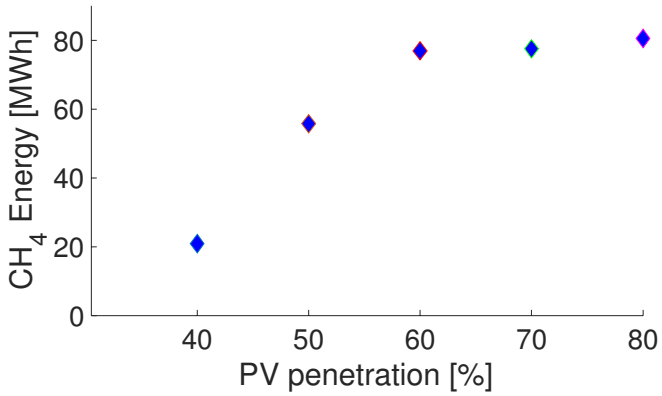

Figure 6-4: SNG production, network #D1, case 0<*L* ≤0.9 km

For the case 2 ≤ *L* ≤ 3 km, the production of SNG is shown in Figure 6-5: the production of SNG is quite similar, but the difference among the production with different PV penetration is lower than the previous case. Again, this can be explained by the relative position between PtG plants and PV plants, that in the case 2 ≤ *L* ≤ 3 km are more concentrated in some portions of the network. It can be seen that for the 40% penetration the energy production is very low, because there are few

problems affecting the network, as in the case of scenario 0 < *L* <0.9 km and thus the use of PtG is very limited.

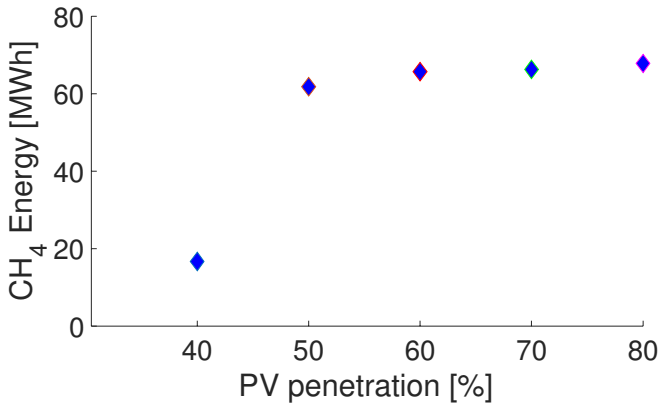

Figure 6-5: SNG production, network #D1, case 2 ≤ *L* ≤ 3 km

6.2.3 Check of the "load factor" of the PtG plants

It is also necessary to investigate how the PtG plants work: for doing this, it has been chosen to show the plant that, in proportion of its size, produces less SNG, i.e., the plants whose "load factor" is lower. In particular, the load factor has been computed as the ratio between the input electricity absorbed when the PV production exists and the energy that the plant should have absorbed if it would work at nominal power. It is evident that the plants are very well used, and are not oversized. The result for the case 0< *L* ≤ 0.9 km is shown in Figure 6-6, whereas the result for the case 2 ≤ *L* ≤ 3 km is shown in Figure 6-7. For all of them is evident the "bell" shape due to the production of PV.

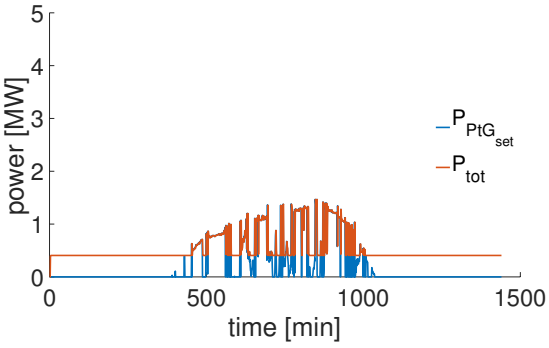

a) Case 50% PV penetration, node 21

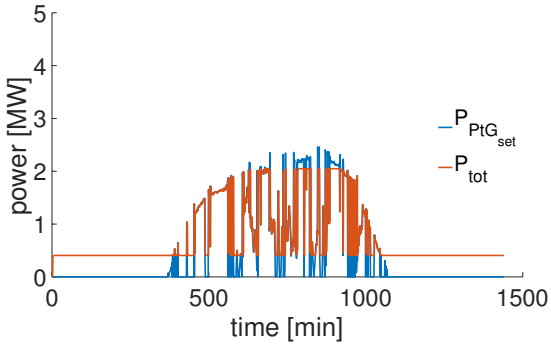

b) Case 60% PV penetration, node 93

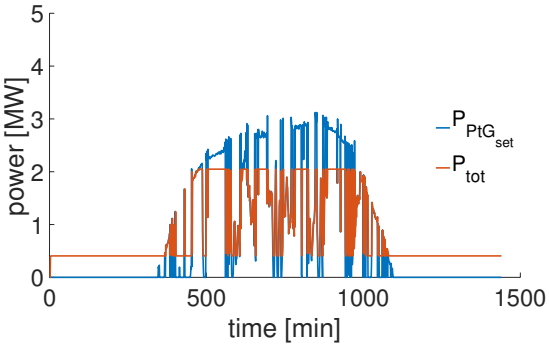

c) Case 70% PV penetration, node 13

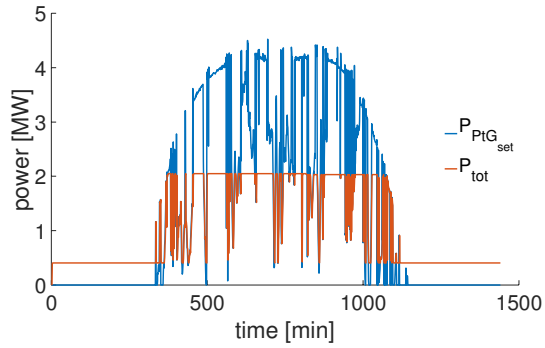

d) Case 80% PV penetration, node 21

Figure 6-6: Set point and actual power of the less productive PtG, network #D1, case 0< *L* ≤0.9 km

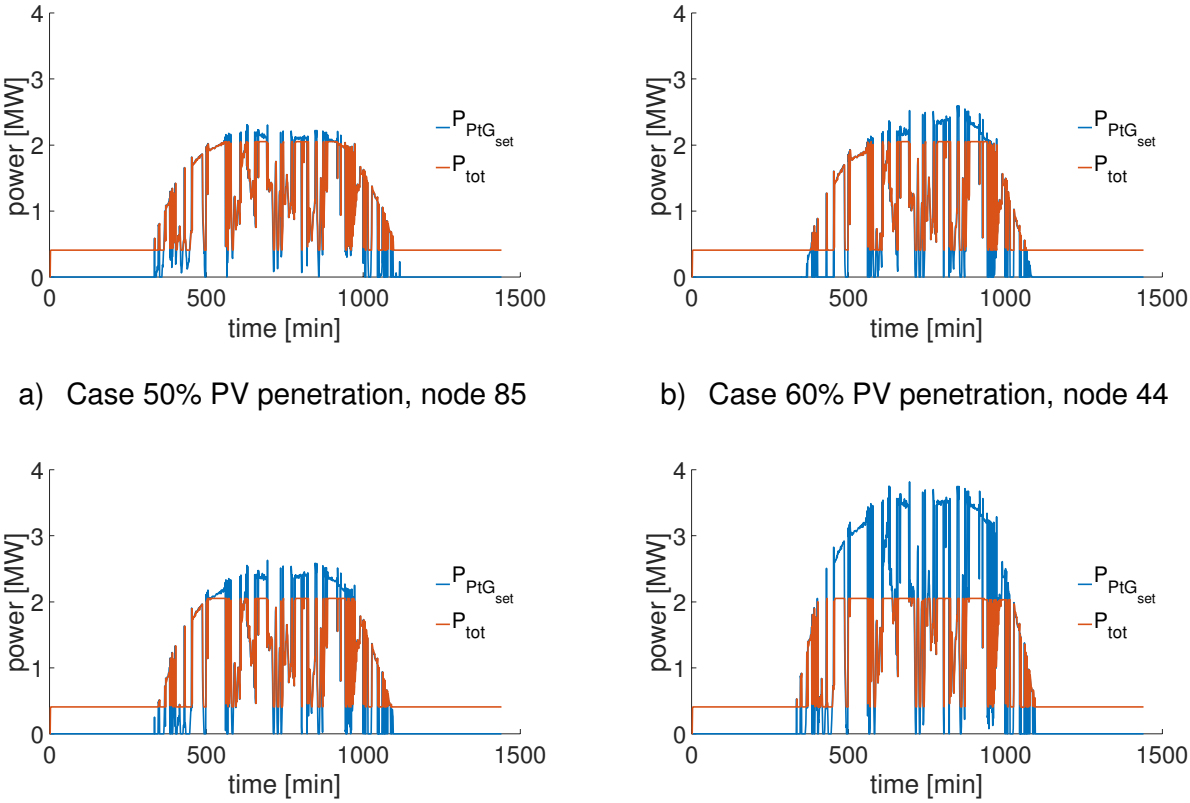

a) Case 50% PV penetration, node 85

b) Case 60% PV penetration, node 44

c) Case 70% PV penetration, node 21

d) Case 80% PV penetration, node 48

Figure 6-7: Set point and actual power of the less productive PtG, network #D1, case 2 ≤ *L* ≤ 3 km

From the figures it is possible to note that even the less productive plant is adequately operated, as also highlighted in Table 6 9.

Table 6-9 Load factors of PtG for each PV penetration level for cases 0< *L* <0.9 km and 2< *L* <3 km

Method PV Placement	PV penet	Node Min Load factor	Load factor [%]	Node Max Load factor	Load factor [%]
0<*L* ≤0.9	40 %	82	70.37	-	-
	50 %	21	68.89	27	81.66
	60 %	93	80.41	100	88.04
	70 %	13	55.07	85	86.59
	80 %	21	64.71	83	87.49
2 ≤ *L* ≤ 3	40 %	87	68.67[7]	-	-
	50 %	85	62.98	81	79.23
	60 %	44	63.38	100	79.69
	70 %	21	58.13	97	87.97
	80 %	48	73.31	97	89.68

[7] Particular case, with only 1 PtG plant installed

6.2.4 Operation during January, April and October

As mentioned before, the optimization method has been run by considering the irradiance condition of July, when the production of energy from solar is maximum. Thus, it is necessary to check if the chosen siting and sizing conditions can affect the network operation during other less challenging conditions.

The results (represented in terms of losses) are summarised in Table 6-10 (for January), in Table 6-11 (for April) and in Table 6-12 (for October). Also in these cases, the installation of new controllable loads (i.e., PtG) is beneficial for the losses in percentage terms.

Table 6-10: Value of power losses for the network #D1, method 1 – Month January

Length [km]	PV penet.	Network losses [MWh]		Network losses [%]	
		pre-installation	post-installation	pre-installation	post - installation
0<*L* ≤0.9	40 %	3.43	3.30	1.93	1.67
	50 %	3.59	4.06	2.20	1.90
	60 %	3.95	3.81	2.45	1.73
	70 %	4.44	3.78	3.00	1.81
	80 %	4.87	4.08	3.56	2.05
2 ≤ *L* ≤ 3	40 %	3.27	3.28	1.84	1.70
	50 %	3.72	4.15	2.11	1.82
	60 %	4.32	4.58	2.69	2.15
	70 %	4.90	4.67	3.26	2.35
	80 %	5.59	5.01	4.02	2.68

Table 6-11: Value of power losses for the network #D1, method 1 – Month April

Length [km]	PV penet.	Network losses [MWh]		Network losses [%]	
		pre-installation	post-installation	pre-installation	post installation
0<*L* ≤0.9	40 %	3.33	3.12	2.32	1.84
	50 %	3.63	3.98	2.64	2.06
	60 %	4.32	3.57	3.83	1.87
	70 %	5.13	3.56	5.70	2.09
	80 %	5.93	3.85	8.26	2.50
2 ≤ *L* ≤ 3	40 %	3.22	2.90	2.25	1.77
	50 %	3.85	4.16	2.83	2.03
	60 %	5.00	4.78	4.47	2.63
	70 %	6.07	5.22	6.48	3.29
	80 %	7.35	5.63	9.75	4.05

Table 6-12: Value of power losses for the network #D1, method 1 – Month October

Length [km]	PV penet.	Network losses [MWh]		Network losses [%]	
		pre-installation	post-installation	pre-installation	post installation
0<*L* ≤0.9	40 %	3.38	3.23	2.04	1.72
	50 %	3.59	4.06	2.20	1.90
	60 %	4.06	3.73	2.80	1.77
	70 %	4.65	3.70	3.63	1.89
	80 %	5.20	4.01	4.53	2.18
2 ≤ *L* ≤ 3	40 %	3.24	3.15	1.95	1.72
	50 %	3.75	4.17	2.31	1.89
	60 %	4.53	4.66	3.13	2.29
	70 %	5.26	4.84	4.01	2.61
	80 %	6.14	5.20	5.22	3.04

It is worth to note that, in terms of currents and voltages, the presence of PtG does not affect the proper operation of the network: for example, for the cases with 40% of PV penetration, a possible risk is a presence of too low voltages due to the presence of an adjunctive load. However, for both cases (i.e., 0< *L* ≤ 0.9 and 2 ≤ *L* ≤ 3) the voltages fall in the usual limits 0.9-1.1 for all the months (as shown in Figure 6-8 only for January, which is the most critical case).

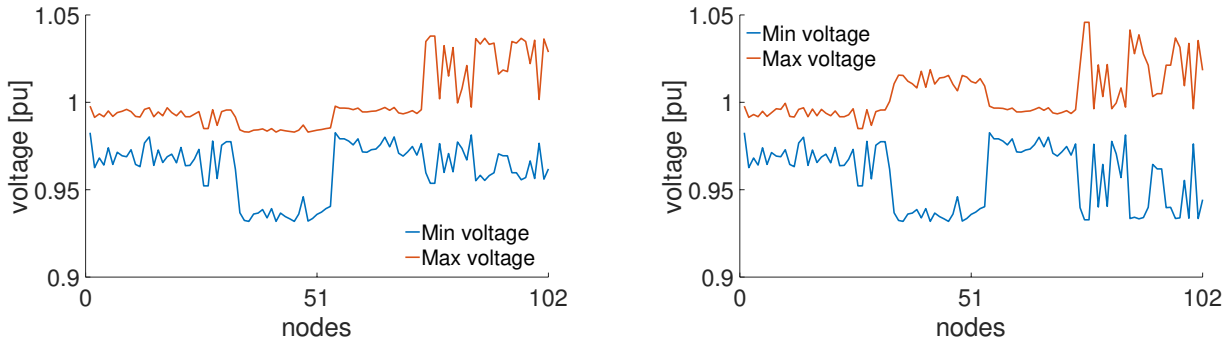

(a) 0< *L* ≤0.9 km, 40% PV penetration, January (b) 2< *L* ≤3 km, 40% PV penetrarion January

Figure 6-8: Maximum and minimum absolute voltage values

The value of reverse power flow (in energy terms) before and after the installation of PtG is shown in Table 6-13, Table 6-14 and Table 6-15 (for January, April and October, respectively). Also in these cases, the presence of PtG helps to reduce the reverse power flow, by eliminating it almost entirely.

For all the cases, the presence of PtG does not overload the network, and so the currents constraints are always verified.

Table 6-13: Comparison of the results before and after the installation of PtG, network #D1, method 1 Energy of reverse power flow - January

Length [km]	PV penet	Rev. PF pre [MWh]	Rev. PF post [MWh]	Reduction [%]
0<*L* ≤0.9	40 %	0.27	0.015	-94.51
	50 %	3.18	0.012	-99.64
	60 %	11.19	0.105	-99.07
	70 %	20.71	0.51	-97.51
	80 %	29.16	3.31	-88.64
2 ≤ *L* ≤ 3	40%	0.25	0.016	-93.67
	50 %	2.30	0.08	-96.70
	60 %	10.66	0.410	-96.15
	70 %	18.39	0.94	-94.90
	80 %	26.56	6.34	-76.13

Table 6-14: Comparison of the results before and after the installation of PtG, network #D1, method 1 Energy of reverse power flow - April

Length [km]	PV penet	Rev. PF pre [MWh]	Rev. PF post [MWh]	Reduction [%]
0<*L* ≤0.9	40 %	1.67	0.062	-96.28
	50 %	5.68	0.095	-98.33
	60 %	20.87	0.27	-98.69
	70 %	37.23	1.51	-95.94
	80 %	51.73	8.54	-83.50
2 ≤ *L* ≤ 3	40 %	1.58	0.076	-95.17
	50 %	5.26	0.14	-97.41
	60 %	19.59	0.61	-96.95
	70 %	32.26	3.35	-89.93
	80 %	46.28	13.77	-70.87

Table 6-15: Comparison of the results before and after the installation of PtG, network #D1, method 1 Energy of reverse power flow - October

Length [km]	PV penet	Rev. PF pre [MWh]	Rev. PF post [MWh]	Reduction [%]
0< *L* ≤0.9	40 %	0.50	0	-100
	50 %	3.18	0.012	-99.64
	60 %	13.81	0.14	-98.96
	70 %	25.24	0.71	-97.18
	80 %	35.73	4.76	-86.67
2 ≤ *L* ≤ 3	40 %	0.45	0	-100
	50 %	2.91	0.018	-99.39
	60 %	13.23	0.31	-97.67
	70 %	22.41	1.44	-93.56
	80 %	32.43	8.37	-74.20

6.3 Case #D1, Method 2

6.3.1 Operation during July

The second method used for siting the PV plants in the network #D1 is based on the loss allocation method: in particular, two different approaches have been used, called 2a and 2b. As shown in Table 6-16, the method 2b allows to have a more dispersed PV generation, throughout the network, whereas the method 2a, at the end, can concentrate only in one feeder the entire PV generation. It is worth to note that the use of this methodology aims to not base the siting of PV according to topological considerations of the network, but only on the basis of the nodes that can worsen the operation of the network (see [47] for more details).

Table 6-16: Distribution of the PV in the different feeders of network #D1, methods 2a and 2b

Method PV placement	Length [km]	Feeder	PV Installed Power [MW]				
			40%	50%	60%	70%	80%
Method 2a		F1	14.62	16.53	20.67	23.62	26.57
		F2	0	0	0	0	0
		F3	0	0	0	0	0
		F4	0	0	0	0	0
		F5	0	0	0	0	0
		F6	0	0	0	0	0
		F7	0	0	0	0	0
Method 2b		F1	5.25	6.33	6.33	7.63	7.63
		F2	3.45	2.11	2.11	2.26	2.66
		F3	5.56	7.65	8.05	8.20	8.20
		F4	0	0.15	0.15	0.20	0.20
		F5	0	0	0	0	5.55
		F6	0	0	0	1.30	1.95
		F7	0	1.95	5.15	5.80	5.80

The results are summarised in Table 6-17: they show that, also in these two cases, the combined use of PtG is able to reduce the problems caused by the high penetration of PV in the distribution network under analysis. It is worth to note that the method 2a, as explained before, creates really strong problems in the network, by mixing up all the three main issues previously cited, whereas the method 2b allows to isolate only one problem (i.e., reverse power flow).

Table 6-17: Comparison of the results before and after the installation of PtG, network #D1, methods 2a and 2b

Length [km]	PV penet	Rev. PF pre	Rev. PF post	Overcurr. pre	Overcurr. post	Overvolt. pre	Overvolt. post
Method 2a	40%	140	2	245	0	-	-
	50 %	201	4	653	5	-	-
	60 %	360	40	1472	57	-	-
	70 %	419	181	1885	269	18	0
	80%	482	261	2493	1186	518	0

Method 2b	40%	142	3	-	-	-	-
	50 %	256	15	-	-	-	-
	60 %	352	29	-	-	-	-
	70 %	429	147	-	-	-	-
	80 %	503	266	-	-	-	-

The levels of overcurrent for the two cases where the installation of PtG almost is able to solve the overcurrent issues (i.e, method 2a, 50% and 60% of PV penetration, respectively) are shown in Table 6-18: in this case, the remaining overloading is not important for the case 50%, especially in terms of time persistence. For the case 60%, even if the installation of PtG is beneficial, it is not resolutive: it is important to highlight here that the case study was characterised by the non-respected constraints, and was built exactly for understanding the contribution of the PtG in the increase of the hosting capacity of the network[8].

Table 6-18: Magnitude of the overloading after the PtG installation, network #D1, method 2a, 50% and 80% of PV penetration

PV penet	#Overloaded branches	Max overload	Max overloaded branch	Max Persistence [min]
50 %	2	28%	21	4
60 %	4	59 %	21	37

The size of the installed PtG plants (corresponding to the solutions reported in Table 6-17) are shown in Table 6-19.

Table 6-19: Size of the PtG plants (expressed in MW) and installation nodes, network #D1, methods 2a and 2b

Method PV Placement	PV penet	Size plant 1	Size plant 2	Size plant 3	Size plant 4	Installation nodes
Method 2a	40 %	2	-	-	-	21
	50 %	2	1	2	-	7, 21, 24
	60 %	2	1	2	2	4, 5, 20, 8
	70 %	1.5	2	2	1.5	10, 20, 24, 8
	80 %	2	1	2	2	7, 3, 20, 14
Method 2b	40 %	2	2	-	-	48, 33
	50 %	2	2	1.5	2	33, 21, 48, 8
	60 %	2	2	2	2	85, 80, 33, 98
	70 %	2	2	2	2	13, 85, 80, 33
	80 %	2	2	2	2	33, 13, 85, 80

For completeness, Table 6-20 shows the value of energy injected in the HV network after and before the installation of the PtG plants. That table shows better performance of PtG in case of concentration of the excess of RES in one feeder up to a penetration of 70%, whereas having a widespread installation of PV in the network over that limit can be faced better from PtG: this is due to the fact

[8] By the way, the complete resolution of the problem should be solved through both a proper planning procedure (not allowing the installation of too much PV in critical nodes) and through novel network operation procedure (e.g., network reconfiguration).

that, over that limit, the load factor of the PtG plants with concentrated PV is reduced, as shown in Section 6.3.2.

Table 6-20: Comparison of the results before and after the installation of PtG, network #D2, methods 2a and 2b Energy of reverse power flow

Method PV Placement	PV penet	Rev. PF pre [MWh]	Rev. PF post [MWh]	Reduction [%]
Method 2a	40 %	1.01	0	-100
	50 %	5.20	0.006	-99.87
	60 %	19.72	0.58	-97.05
	70 %	32.73	3.89	-88.09
	80 %	46.24	9.72	-78.96
Method 2b	40 %	0.86	0.017	-97.92
	50 %	3.76	0.03	-98.98
	60 %	22.37	0.69	-96.92
	70 %	36.21	1.63	-95.49
	80 %	53.82	9.78	-81.82

The losses values are reported in Table 6-21: it is worth to note that, with respect to the values reported in Table 6-8 the values of losses with the method 2a are higher than the ones obtained considering only topological features in the PV installation. With respect to the cases shown in Table 6-8, the installation of a higher load (working to absorb the excess of RES) is beneficial also with penetration equal to 50%, that with the method 1 led instead to an increase of the network losses.

Table 6-21: Value of power losses for the network #D1, methods 2a and 2b

Method PV Placement	PV penet.	Network losses [MWh]		Network losses [%]	
		pre-installation	post-installation	pre-installation	post installation
Method 2a	40%	5.06	4.63	3.75	2.86
	50 %	6.29	4.61	4.96	2.54
	60 %	8.38	4.79	8.28	2.84
	70 %	10.15	5.73	12.50	3.68
	80 %	12.17	7.60	19.87	5.12
Method 2b	40%	3.38	3.21	2.48	1.78
	50 %	3.49	3.22	2.77	1.70
	60 %	4.11	4.09	3.84	2.21
	70 %	4.36	3.77	5.37	2.39
	80 %	4.31	3.68	7.37	2.73

6.3.2 Production of SNG and “load factor” check

The production (in terms of energy) of SNG, for the different PV penetrations of the case method 2a, is shown in Figure 6-9: the production falls in the range 50 MWh – 90 MWh per day in July. It is evident that a higher concentration of PV allows an increasing SNG production, due to the fact that the load factors of the PtG plants are increasing as well (as shown in Table 6-22, method 2a) .

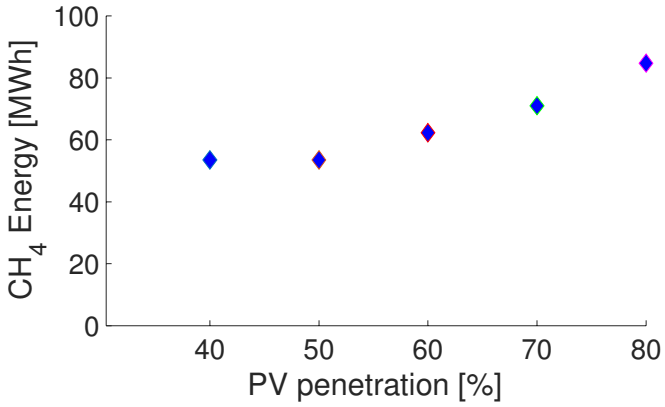

Figure 6-9: SNG production, network #D1, method 2a

For the case method 2b, the production of SNG is shown in Figure 6-10: the production of SNG seems to arrive at an asymptote, which represents the maximum value of CH_4 that can be produced. This depends on the fact that the load factors of the PtG plant with lowest and highest load factor work at the same level when PV penetration reaches 70% and 80% (as shown in Table 6-22, case Method 2b).

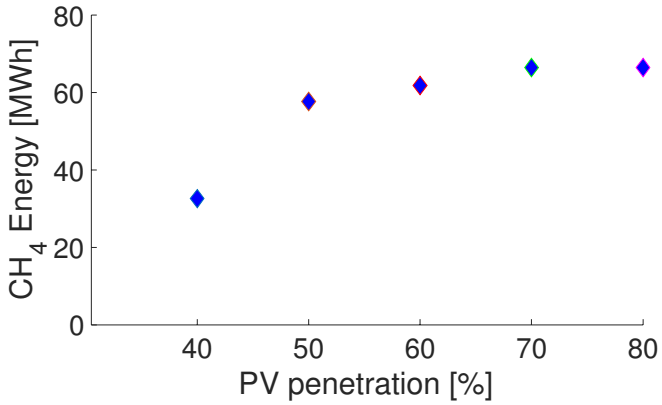

Figure 6-10: SNG production, network #D1, method 2b

Table 6-22: Load factors of PtG of each PV penetration level for the case method2a and method 2b

Method PV Placement	PV penet	Node Min Load factor	Load factor [%]	Node Max Load factor	Load factor [%]
Method 2a	40 %	21	85.63	-	-
	50 %	24	74.65	21	92.67
	60 %	4	58.56	20	83.47
	70 %	10	55.27	20	85.37
	80 %	20	87.39	14	94.14
Method 2b	40 %	48	62.77	33	75.31
	50 %	8	47.70	33	75.80
	60 %	98	63.55	85	77.57
	70 %	80	63.38	33	78.18
	80 %	80	67.35	33	79.15

6.3.3 Operation during January, April and October

In this case, the installation of PtG increases the losses in absolute terms for all the other months and for every PV penetration, as shown in Table 6-23, Table 6-24 and Table 6-25. From the point of view of the percentage losses, the addition of new loads composed of PtG results beneficial, because their value decreases.

Table 6-23: Value of power losses for the network #D1, methods 2a and 2b – Month January

Method PV Placement	PV penet.	Network losses [MWh]		Network losses [%]	
		pre-installation	post-installation	pre-installation	post installation
Method 2a	40 %	4.38	4.17	2.47	2.14
	50 %	5.14	5.40	2.92	2.41
	60 %	6.22	4.64	3.88	2.22
	70 %	7.16	5.06	4.80	2.51
	80 %	8.23	5.93	5.97	2.97
Method 2b	40 %	3.51	3.78	1.94	1.80
	50 %	3.64	3.89	2.09	1.75
	60 %	3.93	4.05	2.46	1.90
	70 %	4.08	3.93	2.74	1.91
	80 %	4.05	3.88	2.98	2.01

Table 6-24: Value of power losses for the network #D1, methods 2a and 2b – Month April

Method PV Placement	PV penet.	Network losses [MWh]		Network losses [%]	
		pre-installation	post-installation	pre-installation	post installation
Method 2a	40 %	5.09	4.64	3.55	2.78
	50 %	6.30	5.90	4.62	3.04
	60 %	8.26	4.72	7.49	2.69
	70 %	9.96	5.62	10.86	3.48
	80 %	11.89	7.48	16.27	4.87
Method 2b	40 %	3.58	3.34	2.43	1.79
	50 %	3.74	3.88	2.26	1.77
	60 %	4.28	3.99	3.89	2.19
	70 %	4.53	3.92	4.92	2.34
	80 %	4.49	3.34	6.34	2.62

Table 6-25: Value of power losses for the network #D1, methods 2a and 2b – Month October

Method PV Placement	PV penet.	Network losses [MWh]		Network losses [%]	
		pre-installation	post-installation	pre-installation	post installation
Method 2a	40 %	4.60	4.31	2.77	2.32
	50 %	5.51	5.54	3.38	2.60
	60 %	6.88	4.67	4.79	2.36
	70 %	8.06	5.21	6.21	2.77
	80 %	9.41	6.39	8.12	3.48
Method 2b	40 %	3.52	3.65	2.08	1.80
	50 %	3.63	3.73	2.26	1.74
	60 %	4.03	4.03	2.82	1.98
	70 %	4.20	3.92	3.24	2.02
	80 %	4.17	3.86	3.65	2.16

As shown in Table 6-17, the configuration obtained by using the method 2b is not affected by any constraint-related issues (i.e., overcurrent and overvoltage) with the data referring to July. So, it is necessary to verify the condition of the network in the other months, for checking the constraints after the installation of PtG. The same check is made for the configuration obtained by using the method 2a. For both the cases the voltages fall in the range 0.9-1.1 pu for all the months, and, as matter of example, the maximum and minimum voltages related to January (Figure 6-11).

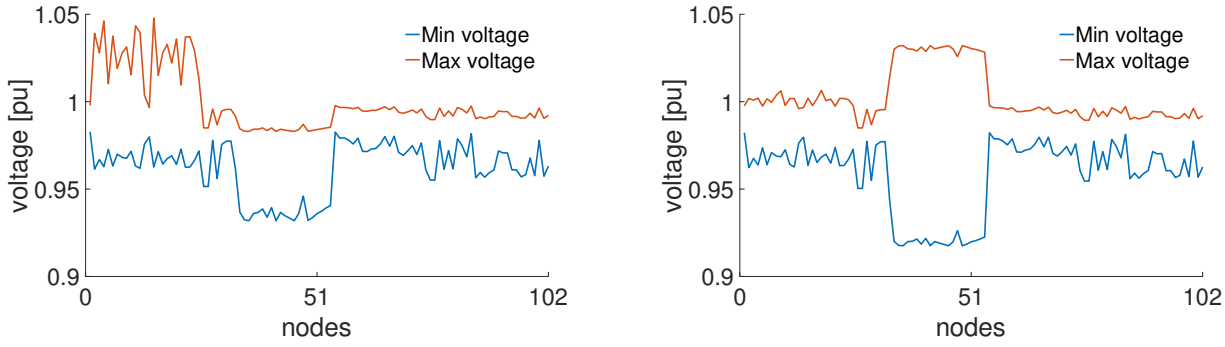

(a) 40% PV penetration, January, method 2a (b) 40% PV penetration, January, method 2b

Figure 6-11: Maximum and minimum absolute voltage values for January, network #D1

As shown for the method 1, also for both the methods 2 the implementation of PtG is really beneficial in terms of reduction of the energy of injected in the HV grid, also for the other months (see Table 6-26, Table 6-27, and Table 6-28).

Table 6-26: Comparison of the results before and after the installation of PtG, network #D1, methods 2a and 2b Energy of reverse power flow - January

Method PV Placement	PV penet	Rev. PF pre [MWh]	Rev. PF post [MWh]	Reduction [%]
Method 2a	40 %	0.12	0	-100
	50 %	2.17	0	-100
	60 %	10.59	0.30	-97.14
	70 %	18.14	0.94	-94.80
	80 %	26.04	3.84	-85.21
Method 2b	40 %	0.08	0.001	-98.09
	50 %	3.53	0.14	-95.77
	60 %	12.19	0.47	-96.14
	70 %	20.17	0.91	-95.26
	80 %	30.35	4.17	-86.26

Table 6-27: Comparison of the results before and after the installation of PtG, network #D1, methods 2a and 2b Energy of reverse power flow - April

Method PV Placement	PV penet	Rev. PF pre [MWh]	Rev. PF post [MWh]	Reduction [%]
Method 2a	40 %	1.01	0	-100
	50 %	5.20	0.006	-99.87
	60 %	19.72	0.58	-97.05
	70 %	32.73	3.89	-88.09
	80 %	46.24	9.72	-78.96
Method 2b	40 %	0.86	0.017	-97.92
	50 %	3.76	0.03	-98.98
	60 %	22.37	0.69	-96.92
	70 %	36.21	1.63	-95.49
	80 %	53.82	9.78	-81.82

Table 6-28: Comparison of the results before and after the installation of PtG, network #D1, methods 2a and 2b Energy of reverse power flow - October

Method PV Placement	PV penet	Rev. PF pre [MWh]	Rev. PF post [MWh]	Reduction [%]
Method 2a	40 %	0.18	0	-100
	50 %	2.85	0	-100
	60 %	13.03	0.23	-98.23
	70 %	21.96	1.65	-92.46
	80 %	31.72	5.27	-83.36
Method 2b	40 %	0.13	0	-100
	50 %	4.34	0.05	-98.81
	60 %	14.87	0.34	-97.77
	70 %	24.44	1.03	-95.78
	80 %	37.19	5.91	-84.11

6.4 Case #D2

6.4.1 Operation during July

The first case study regarding the network #D2 considers PV plants installed in correspondence of the final node of lines having length *L* falling in the range 0< *L* ≤0.45 km (Table 6-29): due to the characteristics of the network lines, this case allows to study a case where all the feeders of the network have a similar amount of PV capacity installed, that means that the number of PtG plants to be used will be higher than in in the network #D1.

Table 6-29: Distribution of the PV in the first case study of network #D2

Method PV placement	Length [km]	Feeder	PV Installed Power [MW]					
			30%	40%	50%	60%	70%	80%
Method 1	0< *L* ≤0.45	F1	5.09	6.79	8.48	10.18	11.88	13.58
		F2	7.90	10.53	13.16	15.80	18.43	21.06
		F3	6.07	8.09	10.12	12.14	14.16	16.19
		F4	8.78	11.71	14.64	17.57	20.49	23.42
		F5	7.07	9.43	11.79	14.14	16.50	18.86
		F6	7.57	10.10	12.63	15.15	17.68	20.20
		F7	7.67	10.23	12.79	15.34	17.90	20.46
		F8	4.94	6.59	8.24	9.89	11.54	13.19
		F9	8.96	11.94	14.93	17.92	20.91	23.89
		F10	3.58	4.78	5.98	7.17	8.37	9.57

The second case study regarding the network #D2 considers PV plants installed in correspondence of the final node of lines having length *L* falling in the range 0.5 ≤ *L* ≤3 km (Table 6-30): due to the characteristics of the network lines, this case allows to study a case where two of the feeders show a really high penetration of PV (i.e., feeders F9 and F10), whereas the other see a lower amount of PV installed.

Table 6-30: Distribution of the PV in the second case study of network #D2

Method PV placement	Length [km]	Feeder	PV Installed Power [MW]			
			30%	40%	50%	60%
Method 1	0.5 ≤ *L* ≤3	F1	2.55	3.41	4.26	5.11
		F2	2.85	3.80	4.76	5.71
		F3	8.26	11.02	13.77	16.53
		F4	1.51	2.02	2.52	3.03
		F5	5.74	7.65	9.57	11.48
		F6	1.04	1.39	1.74	2.09
		F7	1.48	1.97	2.46	2.96
		F8	4.97	6.63	8.28	9.94
		F9	19.04	25.36	31.73	38.08
		F10	20.19	26.92	33.65	40.38

The results are summarised in Table 6-31: they show that, also in these two case studies, the combined use of PtG is able to reduce the problems caused by the high penetration of RES in the distribution network under analysis.

Table 6-31: Comparison of the results before and after the installation of PtG, network #D2

Length [km]	PV penet.	Rev. PF pre	Rev. PF post	Overcurr. pre	Overcurr. post	Overvolt. pre	Overvolt. post
$0<L\leq0.45$	30%	16	1	-	-	-	-
	40%	161	27	-	-	-	-
	50 %	278	32	-	-	-	-
	60 %	362	42	-	-	-	-
	70 %	411	159	2	1	-	-
	80 %	459	203	426	9	-	-
$0.5\leq L\leq3$	30 %	11	0	4	0	-	-
	40 %	161	10	1287	80	17	0
	50 %	268	56	2972	389	909	0
	60 %	354	150	4954	667	1810	0

The size of the installed PtG plants (corresponding to the solutions reported in Table 6-31) is shown in Table 6-32 (for the case $0< L \leq0.45$ km) and in Table 6-33 (for the case $0.5\leq L \leq 3$ km). For the first case, the maximum size allowable is 4 MW, whereas the latter case was forced to work with maximum size 2 MW. As shown from the combination of Table 6-31, Table 6-32 and Table 6-33, the combined presence of widespread and high penetration of RES needs a larger number and size of PtG plants.

Table 6-32: Size of the PtG plants (expressed in MW) and installation nodes, network #D2, $0< L \leq 0.45$ km

	PV penet.											
	30%		40%		50%		60%		70%		80%	
Plants	Size plant	Node	Size plant	Node	Size plant	Node	Size plant	Node	Size plant	Node	Size Plant	Node
1	2.5	95	3	11	2	11	2	11	2	11	3	62
2		-	3	5	2	123	2	123	2	123	2	77
3		-	3	77	4	62	4	62	3	62	2	87
4		-	3	120	3	57	3	57	3	57	2	107
5		-	3	112	2	100	2	100	2	100	4	120
6		-	3	88	1	97	1	97	1	97	2	126
7		-	2.5	62	2	107	2	107	2	107	2	127
8		-		-	3	95	3	95	3	95	3	130
9		-		-	3	117	3	117	2	117	2	11
10		-		-	3	112	3	112	3	112	2	100
11		-		-	4	120	4	120	3	120	4	97
12		-		-	3	130	3	130	3	130	3	117
13		-		-	4	127	4	127	3	127	1	112
14		-		-	3	126	3	126	3	126	2	146
15		-		-	2	146	2	146	2	146	2	149
16		-		-	2	9	2	9	2	9	2	145

17	-	-	3	149	3	149	3	149	3	157
18	-	-	3	145	3	145	3	145	2	57
19	-	-	-	-	-	-	1	157	2	123
20	-	-	-	-	-	-	1	156	1	95

Table 6-33: Size of the PtG plants (expressed in MW) and installation nodes, network #D2, $0.5 \leq L \leq 3$

	PV penet.=30%		PV penet.=40%		PV penet.=50%		PV penet.=60%	
Plants	**Size plant**	**Node**	**Size plant**	**Node**	**Size plant**	**Node**	**Size Plant**	**Node**
1	2	32	2	6	2	6	2	6
2	-	-	1	14	2	14	2	14
3	-	-	1	24	2	24	2	24
4	-	-	1	32	1	31	2	31
5	-	-	2	129	2	32	2	32
6	-	-	2	141	2	129	2	129
7	-	-	1	144	2	141	2	141
8	-	-	1	149	2	144	2	144
9	-	-	1	152	1	149	2	149
10	-	-	1	170	1	152	2	152
11	-	-	2	173	1	170	2	170
12	-	-	2	181	2	173	2	173
13	-	-	-	-	2	181	2	181
14	-	-	-	-	2	188	2	188
15	-	-	-	-	2	192	2	192
16	-	-	-	-	2	198	2	198
17	-	-	-	-	2	200	2	200

For completeness, Table 6-34 shows the value of energy injected in the HV network after and before the installation of the PtG plants. In terms of energy, the reverse power flow is definitely reduced, and even completed eliminated 30% of PV penetration.

Table 6-34: Comparison of the results before and after the installation of PtG, network #D2 – Energy of reverse power flow

Length [km]	PV penet	Rev. PF pre [MWh]	Rev. PF post [MWh]	Reduction [%]
$0<L \leq 0.450$	30 %	0.18	0.002	-98.68
	40 %	27.09	3.20	-88.17
	50 %	81.67	6.49	-92.05
	60 %	152.51	13.10	-91.40
	70 %	231.66	41.97	-81,88
	80 %	316.84	88.61	-72.03
$0.5 \leq L \leq 3$	30 %	0.11	0	-100
	40 %	25.82	0.74	-97.13
	50 %	76.80	4.42	-94.23
	60 %	144.40	26.19	-81.85

Table 6-35 shows that in general the installation of PtG improves the network losses value in percentage terms, for both the case studies (only the case 0<*L* ≤0.45 sees equal value pre and post PtG installation), and for the case 0.5 ≤ *L* ≤ 3 km also in absolute value. This can be referred to the fact that longer lines mean higher resistance and so the reduction of the flows in those lines is beneficial for the entire system.

Table 6-35: Value of power losses for the network #D2

Length [km]	PV penet.	Network losses [MWh]		Network losses [%]	
		pre-installation	post-installation	pre-installation	post - installation
0<*L* ≤0.45	30%	6.14	6.22	0.80	0.80
	40%	5.74	6.31	0.87	0.84
	50 %	5.68	7.14	1.04	0.79
	60 %	6.06	7.00	1.40	0.82
	70 %	6.83	6.97	2.11	0.91
	80 %	7.98	7.46	3.71	1.10
0.5 ≤ *L* ≤ 3	30 %	7.86	7.61	1.03	0.97
	40 %	9.34	8.59	1.43	1.02
	50 %	11.80	10.35	2.17	1.18
	60 %	15.19	11.36	3.51	1.36

6.4.2 Production of SNG and "load factor" check

The production (in terms of energy) of SNG, for the different PV penetrations of the case 0<*L* ≤0.45 km, is shown in Figure 6-12: the production falls in the range 5 MWh – 350 MWh per day in July. With different penetration the production amounts are not so different, due to the fact that in this case the PV is well widespread in all the network and the size of the plants is not so different. In the case of 30% penetration the production of SNG is very low, as the network problems are practically non-existent and only one PtG has been added.

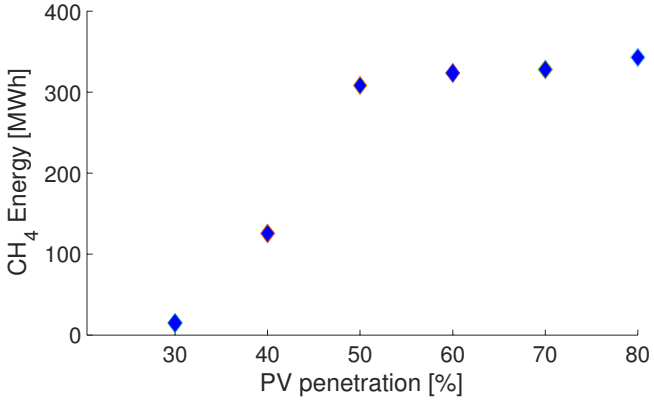

Figure 6-12: SNG production, network #D2, case 0<*L* ≤0.45

For the case 0.5 ≤ *L* ≤ 3 km, the production of SNG is analogous.

Due to the higher number of PtG plants installed, the load factor for the network #D2 is shown as histogram, in Figure 6-13 (case 0< *L* ≤0.45) and in Figure 6-14 (case 0.5≤ *L* ≤3). Every class contains a number of PtG plants.

On one hand, for the case shown in Figure 6-13 it is worth to note that up to 50% most of the PtG plants are characterized of a load factor falling in the range 35-45%, whereas with higher PV penetration the load factor increases.

On the other hand, the case shown in Figure 6-14 is characterized by a higher load factor also with lower penetration, thanks to the lower number of PtG plants installed and their lower sizes.

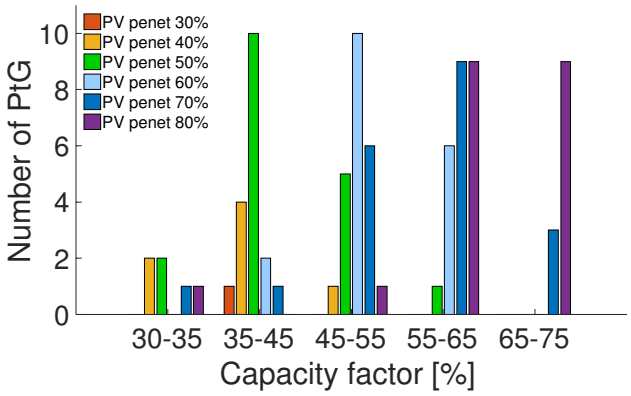

Figure 6-13: Load factors distribution of PtG for every PV penetration, network #D2, case $0 < L \leq 0.45$ km

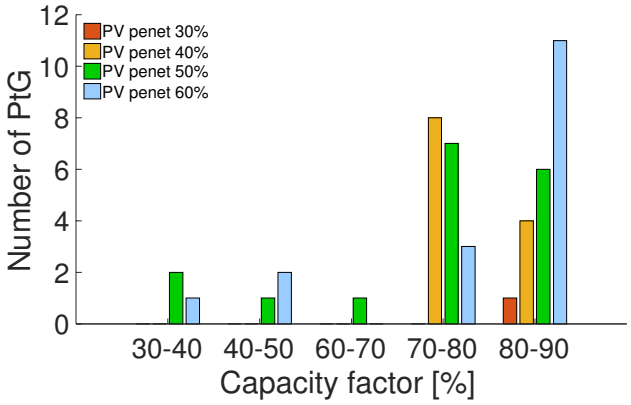

Figure 6-14: Load factors distribution of PtG for every PV penetration, network #D2, case $0.5< L \leq 3$km

6.4.3 Operation during January, April and October

Also in this case, it is necessary to verify the network conditions during the other months: the representation of the network conditions by means of the losses value is shown in Table 6-36, Table 6-37 and Table 6-38. The results confirm what seen before: the network losses increase in absolute terms, but in percentage their value decreases (except for the case $0<L \leq 0.45$, with PV penetration 30%, for which the installation of PtG sees equal percentage losses pre and post PtG installation).

Table 6-36: Value of power losses for the network #D2, – Month January

Length [km]	PV penet.	Network losses [MWh]		Network losses [%]	
		pre-installation	post-installation	pre-installation	post - installation
0<*L* ≤0.45	30%	7.82	7.92	0.85	0.85
	40%	7.42	8.24	0.85	0.84
	50 %	7.23	9.30	0.88	0.85
	60 %	7.19	9.15	0.94	0.85
	70 %	7.32	8.88	1.03	0.86
	80 %	7.60	8.95	1.16	0.90
0.5 ≤ *L* ≤ 3	30 %	8.32	8.35	0.90	0.88
	40 %	8.69	9.25	1.00	0.92
	50 %	9.46	11.64	1.16	1.10
	60 %	10.62	12.10	1.39	1.15

Table 6-37: Value of power losses for the network #2 – Month April

Length [km]	PV penet.	Network losses [MWh]		Network losses [%]	
		pre-installation	post-installation	pre-installation	post - installation
0<*L* ≤0.45	30%	7.04	7.13	0.81	0.81
	40%	6.50	7.26	0.82	0.80
	50 %	6.22	8.08	0.87	0.80
	60 %	6.16	7.76	0.96	0.81
	70 %	6.30	7.45	1.11	0.83
	80 %	6.66	7.56	1.35	0.90
0.5 ≤ *L* ≤ 3	30 %	7.73	7.71	0.89	0.87
	40 %	8.20	8.49	1.04	0.90
	50 %	9.22	10.93	1.29	1.10
	60 %	10.76	11.52	1.68	1.17

Table 6-38: Value of power losses for the network #D2– Month October

Length [km]	PV penet.	Network losses [MWh]		Network losses [%]	
		pre-installation	post-installation	pre-installation	post - installation
0<*L* ≤0.45	30%	7.60	7.69	0.85	0.85
	40%	7.27	8.07	0.88	0.85
	50 %	7.21	9.18	0.95	0.85
	60 %	7.38	9.03	1.06	0.87
	70 %	7.78	8.87	1.24	0.91
	80 %	8.39	9.15	1.50	1.01
0.5 ≤ *L* ≤ 3	30 %	8.49	8.46	0.93	0.95
	40 %	9.27	9.45	0.98	1.12
	50 %	10.62	11.75	1.16	1.40
	60 %	12.50	12.54	1.27	1.81

The check of the correct operation of the network #D2 in the other months has been done and here represented through the results referring to January, shown in Figure 6-15.

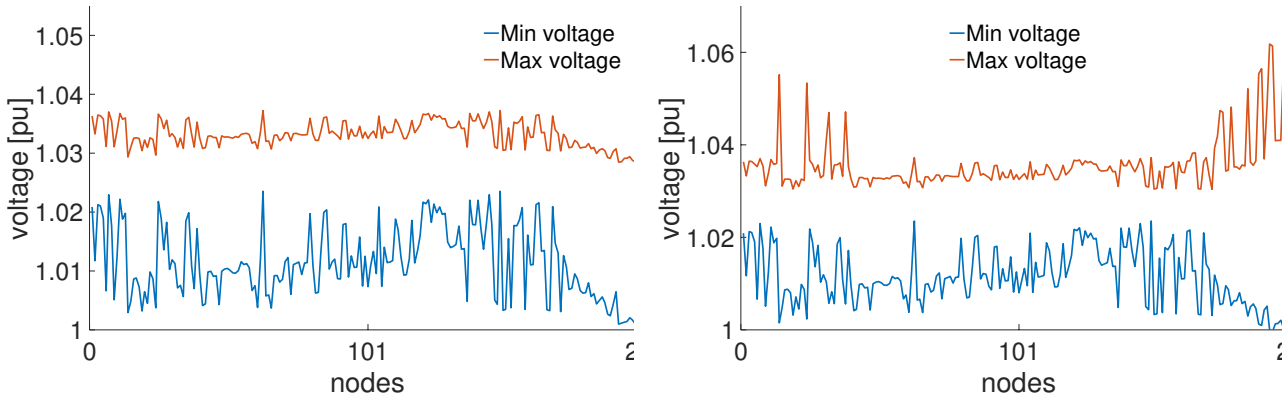

(a) 30% PV penetration, January, case $0<L\leq0.45$ km

(b) 30% PV penetration, January, case $0.5\leq L\leq 3$ km

Figure 6-15: Maximum and minimum absolute voltage values for January, network #D1

6.5 Distribution system result summary

The results obtained are really considered satisfactory, since the network problems (i.e., reverse power flow, overcurrents and overvoltages) have been significantly reduced and, in some cases, completely eliminated. By considering the network #D1 (i.e., the rural network) the case $0< L \leq 0.9$ km sees a reduction of the reverse power flow energy falling in the range 79-95%, whereas in the case $2 \leq L \leq 3$ km the reduction lies in the range 67-95 %. In all cases, the installation of PtG is also able to alleviate the constraints problems, by reaching their complete elimination for the lower PV penetrations. Also the case studies based on the exploitation of the loss allocation factors (i.e., methods 2a and 2b) are in line with the above results, with no particular differences among the concentrated and widespread PV cases.

For the network #D2 (i.e, the semi-urban network), the number and the sizes of the PtG plants are higher than the ones used for the network #D1, due to the higher number of nodes and higher load. The results obtained are really good, with a reduction of the reverse power flow energy falling in the range 72-98%, with better performances for lower PV penetration.

Furthermore, in all the cases the installation of PtG plants did not worsen the percentage losses of the network, and generally led to reduce their values and no problems of undervoltages have been found in the months with lower PV penetration

The load factor of the plants provides information on how much a PtG plant is used: these values are particularly high (even around 90% for some cases of the network # D1) and their variation depends on the PV penetration value, on the positioning of the PtG and on the size. This suggests that, as all the storage facilities, the installation of PtG plants at the level of distribution system has to be made by considering the local characteristics of the network (load, PV penetration and network parameter).

In conclusion, it can be said that the addition of PtG systems in a distribution network can improve the stabilization of the network even for very high (even extreme) penetrations, thus increasing the ability of a network to host a higher penetration of intermittent generation.

7 Conclusions

This Deliverable investigated the impact of PtG on the network operation, both at transmission and distribution level.

For the transmission level three different networks (one test network and two European networks) have been implemented: all the case studies showed that the introduction of PtG is beneficial for the network operation. The benefits have been calculated in technical terms, seen as the reduction of the variation that the traditional generators have to make on their production for facing the RES variation. This has been simulated by making a two level program, where the first part is devoted to simulate an hourly generator dispatching based on the load value and the expected value of the RES, whereas the second part aims to redispatch the traditional generators because of the change of the net load due to the difference between the expected and actual value of RES-based power plants.

For the distribution system, two different networks have been used: the choice of the network has been driven by the demo sites, which are installed either in a rural area (Troia, Italy) or in a semi-urban area (Solothurn, Switzerland). The cases studied in this Deliverable comprise high RES penetration network sample, to understand the potential of PtG in the network stabilisation. In all the cases, the introduction of PtG alleviated the simulated network issues, allowing even the complete resolution of some of the problems. In this case, a network which can cause problem to the HV system was allowed to operate properly. In other cases, the starting network was not respecting the operational constraints: in these cases, the introduction of PtG was able to reduce the network problems a lot, that means an increase of the network hosting capacity.

All the above simulations have been carried out by inserting in the network the “PtG node”, that is the electrical representation of the PtG plant, considering the full production chain (electrolyser, buffer, compressors, methanation step and so on). In this way, the response time of the plant has been properly modelled.

The next steps of this work will be basically two: i) the complete analysis of the impact on the transmission system operation with long term future scenarios, and ii) the impact of PtG on network infrastructure. These two topics are closely connected, because both are related to the future development of the electricity grids (in terms of future investments already scheduled or under investigation). These two aspects will be addressed in the next months and published in D6.6 “Report on the impacts of the PtG on selected scenarios”, that will be delivered in M42 (August 2019).

8 Appendix A: Calculation of the AC power for PV fields

The irradiance can be converted in power though the model shown in this appendix. In particular, the model allows to pass from the irradiance (expressed in W/m^2) to an adimensional value representing the ratio between the power produced by the PV plant at AC side (P_{AC}, expressed in [W]) and the nominal power of the plant (P_{nom}, expressed in [Wp],)i.e., $\frac{P_{AC}}{P_{nom}}$. Eventually, this ratio represents the production profile, i.e., the power produced by the plant expressed in per unit (pu).

This step is made by calculating the temperature of the PV panel T_c by starting from the temperature of the air, as shown in (10), and then using it to calculate the *thermal efficiency* η_{th} which is used for calculating the pu PV production (formulas (11) and (12)) [33]:

$$T_c = T_a + \frac{NOCT-20}{800} \cdot G \quad \textbf{(10)}$$

$$\eta_{th} = 1 - \alpha_{th} \cdot (T_c - 25) \quad \textbf{(11)}$$

$$\frac{P_{AC}}{P_{nom}} = \eta_{DC-AC} \cdot \frac{G}{1000} \cdot \eta_{th} \quad \textbf{(12)}$$

Where T_c is the estimated temperature of the PV panel (expressed in °C), T_a is the air temperature, $NOCT$ is nominal operating cell temperature (imposed equal to 45°C), η_{th} is the reduction of production due to the temperature of the PV panel, G [W/m^2] is the radiation, $\alpha_{th} = 0.45\%$ is the loss coefficient due to the temperature, and $\eta_{DC-AC} = 0.828$ represents the efficiency due to cables, connections, inverter and so on.

9 Appendix B: Day-ahead market and Intraday market

After the deregulation of the electrical system the vertically integrated power system was split up and the state-owned utilities privatized. The deregulation and privatization mainly regarded the electricity production: at supply side, many countries established wholesale markets, where the generators can sell generated electricity under competition. Due to the non-storability of electricity in large scales and the constant need for balancing of generation and demand, a real spot market with immediate delivery cannot exist for power. Hence, most electricity markets perform a day-ahead trading, where the generation/demand schedules and prices for the 24 hours of the following day are determined. The price determination is often done by an auctioning process. In addition to the day-ahead trading, markets with trading shortly before delivery (usually 5-15 minutes), called as real-time or intraday market, also exist. The real-time trading is usually used as a kind of balancing market to adjust the predetermined quantities of the day-ahead market [48].

The day-ahead market is the main area for trading power. The day-ahead energy market is a forward market where generation suppliers sell energy and Load Serving Entities (LSEs) buy energy in advance with respect to the time when energy is produced and consumed. An energy buyer needs to assess how much energy it will need to meet demand in the following day, and how much it is willing to pay for this volume of demanded power, hour by hour. The energy seller also needs to decide how much it can deliver and at what price, hour by hour. The market clearing engine performs an optimization program, generally with the objective function of minimizing total costs or maximizing the social surplus, taking into account some technical and financial constraints.

The real-time market starts physical operations at midnight of the operating day, based on schedules obtained from the day-ahead market and updated in the hours before midnight. The role of the real-time market is mainly to re-dispatch the already committed resources and commit new fast-start resources to meet real-time load and other changes to the system conditions. These changes include weather changes leading to deviations in variable renewable energy sources' production, forced outages of the resources and outages of network facilities.

The real-time market clearing prices reflect the actual operation of the resources participating in the market and are used to re-settle all the generation resources and loads that deviate from their day-ahead schedules. The real-time market calculates real-time marginal prices, usually on a 5-minute basis [49]. It is worth to note that the largest part of the actual energy gets settled in the day-ahead market, and only a small percentage gets settled in the real-time market. Usually in European power system, the market-based ancillary services are provided through an independent market, separated from the energy market; whereas in the American markets, energy and ancillary services are co-optimized in the same market. Inside the United States, all ISOs operate electricity markets in a sequence of day-ahead and real-time markets (sometimes called a two-settlement system). Following day-ahead market closure, real-time (or balancing) energy and ancillary service markets are cleared on an hourly basis during the operation day to ensure resources can meet any changing conditions in an efficient manner, e.g. change of load or renewable production with respect to the day-ahead forecasted values [49].

10 Appendix C: OPF formulation

The presence of a number of generators connected to the same infrastructure leads to consider which of them should be dispatched as first. This kind of choice can be done by making a ranking based on an economic merit order, by minimizing the total cost $f(\mathbf{x})$ through on an optimization problem, i.e.:

$$\min_{\mathbf{x}} f(\mathbf{x}) \tag{13}$$

subject to equality $\mathbf{g}(\mathbf{x})$ and inequality $\mathbf{h}(\mathbf{x})$ constraint, as well as to the limits of the state variables $\mathbf{x}$:

$$\mathbf{g}(\mathbf{x}) = \mathbf{0} \tag{14}$$

$$\mathbf{h}(\mathbf{x}) \leq \mathbf{0} \tag{15}$$

$$\mathbf{x}_{min} \leq \mathbf{x} \leq \mathbf{x}_{max} \tag{16}$$

In our cases, the problem variables are the angle of the voltages and the generated power of the generators, which cannot exceed their limits. The existence of time variant loads implies a variation in the production of the different units: this variation is physically limited by ramp rate constraints, which do not allow the sudden change of the generation[9].

[9] This condition affects only the structure of the inequality constraints, which should consider also the transition from one state to the other during the time

11 Appendix D: Description of the script for the transmission network case studies

11.1 Network #T1

The script developed and tested with the network #T1 contains some simplifications, i.e.:

- no OPF existing: the distribution of the load is made according to the size and the ramp rates of the generators.
- the network calculations are made by means of Newton-Raphson power flow algorithm and so it is possible to find one slack node, which has to face the load variations and supply the network losses
- only one RES power plant is considered

By the way, its implementation allowed to study the impact of different generation types, creating a re-dispatching algorithm based on the generator technical features and implementing a raw model of a PtG plant (considering in that case only the electrical interface, i.e., the electrolyser characteristics). Furthermore, a complete and scalable input data format has been introduced. The main loop of the code is shown in Figure 11-1.

Different blocks have different aims, in particular:

- time.m: manages time-related operations, for example it updates the loads and generation based on the load and generation profiles in the current time step
- dPredist.m: evaluates the existence of residual load dP, caused by new scheduled values of the generation (due to the variation of the load). By considering the generator characteristics (i.e. current generation value and ramp rates values), it redistributes dP among generators that can do it, based each generators ramp value and size
- feasibility.m: checks the feasibility of the system, and adds warnings to the mpc if violations are found, resets the warnings if no violations have been detected. Also calculates apparent power flowing in the network branches
- protection.m: it triggers protections based on warnings and timers. This functionality has been used
- runpf: it calculated the solution of the network based on the Newton-Raphson algorithm. The native code of Matpower [38] has been modified for accepting further fields not existing in the original version

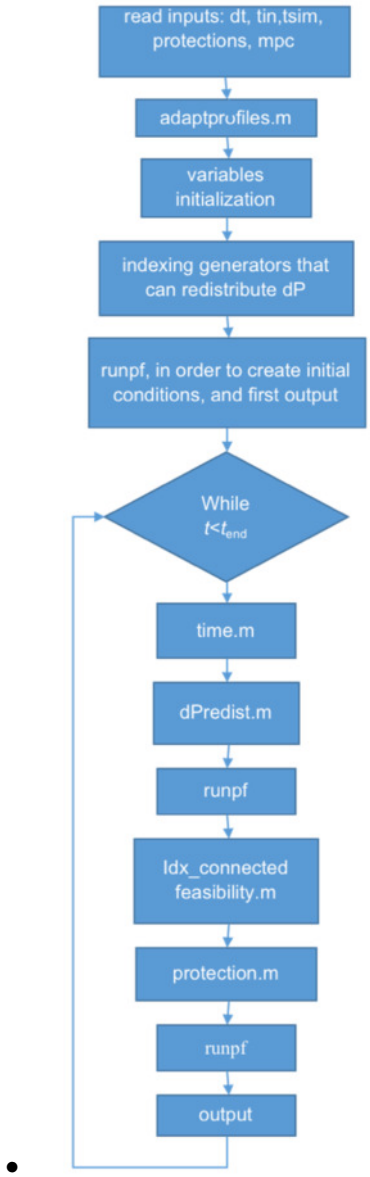

Figure 11-1: Main loop of the script applied at the network #T1

11.2 Networks #T2 and #T3

11.2.1 Main characteristics

The script is composed of two main files, called DayAheadMarket.m and RealTimeMarket.m. They run two optimizations:

- the first one, based on expected values of load and non-dispatchable generation (emulating a day-ahead market, DAM),
- the latter one based on the actual values of PV and wind generation (emulating a real time IDM market).

By comparing the results of the two markets it is possible to evaluate the impact of the variability of PV and wind on the system, and thus, inserting PtG units, also the effect that these units can have on the electrical system.

PtG units are modelled within Matpower as dispatchable loads, which are modelled as negative generators. Within the day-ahead script they are considered as constant loads, working at a fixed percentage of their rated power.

As mentioned in Section 3.8.3, the script is based on Matpower [38]: this choice allows to take advantage of Matlab flexibility, and of the possibility to easily adapt the input data at the ones referring to new networks. The model does not account for frequency variation and reactive power managing, since it relies on DC power flow (for reducing the computational time).

11.2.2 Description of the input data

Both scripts contain a similar input section, in which the Matpower case-file (called later mpc) is loaded. A file “mpc” is a structure that gathers all the necessary network parameters.

The main fields contain all the information regarding:

- buses (location, load value)
- AC lines (starting and ending nodes, capacity, number of equivalent lines in parallel)
- generators (type, status, size, ramp up and ramp down, location, marginal cost, minimum power)
- DC lines (starting and ending nodes, capacity)

The types of generators considered are the following:

- biomass
- coal
- geothermal
- lignite
- nuclear
- Closed Cycle Gas Turbine (CCGT)
- Open Cycle Gas Turbine (OCGT)
- oil
- onwind
- offwind
- solar
- Run on River (ROR) power plant
- Hydro-pump

In the scripts developed, additional columns have been added in order to store more information without interfering with Matpower functionality. For example, within the bus field has been added a

column that stores all the information regarding the bus country, and in generator field a new column allows to store the type of generator. This simplifies a lot the application of properties to some elements, as well as the filtering of the data along the script execution.

Load profiles are expressed in MW and are network specific, due to the fact that every network has its own different redistribution of loads within every country.

PV profiles are based essentially on irradiance profiles and the given installed PV capacity. Thanks to the formulation reported in Appendix A: Calculation of the AC power for PV fields, the power profiles is calculated [33]. It is worth to note that in the day-ahead script wind and PV profiles are hourly values, whereas in the real-time script the time step is chosen by the users and lies in the range 5 to 15 minutes, as it can be seen in Appendix B: Day-ahead market and Intraday market.

11.2.3 Limitations

From the time calculation point of view, the script performance is strongly depending from the DC Unit De-commitment OPF (DUOPF) implemented in Matpower, which is used for the solution of the DAM.

Matpower DUOPF routine is a basic deterministic routine that changes generators' status with a logic similar to the one of the branch exchange method. As stated by [38], the routine is not efficient as the number of generators increases. The original deterministic logic has been modified to include a basic heuristic, which excludes some of the most expansive generators at the minimum power output. By doing this the computational time required decreases significantly, from 1500 seconds circa down to 500 seconds for network #T3.

Another example can show how much DUOPF computational time is directly linked to the number of generators: in network #T3 a single execution of DUOPF takes about 400 to 600 seconds, while in network #T2, which has less generators, computational times are from 40 to 60 seconds for a single execution.

Despite this inconvenient, the split nature of the implemented script allows to solve multiple IDM conditions (for example, with different number of PtG) given only one DAM calculation. Security and emergency problems are not taken in account in the current implementation.

11.2.4 Execution of the DAM script

As shown in Figure 11-2, the DAM is modelled as loop, in which each iteration represents an hour. For each iteration:

- A function updates all the time related variables, for example the nodal load for the current hour, and the current PV and wind generation forecasts for the hour.
- Then a DUOPF is performed, and it provides the list of generators that are required online in order to supply optimally the load in that iteration, without violating any generator or branch constrain.
- This list of online generators is saved and assigned to the current hour.
- Since it is expected for the RES production to have variation in the intraday market, it is necessary to add more generators online in order to provide security/reserve/reserve/ramp services. These generators are chosen among the cheapest that could not participate to the day-ahead market, and the added capacity depends on two factors, seasonality and time.

- After adding additional generators, a DCOPF is performed, in order to update the market clearance for this iteration. The current output is saved, and the iteration ends. When all the hours of the day have been processed, the day-ahead market script ends.

The loop iteration ends, the time variable is increased, and another iteration begins.

Additional generators are necessary since there are two time intervals in which the ramp service is highly required: the first is at sunrise when PV production rapidly increases, whereas the second one is at sunset, when PV production rapidly decreases. This is needed since in those hours the averages at five to fifteen minutes do not oscillate around the hourly averaged value, but steadily increase or decrease. Because of this, more generators are needed for ramp service. Seasonality changes the time when these two conditions occur, and this affects also the number of generators required to change along the year.

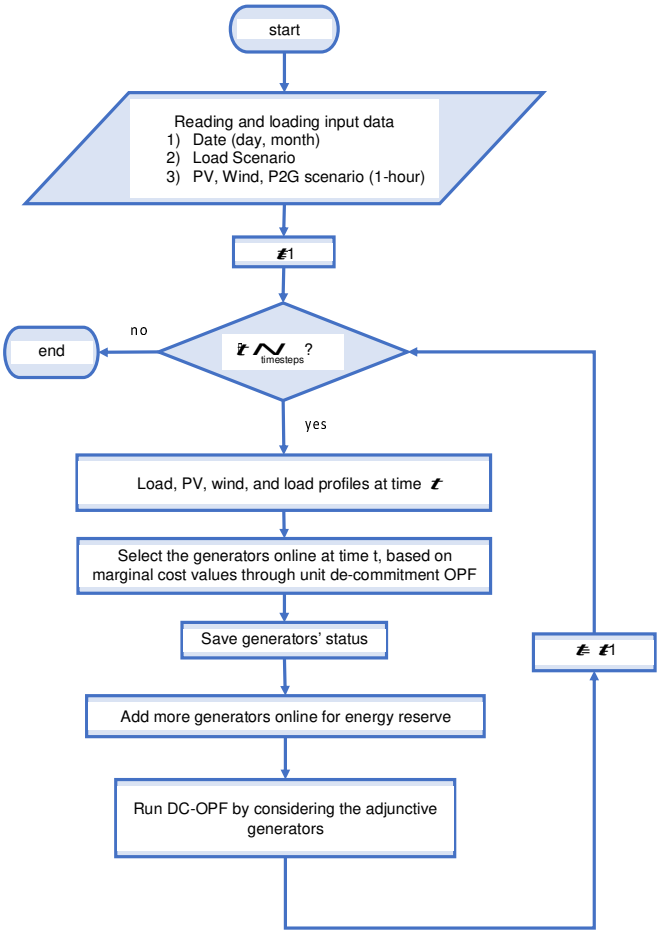

Figure 11-2: Flow chart describing the DAM

11.2.5 Execution of the real time IDM script

The real time market flowchart is shown in Figure 11-3.

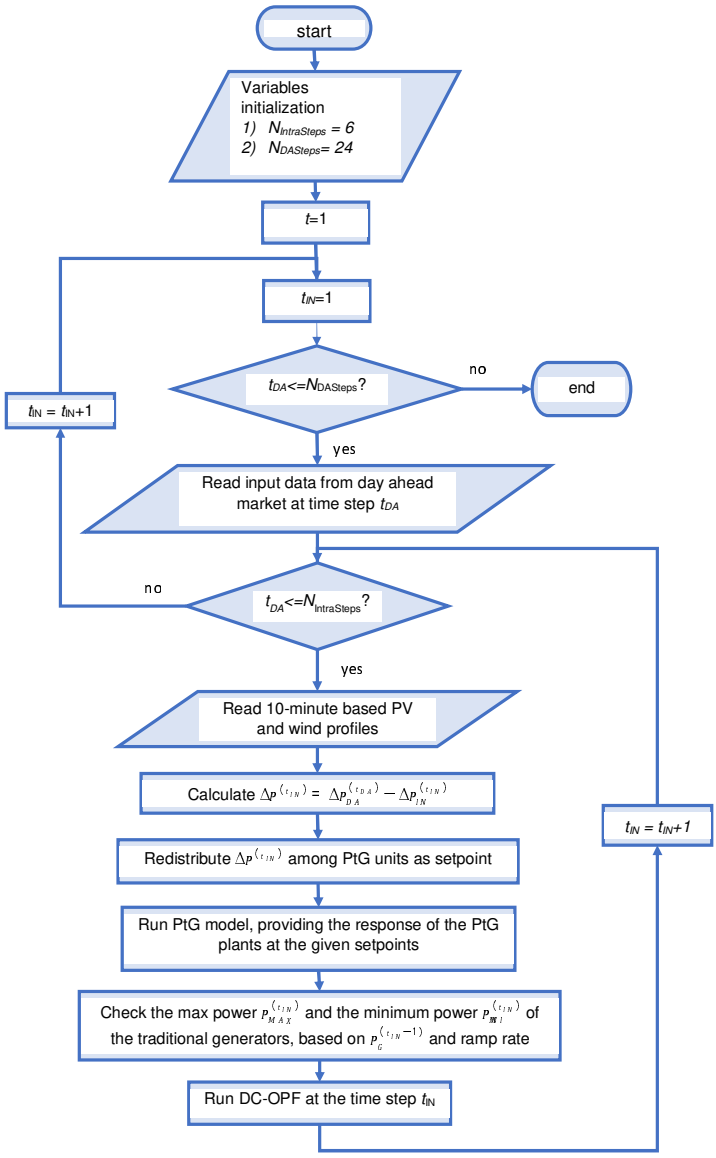

Figure 11-3: Flowchart of the real time (or ID) market

The real time IDM market script shares most of the input part with the script emulating the DAM. Moreover, it receives as input the status of the generators for every hour from the day-ahead market. There is an hourly time loop that updates every variable that changes hourly (DAM time loop), and, within each hour-iteration, another time loop represents the user defined time steps within the hour (IDM time loop), e.g., twelve five-minutes time steps, six ten-minutes time steps, four fifteen-minutes time steps.

Within each ID time loop, the PV and wind profiles are averaged according to the user time-step, and the difference of the actual renewable power with respect to the hourly one is calculated for each PV/wind generator. Part of this difference between the actual IDM generation and the DAM forecast can be assigned to every PtG unit as setpoint. If this quantity is positive it means that currently there is more PV/wind generation than forecasted, then PtG units can increase their power absorption. Vice versa, if this quantity is negative, there is less PV/wind generation than forecasted, therefore PtG units will have to lower their power absorption in order to help the network.

When PtG unit setpoints for the current iteration are known, PtG model is launched for each PtG unit. Given the fast response of PtG, the model runs with one-minute time steps, for a number of

times equal to the user defined time step for IDM market. For each PtG unit the average power (energy) within the user defined time step for IDM market is the response of the unit at this time iteration.

Since Matpower OPF offers a static resolution of the network, the ramp constrains are enforced through the maximum and minimum power constrains of generators. In each iteration the generation results of the previous time iteration are taken in account, and the maximum/minimum power constrains are updated as the previous results plus/minus the ramp rate applied to the user-defined time step for IDM market.

A DCOPF is performed, and the output is saved as the results for the current iteration, ending the iteration.

12 Appendix E: Simulated Annealing

The simulation annealing is a probability-based heuristic optimization method based on the simulation of the annealing process in which a melting metal is slowly cooled to solidify in its minimum energy state (single solution update). It was introduced the first time in [50], and successfully used in network reconfiguration (see as example [51]). In this Deliverable, this algorithm has been used for deciding where to install the PtG plants, and decide their size.

The algorithm is composed of two cycles, namely the external cycle and the internal cycle. The external cycle (shown in in Figure 12-1) depends on a control parameter called C, whose initial value is named C_0. For every iteration *m* of the external cycle, the control parameter is updated with a certain velocity described by the cooling rate α, i.e.:

$$C_m = \alpha \cdot C_{m-1} \quad \textbf{(17)}$$

The stop criterion of the external cycle is based on the persistence of the solution found so far: once the solution found persists (or the changes are below a certain threshold) for at least N_R successive iterations, the external cycle stops[10]

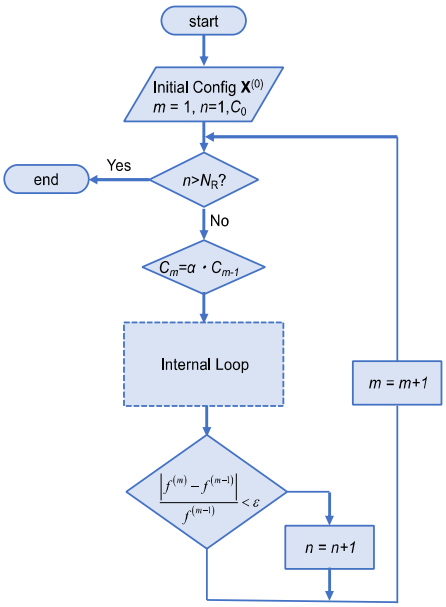

Fi

At every iteration of the external cycle, the internal cycle is run (shown in Figure 12-2). For every iteration *m* of the external the input of the internal cycle are:

1. Initial configuration: it is the best configuration found so far (the solution provided as output at the iteration *m*-1)
2. Value of the control parameter C_m
3. Number of solution to be analysed N_A

[10] This kind of stop criterion is typical of many heuristics existing in literature and allows to not fix a priori a total number of iteration, but only the number of iteration in which the same solution persists.

4. Number of solution to be accepted N_C

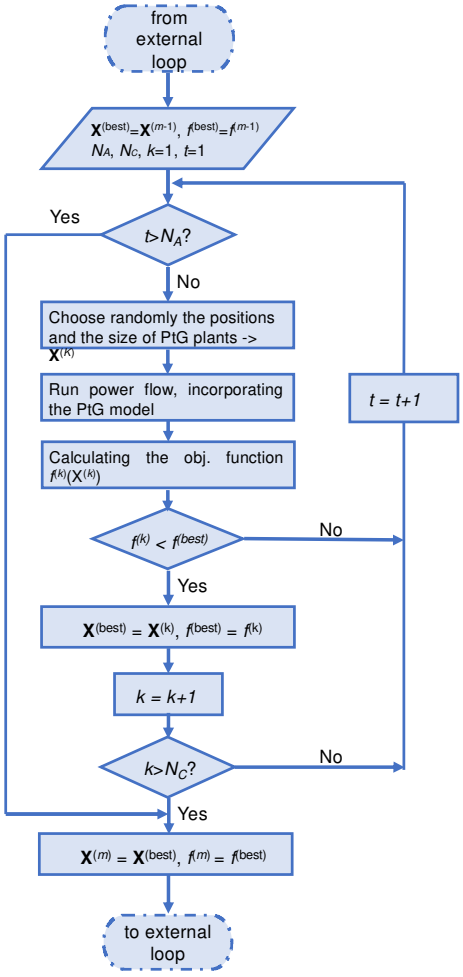

Figure 12-2: Flowchart of the internal loop of SA

The last two inputs are necessary for the stopping criterion of the internal cycle, which is composed as follows: the internal cycle stops when either N_A or N_C are reached. The first condition is usually reached with high C_m, wherease the second condition is usually reached with low C_m.

The objective functions change according to the goal of the optimization:

1. Presence only of reverse power flow: as pointed out in Section 5, the presence of reverse power flow is not violating any operational constraints of the network, even whether this is a not desirable condition. In this case, it is necessary to avoid that the placement of PtG plants can lead to a condition with low or null reverse power flow, but with violated constraints. For that reason, it has been used a penalised objective function, written as follows:

$$f_k(\mathbf{X}) = \frac{RPF_k}{RPF_0} \cdot \left(1 + \sum_{j \in \mathbf{J}} \rho_V \left(\frac{V_j^{(max)} - V_j}{V_j^{(max)}} \right)^2 + \right.$$
$$\left. + \sum_{j \in \mathbf{J}} \rho_V \left(\frac{V_j^{(min)} - V_j}{V_j^{(min)}} \right)^2 + \sum_{b \in \mathbf{B}} \rho_I \left(\frac{I_b^{(th,max)} - I_b}{I_b^{(max)}} \right)^2 \right) \quad (18)$$

Where RPF indicates the minute of reverse power flow (the subscript refers to the iteration of the internal cycle), $\mathbf{J}$ indicates the set of nodes, $\mathbf{B}$ indicates the set of branches and ρ_V and ρ_I indicate the penalisation of voltage (minimum and maximum) and current (thermal limits), respectively. In this way, the objective function considers the constraints violation, and this can be, in case, rejected during the optimization process.

2. Presence of reverse power flow and overcurrent, or reverse power flow and overvoltage: in this case, one of the objective to be optimized is actually a violated constraint. However, still it is necessary to use the penalized objective function, for properly representing the violation of the other objective function.

   a. Case reverse power flow and overcurrent:

$$f_k(\mathbf{X}) = \left(\frac{RPF_k}{RPF_0} + \frac{OC_k}{OC_0}\right) \cdot \left(1 + \sum_{j \in \mathbf{J}} \rho_V \left(\frac{V_j^{(max)} - V_j}{V_j^{(max)}}\right)^2 + \sum_{j \in \mathbf{J}} \rho_V \left(\frac{V_j^{(min)} - V_j}{V_j^{(min)}}\right)^2\right) \quad \textbf{(19)}$$

   Where OC indicates the number of minutes of overcurrent affecting the network

   b. Case reverse power flow and overcurrent:

$$f_k(\mathbf{X}) = \left(\frac{RPF_k}{RPF_0} + \frac{OV_k}{OV_0}\right) \cdot \left(1 + \sum_{j \in \mathbf{J}} \rho_V \left(\frac{V_j^{(min)} - V_j}{V_j^{(min)}}\right)^2 + \sum_{b \in \mathbf{B}} \rho_I \left(\frac{I_b^{(th,max)} - I_b}{I_b^{(max)}}\right)^2\right) \quad \textbf{(20)}$$

   Where OV indicates the number of minutes of overvoltage affecting the network. It is worth to note that the penalization on the presence of undervoltages is still active, for avoiding that the installation of a further load (i.e., PtG plants) can lead to worse the voltage values.

The method allows to accept (temporary) configurations having a worsening Δf in the objective function, only if they respect the following condition:

$$e^{-\Delta f / C_m} > r \quad \textbf{(21)}$$

Where r is a random number extracted in the interval (0,1].

The initial value C_0 of the control parameter can be customized according to the problem under analysis, by calculating an average worsening $\overline{\Delta f}$ obtained by considering some configuration having a worse objective function than the one of the initial configuration of the method. Then, by imposing an initial probability p_0 to accept worse solutions, the initial value of the control parameter C_0 can be calculated as follows:

$$C_0 = \frac{\overline{\Delta f}}{\ln(1/p_0)} \quad \textbf{(22)}$$

References

[1] E. Bompard, F. Boni-Castagnetti, G. Chicco, A. Mazza, L. Piantelli, and E. Pochettino, “D6.1: Report on opportunities and options for PtG in power systems”, STORE&GO, May 2017

[2] Task Force C6.04 “Benchmark Systems for Network Integration of Renewable and Distributed Energy Resources”, CIGRE, April 2014

[3] ENTSO-E, Union for the Coordination of the Transmission of Electricity (UCTE), https://www.entsoe.eu/news-events/former-associations/ucte/Pages/default.aspx (on line on 8th March 2018)

[4] ENTSO-E, Home page, https://www.entsoe.eu/Pages/default.aspx (on line on 8th March 2018)

[5] ENTSO-E, TYNDP, http://tyndp.entsoe.eu/maps-data/ (on line on 17th July 2018)

[6] Progetto Atlantide http://www.progettoatlantide.it/archivioReti/home.do;jsessionid=D9D16768154B56633168700BFA5E532A

[7] G. Prettico, F. Gangale, A. Mengolini, A. Lucas, and G. Fulli, Distribution System Operators Observatory, JRC Technical Reports, 2016.

[8] EU Commission, A policy framework for climate and energy in the period from 2020 to 2030 Communication from the Commission to the European Parliament, the Council, the European economic and social committee and the Committee of the regions, 22 January 2014, http://eur-lex.europa.eu/legal-content/EN/TXT/PDF/?uri=CELEX:52014DC0015&from=EN, (on line 4th April 2018)

[9] B. A. Ogunnaike, W. H. Ray, Process Dynamics, Modeling, and Control, Oxford University Press, 1994.

[10[D. E. Seborg, T. F. Edgar, D. A. Mellichamp, Process Dynamics and Control, 2nd ed., John Wiley & Sons, 2004

[11] K. R. Sundaresan and P. R. Krishnaswamy, "Estimation of Time Delay Time Constant Parameters in Time, Frequency, and Laplace Domains", The Canadian Journal of Chemical Engineering, 56(2), 1978, pp. 257–262, http://dx.doi.org/10.1002/cjce.5450560215.

[12] O. Schmidt, A. Gambhir, I. Staffell, A. Hawkes, J. Nelson, S. Few, “Future cost and performance of water electrolysis: An expert elicitation study, International Journal of Hydrogen Energy, Volume 42, Issue 52, 2017, pp. 30470-30492, DOI:https://doi.org/10.1016/j.ijhydene.2017.10.045.

[13] S. McDonagh, R. O'Shea, D. M. Wall, J.P. Deane, J. D. Murphy, "Modelling of a power-to-gas system to predict the levelised cost of energy of an advanced renewable gaseous transport fuel", Applied Energy, Volume 215, 2018, pp. 444-456, https://doi.org/10.1016/j.apenergy.2018.02.019.

[14] E. Giglio, F.A. Deorsola, M. Gruber, S. R. Harth, E. A. Morosanu, D. Trimis, S. Bensaid, and R. Pirone, Power-to-Gas through High Temperature Electrolysis and Carbon Dioxide Methanation: Reactor Design and Process Modelling, Ind. Eng. Chem. Res., vol. 57, pp. 4007–4018, 2018.

[15] F. Petipas, A. Brisse, and C. Bouallou, Model-based behaviour of a high temperature electrolyser system operated at various loads, J. Power Sources, vol. 239, pp. 584–595, 2013.

[16] R. K. Sinnott, Coulson & Richardson’s Chemical Engineering Design, 4th ed., vol. 6. Oxford, 2005.

[17] A. Mazza, E. Bompard, and G. Chicco, Applications of power to gas technologies in emerging electrical systems, Renewable and Sustainable Energy Reviews, vol.92, pp. 794-806, 2018

[18] ENTSO-E, Ten Years Network Development Plan 2016: Grid data, https://docstore.entsoe.eu/stum/, (on line 18th July 2018)

[19] DIW Berlin, ELMOD: The original Version of Europe, https://www.diw.de/de/diw_01.c.528493.de/forschung_beratung/nachhaltigkeit/umwelt/verkehr/energie/modelle/elmod.html#ELMOD, (on line 18th July 2018)

[20] F.U. Leuthold, H. Weigt, and C. von Hirschhausen, A Large-Scale Spatial Optimization Model of the European Electricity Market, Nework and Spatial Economics, vol.12, pp. 75-107, 2012

[21] Power World, Updated and Validated Power Flow Model of the Main Continental European Transmission Network, https://www.powerworld.com/knowledge-base/updated-and-validated-power-flow-model-of-the-main-continental-european-transmission-network (on line 8th March 2018)

[22] T. Jensen, H. de Sevin, M. Greiner, P. Pinson, The RE-Europe data set, https://zenodo.org/record/999150#.W303ry1aagQ

[23] B. Wiegmans, Unofficial ENTSO-E dataset processed by GridKit, https://zenodo.org/record/55853#.WpA8cjtG2Co (on line 18th July 2018)

[24] J. Hörsch, and T. Brown, The role of spatial scale in joint optimisations of generation and transmission for European highly renewable scenarios, 14th Int. Conference of the European Energy Market, Dresden, Germany, 2017

[25] J. Hörsch, F. Neumann and T. Brown, Python for Power System Analysis (PyPSA), Model of the European Energy System, https://github.com/PyPSA/pypsa-eur

[26] J. Hörsch, F. Hofmann, D. Schlachtberger, and T. Brown, Supplementary Data: Code, Input Data and Model data: PyPSA-Eur: An Open Optimisation Model of the European Transmission System, https://zenodo.org/record/1246852#.W307ay1aY_V (on line 19th July 2018)

[27] J. Hörsch, F. Hofmann, D. Schlachtberger, and T. Brown, PyPSA-Eur: An Open Optimisation Model of the European Transmission System, Preprint submitted to International Journal of Energy Strategy Reviews, June 2018, https://arxiv.org/pdf/1806.01613.pdf

[28] ENTSO-E, Power Statisics - Load, https://www.entsoe.eu/data/power-stats/hourly_load/ (on line on 17th July 2018)

[29] ENTSO-E, European Grid Map, https://www.entsoe.eu/data/map/ (on line on 17th July 2018)

[30] D. Oeding, B. Oswald, Elektrische Kraftwerke und Netze, 7th Edition, Springer, 2011 (in German)

[31] European Commission, European Meteorological derived high resolution renewable energy source generation time series, https://ec.europa.eu/jrc/en/scientific-tool/emhires (on line 18th July 2018)

[32] Bright Solar Resource Model, http://jamiembright.github.io/BrightSolarModel/, (online 18th July 2018)

[33] F. Spertino, F. Corona and P. Di Leo, "Limits of Advisability for Master–Slave Configuration of DC–AC Converters in Photovoltaic Systems," in IEEE Journal of Photovoltaics, vol. 2, no. 4, pp. 547-554, Oct. 2012. doi: 10.1109/JPHOTOV.2012.2203793

[34] Matlab, *k-means algorithm*, https://www.mathworks.com/help/stats/kmeans.html (on line 24th October 2018)

[35] ENTSO-E, Power Statisics - Generation, https://www.entsoe.eu/data/power-stats/net-gen-capacity/ (on line on 17th July 2018)

[36] ENTSO-E, TYNDP 2018 Scenario Report, https://tyndp.entsoe.eu/tyndp2018/scenario-report/

[37] J.J. Grainger, and W.D. Stevenson, Power System Analysis, McGraw-Hull Series in Electrical and Computer Engineering, 1994.

[38] R. D. Zimmerman, C. E. Murillo-Sanchez, and R. J. Thomas, Matpower: Steady-State Operations, Planning and Analysis Tools for Power Systems Research and Education, IEEE Transactions on Power Systems, vol. 26, pp. 12-19, Feb. 2011 http://dx.doi.org/10.1109/TPWRS.2010.2051168

[39] M.Rubino, H.Andrei, A.Mazza, and G.Chicco, Ranking the Radial Configurations for Minimum Losses Distribution System Reconfiguration. Part 1: Benchmark Results, The Scientific Bulletin Of Electrical Engineering Faculty. - ISSN 1843-6188, vol.1, pp. 23-28, 2014

[40] C.M. Domingo, T.G.S. Román, A. Sánchez-Miralles, J.P.P. González, and A.C. Martínez, A reference network model for large-scale distribution planning with automatic street map generation, IEEE Transaction on Power Systems, vol. 26, pp. 190-197, 2011.

[41] J. Gorre, et al, Interim report of benchmarks and analysis description and load profile definitions, Deliverable project STORE&GO, October 2017.

[42] J.M. Bright, C.J. Smith, P.G. Taylor, and R. Crook, “Stochastic generation of synthetic minutely irradiance time series derived from mean hourly weather observation data”, Solar Energy, vol. 115, pp. 229-242, 2015, DOI: http://dx.doi.org/10.1016/j.solener.2015.02.032

[43] JRC, “Photovoltaic Geographical Information System-Intercactive maps” http://re.jrc.ec.europa.eu/pvgis/apps4/pvest.php#

[44] N. Jenkins, J.B. Ekanayake and G. Strbac, Distributed Generation, IET Renewable Energy Series, London, 2010

[45] Enel Energia, “Enel Energia a tutto storage”, https://corporate.enel.it/it/media/news/d/2015/12/enel-energia-a-tutto-storage (on line of 17th July 2018)

[46] E. Carpaneto, G. Chicco and J. Sumaili Akilimali, “Characterization of the loss allocation techniques for radial systems with distributed generation,” Electric Power Systems Research, vol. 78, no. 8, pp. 1396–1406, 2008.

[47] A.Mazza, E.Carpaneto, G.Chicco, and A.Ciocia, Creation of Network Case Studies With High Penetration of Distributed Energy Resources, UPEC 2018, Glasgow, 4th-7th September 2018

[48] K. Mayer, S. Truck, Electricity markets around the world, Journal of Commodity Markets, Volume 9, March 2018, pages: 77-100

[49] EPRI, Wholesale electricity market design initiatives in the United States: Survey and research needs, Electric Power Research Institute, 2016 Technical Update

[50] P.J.M.van Laarhoven and E.H.L.Aarts, Simulated Annealing: Theory and Applications, D.Reidel Publ. Company, Dordrecht, Holland, 1987.

[51] E. Carpaneto, G. Chicco, and E. Roggero, Comparing deterministic and simulated annealing-based algorithms for minimum losses reconfiguration of large distribution systems, IEEE Powertech Conference 2013, Bologna, Italy